KANSAS GEOLOGICAL SURVEY
OPEN-FILE REPORT 90-34

STRATIGRAPHY, CARBONATE PETROLOGY, DIAGENESIS, AND TRACE ELEMENT CEMENT GEOCHEMISTRY OF THE WYANDOTTE LIMESTONE (UPPER PENNSYLVANIAN), MIAMI COUNTY, KANSAS

By

R.S. Arvidson

Kansas Geological Survey
1930 Constant Avenue
University of Kansas
Lawrence, KS 66047-3726

STRATIGRAPHY, CARBONATE PETROLOGY, DIAGENESIS, AND TRACE ELEMENT CEMENT GEOCHEMISTRY OF THE WYANDOTTE LIMESTONE (UPPER PENNSYLVANIAN), MIAMI COUNTY, KANSAS

by

Rolf Solheim Arvidson

A thesis submitted in partial fulfillment
of the requirements for the
Master of Science degree in Geology
in the Graduate College of
The University of Iowa

December 1990

Thesis supervisor: Professor Philip H. Heckel

The Graduate College
The University of Iowa
Iowa City, Iowa

CERTIFICATE OF APPROVAL

MASTER'S THESIS

This is to certify that the Master's thesis of

Rolf Solheim Arvidson

has been approved by the Examining Committee for the thesis requirement for the Master of Science degree in Geology at the December 1990 graduation.

Thesis committee: _____
Thesis supervisor

_____
Member

_____
Member

ABSTRACT

The Upper Pennsylvanian Wyandotte Limestone and Lane Shale, exposed in the eastern Kansas outcrop just south of Kansas City, are a sequence of cyclic limestones and shales deposited during two discrete, transgressive-regressive, eustatic marine cycles. These rocks preserve both a record of intimate feedback controls between carbonate and siliciclastic depositional systems, and complex associations of diagenetic fabrics related to rock/water ratios established during early stabilization history.

The first cycle terminated progradation of prodeltaic shale lobes, whose topography then controlled the local development of phylloid algal mud mounds during both the initial transgressive and later regressive phases of deposition. Shallow, well-lit, and well-circulated environments, slightly off the axis of shale lobes, favored luxuriant algal growth and carbonate mud production. Carbonate beds deposited in off-lobe areas of deeper water were thin and poor in algae by comparison. Regression brought about the growth of new delta lobes, whose paths of progradation were in turn controlled by the geometry of the underlying carbonate mound complex. Feedback between carbonate and clastic systems was also expressed during the second marine cycle, with deposition of algal mound and shoal water carbonate facies influenced by the topography of the underlying delta, as well that inherited from carbonate mounds of the previous marine cycle.

Petrographic, cathodoluminescent, and trace element geochemical data suggest that the path and extent of early meteoric diagenesis of phylloid algal mound carbonates was controlled by rock/water ratio, which can be seen to increase with depth through the mound pile. Low rock/water ratios through the top of the mound tended to remove metastable algal debris and marine cements, and cannibalize early meteoric cements, and thus skeletal voids here typically host only unzoned, lucid calcites precipitated in what was probably a burial regime. In contrast, the basal strata of the mound preserve neomorphic algal relics, and voids here retain both marine and early meteoric zoned cements, whose zonation of temporally increasing Sr suggests the maintenance of high rock/water ratios during early diagenesis.

ACKNOWLEDGEMENTS

I would like to extend sincere thanks to my committee: Professor Philip H. Heckel, who suggested the topic, for inspiration and guidance in the unique problems of Pennsylvanian field stratigraphy and depositional environments; to Professor Greg Ludvigson, for stimulating my interest in the application of trace element techniques to carbonate diagenesis; and to Professor Robert Brenner for introducing me to cathodoluminescent petrography. My thanks also go to W. Lynn Watney and the Kansas Geological Survey for financial support of field work; to Professor Nancy Budd for encouraging my interest in computer applications in geology; to Professor Ian Steele of the University of Chicago for assistance in acquisition of microprobe data; and to the faculty and staff of the Department of Geology at The University of Iowa and the Iowa Geological Survey Bureau for their assistance and friendship.

Lastly, my loving thanks to my dearest friend Mara Soloway, for her constant encouragement and patience, and for sharing her life with me during writing and after.

TABLE OF CONTENTS

LIST OF TABLES

LIST OF FIGURES

CHAPTER I

INTRODUCTION

Background, organization, and purpose of the project

The Wyandotte Limestone is one of a series of cyclic limestone and shale sequences found throughout the upper Desmoinesian, Missourian, and lower Virgilian stages in the Pennsylvanian Midcontinent outcrop belt of Oklahoma, Kansas, Missouri, Nebraska, and Iowa. A basic depositional model of HECKEL (1977, 1980) has related these sequences to glacioeustatic cycles of marine transgression and regression, and has successfully explained their lateral and vertical facies distribution. This model identified the Kansas-type cyclothem as composed of one nonmarine to nearshore and three open marine units. The marine members include a basal, thin, dense, dark skeletal calcilutite that is abundantly and diversely fossiliferous, and reflects deposition under a deepening water column; a thin, nonsandy, often phosphatic, conodont-rich shale having great lateral persistence, recording maximum water depth and transgression of the sea; a thick, fossiliferous, skeletal calcilutite, with shoal-water facies commonly present at the top, deposited in shallowing water.

These transgressive-regressive marine sequences are separated by relatively thick, sandy shales that contain remains of nonmarine flora, with marine fossils either lacking entirely or at best meager in abundance and diversity. These shales are deposits of the eustatic low stand, formed during progradation of the shoreline over the shelf, and represent a spectrum of nonmarine or nearshore environments, including deltaic complexes, coals, soil profiles, etc.

Application of this model to the Wyandotte Limestone (HECKEL, in review) resolves the formation into two discrete eustatic marine cycles. The basal transgressive Frisbie Limestone Member, offshore Quindaro Shale Member, and regressive Argentine Limestone Member constitute the lower cycle. The upper cycle, represented by the Farley Limestone Member, is separated from the lower by the nonmarine to nearshore deltaic Island Creek Shale. Recognition of the lateral persistence of the offshore conodont-rich Quindaro Shale has revealed errors in regional stratigraphic correlation, due largely to the transitional facies of the Wyandotte in Miami County, Kansas. Here, close to the southern limit of their outcrop exposure, the three lower members of the Wyandotte descend in the section over a slope that formed the boundary between a shallow carbonate shelf to the north and more offshore environments to the south.

The documentation of this transition, as well as presentation of the complete Wyandotte lithostratigraphic correlation along its outcrop belt, are the subjects of Chapter II.

Chapter III organizes the carbonate members of the Wyandotte into a scheme of microfacies based on standard petrographic examination, maps the lateral and vertical distribution of facies, and briefly discusses depositional environments. This scheme recognizes seven basic lithofacies: phylloid algal wackestone, phylloid algal packstone, geopetal brachiopod-algal calcilutite, onkoid-sponge calcilutite, oosparite, peloidal grainstone, and mixed skeletal calcarenite. Lastly, specific petrographic aspects of diagenesis (visible under transmitted light or excited by cathodoluminescence) are addressed. A model relating general petrographic features of cyclothemic sequences to their diagenesis in marine, meteoric, and burial environments (HECKEL, 1983) is also applied here. The discovery of marine cements (aragonite or magnesian calcite), preserved not as relics but crystallographically intact within the Frisbie Limestone, is an uncommon and exciting feature of rocks that have otherwise undergone substantial neomorphism.

Extensive petrographic examination of abiotic, void-filling calcite cements of the Wyandotte using

cathodoluminescent excitation also reveals a complex and striking pattern of cement growth zones. These growth zones preserve a record of changes in pore water chemistry during early meteoric diagenesis from a marine carbonate, composed of metastable aragonite and magnesian calcite, to diagenetic calcite. This cement record has been exploited through microprobe analysis of the spatial distribution of trace quantities of Mg, Mn, Fe, and Sr.

Proper interpretation of these data demanded construction of a qualitative model designed to predict the sequential evolution of trace metal ratios in meteoric pore waters. Studies of meteoric diagenesis in the modern environment have recognized that both Sr and Mg, sourced from the original marine components of the rock, are redistributed and partitioned between solid cement and aqueous reservoirs. The extent of this bulk partitioning is controlled by the number of dissolution-reprecipitation cycles, and is thus an index to the interaction of rock and water (VEIZER, 1983; LOHMANN, 1988).

In contrast, Fe and Mn are sourced primarily from terrestrial reservoirs, and the major control of Fe and Mn dissolved in groundwater is redox potential. Eh changes in groundwater systems are driven principally by oxidation of soil organic matter, which thus controls the boundary between surface oxic and subsurface anoxic regimes. The

concentrations of reduced Fe and Mn in a diagenetic cement thus reflect its position up- or downflow of this interface. Comparisons of the ideal behavior of Sr, Mg, Fe and Mn under closed versus open system diagenesis were made through computer simulation of equilibrium dissolution-reprecipitation reactions.

Using these criteria, detailed comparison was made of the trace element trends in cement samples collected from a thick vertical section of algal mound facies of the Wyandotte exposed close to the facies transition mentioned above, and from other selected sites as well. Calcite cements filling primary skeletal or sheltered cavities were selected with the requirement that they retain some vestige or relic of early marine cements, as well as host as complete a zoned sequence as possible in one void fill. Once the spatial and temporal relationship of zones was mapped through CL microscopy, microprobe transects were then made across each void fill. All CL and microprobe data are presented and discussed in Chapter IV, and Chapter V provides thesis summary and conclusions.

This thesis has thus three basic objectives:

1. to describe and map the lithostratigraphy and general facies distribution of the Wyandotte Limestone in Miami County and surrounding area;

2. to describe and discuss the transmitted light and CL petrography of the carbonate members;
3. to analyze the sequence of changes in trace element composition of calcite cements, and thus reconstruct physico-chemical conditions under which stabilization of carbonate mineralogies was accomplished.

Previous investigations

The generalized stratigraphy of the Wyandotte Limestone in Miami County was first described by NEWELL (1935), and later by MILLER (1966). The Wyandotte has also been described in the surrounding counties of Franklin (BALL, BALL, and LAUGHLIN, 1963), Linn (SEEVERS, 1969), and Johnson (O'CONNOR, 1971). As mentioned above, tracing of a conodont-rich horizon within the Quindaro Shale by HECKEL (in review) has provided the key to accurate correlation of Wyandotte members. Earlier investigations suffer in this regard due to their lack of genetic criteria for distinguishing offshore from nearshore shales, resulting in an arbitrary discrimination between limestone members, leading to the misidentification of the Farley Limestone as Argentine, or as Argentine plus Frisbie.

To the north in Johnson County, phylloid algal mounds are locally well-developed within all Wyandotte carbonate members. In an extensive litho- and biofacies analysis of the Wyandotte in this area, CROWLEY (1969) defined seven

facies: terrigenous, stromatolite-sponge, algal-bank, Archaeolithophyllum cap, calcarenite, oolite, and shelly mud. He related the lateral and vertical distribution of these facies to depositional topography (particularly that inherited from underlying deltaic platforms), water depth, and growth of algal mounds that in turn exerted unique feedback depositional controls. This work was basically accurate, except for his inclusion of the offshore Quindaro and nearshore Island Creek Shales within the same (terrigenous deltaic) facies. As a genetic understanding of cyclothemic deposition was still in its infancy, Crowley also made no attempt to cast the succession of facies and paleoenvironments within a framework of Pennsylvanian eustatic fluctuations.

Field and analytical methods

Detailed description and measurement were made of stratigraphic sections exposed at 42 sites through Miami, Johnson, Franklin, and Linn Counties (see Figure 2.1). Relatively new roadcuts and working quarries constitute the principal sections, although the complete Wyandotte succession is rarely exposed at any one given locality. Five to ten kg samples were collected at intervals appropriate to the scale of lithologic change, generally five feet or less. Shales were collected adjacent to base of the overlying limestone. Separation of conodont material

from shales was made by immersing samples saturated with Stoddard's solvent in hot water. Identification of conodonts faunas and the respective stratigraphic units that they help to identify was made by Philip H. Heckel (in review), and conodont data do not appear in this thesis.

Slabs of selected lithologies were polished for ease of recognition in additional field work. Over 200 thin sections (1" x 2" and 2" x 3") of carbonate samples were prepared for routine petrography. Selected thin sections and slabs were stained with Alizarin Red S and potassium ferricyanide for identification of carbonate mineralogy and ferroan carbonate, respectively, (LINDHOLM and FINKELMAN, 1972). To ensure precision, staining solutions were prepared in one liter batches at controlled temperature, and no more than fifty standard thin sections were stained before solutions were discarded.

Eighty-two additional standard petrographic thin sections were cut and micropolished from vacuum-resin-impregnated samples for cathodoluminescent petrography. Eight of these sections were ultimately selected for microprobe analysis.

Transmitted light photomicroscopy used a Nikon Optifot polarizing microscope with automatic exposure control, with KODAK EKTAR color print film, 125 ASA. All petrographic description and facies classification used the standard

terminology of Grabau or Dunham, and chose to adopt a given scheme where it best delivered an accurate description of the material.

CL petrography used a modified NUCLIDE ELM-2B LUMINOSCOPE. Best results for CL photomicrography were obtained using KODAK EKTAR color print film, 1000 ASA, with exposures ranging from 1 to 10 seconds, with operating conditions of 10-14 kV accelerating voltage at 0.4-0.75 milliamperes, measured at the anode. The CL apparatus was modified to introduce helium gas until residual chamber atmosphere was evacuated to 45-50 millitorr (mT), and total chamber pressure was stabilized at 190-200 mT. This atmosphere produced very stable operating conditions for the instrument, and appeared to enhance luminescence intensity while minimizing sample heating and damage.

Elemental data (Mg, Ca, Mn, Fe, Sr) were collected on 190 cement sites using an automated CAMECA SX-50 electron microprobe, operated under the direction of Dr. Ian Steele at the University of Chicago. A focused, 15 kV, 50 nannoampere beam was used. Sample damage from beam heating in the form of micropits was sustained, resulting in generally high elemental totals. These errors were viewed as acceptable due to the overall qualitative use of the dataset. The detection limit for all elements was assumed to be approximately 100 ppm.

CHAPTER II

STRATIGRAPHY

Introduction

Previous work on the Wyandotte Limestone in Miami and Johnson County (NEWELL, 1935; MILLER, 1966; CROWLEY, 1969) recognized the division of the formation into five formal members: in ascending order, the Frisbie Limestone, Quindaro Shale, Argentine Limestone, Island Creek Shale, and Farley Limestone (see general reference section, Figure 2.2). The shale sequence separating the Wyandotte from the underlying carbonates of the Iola Limestone has been traditionally regarded as the Lane Shale, named for thick shales and sandstones just outside the town of Lane in eastern Franklin County. The topmost Farley Limestone Member is in turn separated from the overlying carbonates of the Plattsburg Limestone by clastics of the Bonner Springs Shale. The Farley is locally divisible in Johnson County into two limestone beds separated by an intervening shale: the upper and lower Farley limestone and middle Farley shale, respectively. These beds show high variability in thickness and lithic character on an outcrop scale (CROWLEY, 1969; HARRIS, 1985), and have informal, local recognition only.

Historically, the fivefold division of the Wyandotte Limestone accommodated the outcrop belt in Johnson and Wyandotte Counties (see index map, Figure 2.1), where these units were typically well exposed as distinct lithologic entities, and stratigraphic correlation could be accomplished with relative ease. This organization also lent itself to the problem of apparent discontinuity of the upper Wyandotte members Island Creek Shale and Farley Limestone to the south in Miami County. Here these units were not recognized with certainty, and carbonate rocks at the stratigraphic position of the Wyandotte in Miami County were assumed to be predominately represented by the Argentine Limestone only (MILLER, 1966, p.17). Alternatively, it was assumed that the Farley merged with the top of the Argentine, thus becoming indistinguishable from it, through pinchout of the Island Creek Shale.

The Frisbie Limestone and Quindaro Shale were also recognized at only a few localities in northeastern Miami County. However, tracing of conodont-rich horizons through central Miami County in thin shales lying not far above the main bench of the Raytown Limestone, the upper member of the Iola Limestone, by MITCHELL (1981) allowed identification of the Quindaro Shale at localities PW1 and PW11 (index map, Figure 2.1). This conodont horizon has also been identified at the top of the Raytown farther to the southwest at

locality LA10. Thus the thin limestone immediately overlying this conodont horizon at these localities, previously regarded as "upper Raytown" (MILLER, 1966, p.17) is indeed true Argentine Limestone, now condensed dramatically from its thickness in algal mounds exposed in northeastern Miami and much of Johnson County. At localities PW11 and LA10, this limestone is in turn overlain by thick sandstones and shales of the type Lane Shale. Herein lies the basic evidence for miscorrelation of most of the Wyandotte Limestone in western Miami County, i.e., recognition of thinned Argentine Limestone at the top of the Iola Limestone. It follows that type Lane Shale overlying the Argentine at these localities cannot be correlated with shales that underlie the Argentine to the northeast in the Kansas City area, but instead must be correlated with the Island Creek Shale, which was traditionally regarded as thin or absent in Miami County. Lastly, limestones that overlie the Lane Shale in western Miami County, formerly regarded as Argentine or Argentine-Farley, must be entirely Farley Limestone, which thus enjoys much wider distribution than previously realized.

Thus the traditional stratigraphic correlation of the Wyandotte in Miami County suffers from the following defects:

1) a lack of understanding of the lateral distribution of the upper members, Island Creek Shale and Farley Limestone, and confusion and widespread misidentification of Farley as Argentine in western Miami County;

2) miscorrelation of the thinned Argentine Limestone in western Miami County with beds at the top of Iola Limestone;

3) miscorrelation of the type Lane Shale with shales underlying the Wyandotte Limestone in the Kansas City area, that have thus provisionally been given the revived name Liberty Memorial Shale (HECKEL, in review).

Tracing of conodont-rich horizons marking the position of the Quindaro Shale has thus provided the basic skeleton for recorrelation of the Wyandotte Limestone in Miami County. It is thus a central task of this thesis to document the true lithostratigraphy of the constituent members of the Wyandotte in this area, to show their relationship with the sections exposed to the north in Johnson County, and to describe and map southwestward changes in lithology and thickness as the Wyandotte nears its pinchout in the shallow subsurface of northeastern Anderson County.

Description of measured sections

The following description of outcrop localities will refer to six measured sections (Figures 2.3, 2.5, 2.7, 2.9, 2.11, and 2.13) of key Wyandotte exposures in Miami County that have been drafted to illustrate important lithologic features and relationships. In addition, later discussion will refer to the suite of isopach maps constructed from measured thicknesses of each Wyandotte member (Figures 2.18, 2.19, 2.20, 2.21, 2.22, and 2.23). Additional supporting data used in preparation of these maps were culled from published reports of now largely inaccessible outcrops (MILLER, 1966; NEWELL, 1935; CROWLEY, 1969), excluding localities with a likelihood of having errors in correlation. The index map of the study area (Figure 2.1) illustrates the location of Wyandotte outcrops and other landmarks referenced in the text. Lastly, two stratigraphic cross sections, A-A' and B-B' (Figures 2.24 and 2.25), are presented: the first along new State Highway K68 transecting the county from east to west, the second a SW-NE line that ties the southwesternmost portion of the Wyandotte in Miami County to the algal bank complexes exposed at Stilwell in southeast Johnson County and documented by CROWLEY (1969). Please note that the cross sections do embrace the revised correlation (HECKEL, in review) in which the Island Creek Shale, Farley Limestone, and Bonner Springs Shale are

included as members of the Lane Shale, and the Wyandotte Limestone thus comprises only the Frisbie Limestone, Quindaro Shale, and Argentine Limestone Members.

Liberty Memorial Shale

As mentioned above, shales residing between the base of the Wyandotte and the top of the Raytown Limestone Member of the Iola Limestone have suffered miscorrelation with those belonging to the type Lane Shale. This error reflects a failure to recognize true Argentine Limestone below type Lane in Miami County. This confusion has been remedied by the revival of the name Liberty Memorial Shale for the sub-Wyandotte nearshore and nonmarine clastics of the Kansas City area (HECKEL, in review).

The maximum thickness of Liberty Memorial in Miami County was measured by MILLER (1966) as 65.7 feet south of Louisburg at LO6, of which only the uppermost 7 feet of sandy, slightly calcareous, bioturbated light grey shale are currently available for inspection. At PE15, a roadcut on U.S. Highway 169-K7 southeast of Lake Miola, approximately 28 feet of grey to tan, slightly calcareous Liberty Memorial Shale were measured over the Iola Limestone. The Liberty Memorial here is overlain by the thin, conodont-bearing Quindaro Shale, followed upsection by the Argentine Limestone (see measured section and photo, Figures 2.3 and 2.4). One half mile to the SE, a section measured by Newell

"0.3 miles W of NE corner of section 14, T17S R23E" (PE16; NEWELL, 1935, pp.140-141, locality 141) recorded over 38 feet of (covered) "Lane" Shale, whose elevation, local thickness, and stratigraphic position over the Iola Limestone reveal it to be Liberty Memorial Shale. Farther to the west, at a quarry west of Paola (PW11; see measured section and photo, Figures 2.5 and 2.6), 8.5 feet of grey, occasionally silty, clay shale that lacks macrofossils overlie the Raytown Limestone Member of the Iola. At the top of this shale is a thin, fossilferous, marine horizon overlain by several feet of dense skeletal calcilutite. Conodonts recovered from this marine horizon again reveal it to be the Quindaro Shale with thin overlying Argentine Limestone. To the north at PW1, the Raytown Limestone is directly overlain by the Quindaro Shale (identified again by its distinctive conodont fauna) and Argentine Limestone, with little or no intervening Liberty Memorial Shale, thus recording its distal pinchout.

Outcrop control of the Liberty Memorial is poor in southeast Miami County. NEWELL (1935) described several outcrop localities in Paola East quadrangle (see index map, Figure 2.1, PE23 through PE28, his localities 139, 138, 137, 148, 147, 151, respectively) having shale sections overlying the Raytown of roughly twenty feet in thickness. Although these outcrops are no longer available for inspection, his

descriptions of a uniform, olive-buff or olive-drab, argillaceous shale are consistent with the general character of Liberty Memorial Shale exposed SE of Lake Miola at PE15.

Frisbie Limestone

The Frisbie Limestone is the basal member of the Wyandotte, embraced by the underlying Liberty Memorial Shale and overlying Quindaro Shale. The Frisbie in Miami County ranges from approximately 10 feet (and possibly slightly greater) to zero. The thickest exposures occur at a quarry south of Wagstaff (locality SP5, see index map, Figure 2.1) where the unit is a complex of thin carbonate and shale interbeds, each ranging from a fraction of a foot to two feet in thickness (see measured section and photo, Figures 2.11 and 2.12). The Frisbie carbonates here are dark grey skeletal calcilutites containing scattered crinoid columnals, small brachiopods, phylloid-algal-sheltered voids, and irregular argillaceous partings. The tops of carbonate interbeds are somewhat rubbley, although the top of the unit itself is in sharp contact with the overlying Quindaro Shale. The base of the Frisbie is not exposed here.

Unequivocal recognition of the Frisbie is possible elsewhere in Miami County only at two other exposures east of SP5 near Louisburg. Just west of Louisburg at the intersection of State Highways K68 and K69 (LO1), 0.9 feet

of Frisbie Limestone are exposed, consisting of dark grey, dense skeletal packstones containing abundant crinoid debris, small brachiopods, and large calcisponges (see photo, Figure 2.15). South of Louisburg at LO6, 2 feet of Frisbie having similar lithology are also exposed. The division of the Frisbie into interbedded limestones and shales seen at SP5 was also described by MILLER (1966, p.16) several miles SE of LO6, but the total thickness was not given. At all other localities where the base of the Argentine can be recognized with certainty (through identification of underlying Quindaro conodont faunas), the Frisbie is absent.

Quindaro Shale

The Quindaro Shale is exposed as a distinct bed at the same localities just described for the Frisbie Limestone, and is thickest in the Louisburg area.[1] At SP5 the Quindaro is a 0.6 foot thick bed of light to dark grey shale containing scattered traces of fine skeletal debris. At LO1, 1.9 feet of dark grey, fossilferous Quindaro Shale are present containing abundant crinoid columnals and large calcisponges (see photo, Figure 2.15). The abundant conodont fauna taken from this shale are similar to those taken from reference sections in Johnson County. Contact

[1]Regionally, the thickest Quindaro sections (>5 feet) exist in northern Johnson County near the Kansas River.

with the overlying Argentine Limestone at both these localities is sharp. At LO6, the Quindaro carries abundant crinoids, bryozoans, and small brachiopods (MILLER, 1966). In addition, where the Frisbie Limestone is otherwise absent elsewhere in Miami County, the Quindaro (identified by its abundant conodonts) resides in gradational contact with underlying Liberty Memorial Shale at four localities: PE16, LA10, PW11, and PW1. Less than 0.5 feet of dark grey fossiliferous Quindaro lie exposed above grey to tan Liberty Memorial Shale at PE16. At PW11 and LA10, a similar thickness of Quindaro is present, in the latter locality resting directly atop Raytown Limestone due to the pinchout of the Liberty Memorial Shale.

Argentine Limestone

The Argentine is the most variable in terms of thickness and lithic character of all the Wyandotte members in Miami County. The greatest measured thickness, 36 feet, occurs at SP5, the quarry south of Wagstaff (see measured section and photo, Figures 2.11 and 2.12).[2] The basal 20 feet of Argentine here is a light grey skeletal calcilutite exhibiting small sponges, brachiopods, bryozoans and

---

[2]The section exposed 3 miles south of Bucyrus by North Wea Creek (BU2), measured at 37 feet by MILLER (1966, p.17), may be incrementally thicker, but this outcrop is badly weathered and the basal section is not accessible (see also NEWELL, 1932, p.115, locality 71).

crinoids. Although skeletal material is sparsely distributed through this section, locally greater concentrations of fossil debris do occur. The upper section of Argentine here displays an increasing frequency of thin (<0.1 foot), discontinuous shale partings, often containing crinoid debris, and subhorizontal stylolitic seams. Overall fossil content also changes upsection, displaying a decrease in visible abundance (relative to carbonate mud volume), and an appearance of thick phylloid algal blades and small, rugose horn corals. The top 10 feet reveal a climax in algal abundance, with fossils other than small brachiopods and corals rare, followed thereafter upsection by a decrease in algae and an increase in irregular shale partings. The top of the Argentine here is a grey, massive, silty carbonate mudstone grading into calcareous siltstone, with few fossils save isolated bryozoans and fusulinids. Black nodular chert is also present.

To the east of SP5, the Argentine is exposed at several localities along State Highway K68. At LO1 (the intersection of K68 and K69), the Argentine consists of 20 feet of wavy, medium bedded, mixed skeletal calcilutite containing algae, bryozoans, small and large brachiopods, and crinoids (Figure 2.15). Beds here are roughly 2 feet thick and separated by thin zones of nodular chert. At LO3 and BU6, just west and north of Louisburg, respectively, the

top of the Argentine is a molluscan (bivalve) calcarenite overlain by the Island Creek Shale. This calcarenite forms a 0.5 foot bed capping medium bedded phylloid algal calcilutite, itself having abundant sparry, sheltered voids. Farther to the west at PE2, just north of Somerset and east of North Wea Creek, beds of the Argentine are seen to dip to the northwest approximately 20 degrees. The lithology here is a algal skeletal calcilutite with conspicuous veins and void fills of coarsely crystalline calcite spar. Rocks belonging to the Argentine are missing at localities just to the west of North Wea Creek (PE3 and PE17), although three feet of skeletal calcilutite and underlying shale probably belonging to the Farley Limestone and Island Creek Shale, respectively, are found just west of PE3 at PE4. This area is structurally disturbed and will be discussed shortly.

The thick sequence of algal- and mud-dominated, calcarenite- or siltstone-capped Argentine represented at SP5 and in the Louisburg area stands in vivid contrast with the section present approximately two miles southwest of SP5 at PE8 and PE9 (see measured section and photo, Figures 2.7 and 2.8). Although the base of the Argentine is not exposed here, its total thickness is estimated at 10 feet. Lithology is a dark grey, massive, dense, mixed skeletal calcilutite, with abundant small brachiopods, crinoids, cephalopods, high-spired gastropods, small sponges, small

rugose corals, and fenestellid bryozoans. Most notable is the algal encrustation of skeletal grains, forming mm-thick oncolitic sheaths. Laminations of these crusts also shelter cm-sized, spar-filled voids. The top weathered surface forms a prominent bench, and is littered with abundant loose echinoid spines and spirifer debris. The top three feet of Argentine are separated from the remaining basal carbonate section by 0.5 feet of calcareous, grey shale. The exposed basal limestone is identical in lithology to the upper section.

This unique lithology is also found in Argentine strata that directly overlie the Quindaro at localities PW1, PW11 and LA10. At PW1 west of Bull Creek on K68, 5.5 feet of dense, skeletal calcilutite belonging to the Argentine are separated from the underlying Raytown Limestone (the Liberty Memorial Shale is essentially absent by pinch out) by the conodont-rich Quindaro Shale (see photo, Figure 2.16). At PW11 as previously mentioned, the Argentine had been misidentified as belonging to the upper Raytown (MILLER, 1966). Here slightly less that 6 feet of Argentine are exposed over a conodont-rich horizon identifying the Quindaro Shale, and consist of a lower 5 feet and upper 2 feet of reddish-grey, ferruginous, skeletal calcilutite separated by an intervening 0.5 foot of calcareous shale (see measured section, Figure 2.5). Still farther to the

southwest at LA10, this sequence is again repeated with approximately five feet of Argentine exposed, separated from the underlying Raytown Limestone by less than 0.5 foot of shale (see measured section, Figure 2.19). At all these localities, the distinctive overall rock fabric and fossil constituents are identical to those exposed at PE8, and little doubt exists that they represent the same marine horizon (see photos, Figure 2.10).

In the north half of the Paola East quadrangle, the transition between thick phylloid algal-dominated calcilutites and dark, thin but fossiliferous skeletal calcilutites can be located with relative accuracy. The five localities that form a north-south line one mile east of Lake Miola (PE10 through PE14, see index map and map inset, Figures 2.1 and 2.26) expose the very top of the Argentine roughly one half mile east of PE8 and PE9. These exposures are rich in phylloid algal blades and have none of the lithologic characteristics of the condensed Argentine section exposed one half mile to the west at PE8 and PE9. The Argentine's transition in thickness and lithologic character is also expressed topographically by a mild N-S scarp paralleled by U.S. Highway 169-K7 and the eastern shore of Lake Miola.

At PE15 just SE of Lake Miola, the Argentine is exposed overlying conodont-bearing Quindaro Shale and Liberty

Memorial Shale (see measured section and photos, Figures 2.3 and 2.4). The Argentine here is a mixed skeletal calcilutite with abundant crinoids, small corals, brachiopods, ramose bryozoans, and thin argillaceous partings, and although it resembles exposures at SP5 in general lithologic aspect, it has thinned to approximately 11 feet and lacks abundant phylloid algae. However, it also differs from the Argentine at PE9 through lack of an abundant encrusting (onkoid) biota.

In southern Paola East quadrangle, the previously mentioned poor outcrop control frustrates precise mapping of the Argentine's change in thickness. It is possible that South and North Wea Creeks may locate the margin of thicker Argentine represented by positive surface topography at localities PE10 through PE14 (see map inset, Figure 2.26). In addition, the thin Wyandotte carbonates overlying the Liberty Memorial in the south half of Paola East quadrangle measured by NEWELL (1935) and MILLER (1966) most probably belong to the Argentine (PE23 through PE28).

Island Creek Shale

The Island Creek Shale also exhibits considerable variation in thickness and lithologic character throughout Miami County. The Island Creek can be traced from Stilwell in Johnson County, where it overlies a prominent algal mound complex of the Argentine mapped by CROWLEY (1969), along new

State Highway K69 south into Miami County as a thin calcareous, fusulinid-rich shale. MILLER (1966) tentatively identified the Island Creek at BU2 (1.6 feet) and BU1 (0.4 feet). In the Louisburg area where it overlies thick phylloid algal calcilutites of the Argentine (LO3 and BU6), the Island Creek is also typically a 0.5 to 1 foot thick calcareous, fossiliferous shale containing abundant crinoids, fenestrate bryozoans, and fusulinids. It can be traced to the west at the SP5 quarry, where it is 0.5 to 0.7 feet thick, and grades from a blocky grey at the top to a light brown shale at the base, albeit with no conspicuous fossils. Directly to the west at PE8 where it drapes over thinning Argentine and is overlain by the Farley Limestone, the Island Creek thickens dramatically to more than 45 feet (PE8, see measured section, Figure 2.7) of grey, buff-weathering shale having abundant ironstone concretions. At SP1 due west of Wagstaff, three miles directly north of PE8, 31.2 feet of grey to grey-brown clay shale having impressions of woody plant material and thin beds of grey, micaceous sandstone underlie the Farley Limestone. This represents only a minimum thickness as the top of the Argentine is not exposed here.

West of these localities, this interval thickens into a sandy shale with interbedded sandstones having plant impressions and carbonaceous streaks, reaching a maximum

thickness of more than 100 feet in the area of the type Lane Shale (measured by NEWELL, 1935, at LA12, PW16, and PW15, his localities 110, 143, and 112, respectively). This thick sequence persists near the southwestern corner of Miami County at LA10/LA11, where a composite shale section of 95 feet (although mostly covered) can be measured between the Argentine and Farley Limestones (see measured section, Figure 2.9). Here the type Lane Shale thus occupies the stratigraphic position between the Argentine (identified at PW11 and LA10) and Farley Limestones (LA11). To the north around Hillsdale Lake, a now inaccessible section (AN6) of Lane Shale was also measured by NEWELL (1935, his locality 88) at over 100 feet in thickness.

Farley Limestone

The Farley Limestone can be identified with certainty throughout Miami County except for the southeast quarter. In the northeast quarter it is typically 5 to 15 feet thick, separated from thick Argentine Limestone by thin Island Creek Shale. At LO3 and BU6, the basal Farley is a fusulinid grainstone (0.5 feet), succeeded by phylloid algal calcilutite (0.5 feet), with the remaining upper section a mixed skeletal calcilutite containing brachiopods, phylloid algae, crinoids, and other skeletal debris. To the west on K68 at PE1, the top of the Farley underlying the Bonner Springs Shale is a peloidal calcarenite. Farther to the

west at SP5, the Farley is exposed as a medium to thinly bedded, ferruginous, geopetal brachiopod calcilutite having abundant void-filling calcite spar (see measured section and photo, Figures 2.11 and 2.12). Although thought to be the Merriam Limestone by MILLER (1966), it can be positively identified here by its stratigraphic position between underlying thin Island Creek and overlying Bonner Springs Shale (in turn overlain by the characteristically thickly bedded and Composita-rich Merriam Limestone) outcropping one mile to the northwest at SP6.

As the Farley begins to separate substantially from the Argentine due to thickening of the underlying Island Creek-Lane Shale section, it also exhibits local thickening and a more complex internal stratigraphy. At PE6/PE7 and SP1, the base of the Farley in contact with the Island Creek-Lane Shale is an argillaceous, dark grey, skeletal calcarenite, with the remainder of the unit a sparry, algal-brachiopod calcilutite. Total thickness at SP1 is 14 feet. To the west at PW2, the lower part of the Farley is a massive oolite, grading up into ferruginous, thinly bedded, flaggy-weathering calcilutite containing molluscs and oolite intraclasts. The upper Farley section is massive and contains abundant brachiopods, fenestrate bryozoans, and phylloid algae, including a conspicuous bed of large productids. Farley thickness here exceeds 19 feet.

A slightly thinner but otherwise virtually identical Wyandotte section having basal oolite and a zone of large brachiopods was described by NEWELL (1935) three miles to the south at PW14 (his locality 104). Basal Farley oolite is also found above thick Lane Shale at PW7, where its thickness is estimated at 10 feet.

At PW4, two miles to the west of PW2, approximately 8 feet of Farley are exposed. The thick to medium wavy bedded, ferruginous, skeletal calcilutite containing bryozoans, crinoids, and rare large brachiopods is similar in general appearance to PW2, but differs in the absence of basal oolite.

At RA9 just west of the Miami County border in Franklin County, 14 feet of Farley are exposed above sandy shale and sandstone of the Lane-Island Creek Shale (see photo, Figure 2.17). The Farley grades from sandy, flaggy, brachiopod calcilutite up into ferruginous, algal-brachiopod calcilutite. The unit is thickly bedded, although certain zones exhibit a distinctive style of weathering into small chips or lentils. Stringers of prominent cm-sized solution cavities high in the section probably mark zones of original skeletal concentrations. Ferruginous, grey, brachiopod or brachiopod-algal calcilutites ranging from five to fifteen feet also characterize most of the other Farley exposures in

western Miami and eastern Franklin Counties (localities LA11, RA8, and LA9).

Close to the four corners of Miami, Linn, Franklin, and Anderson Counties, the Farley thickens to greater than 40 feet. At LA8 quarry in Linn County, over 34 feet of visibly mounded Farley can be measured (see measured section and photo, Figures 2.13 and 2.14, respectively). Close to its basal contact with Island Creek-Lane Shale (visible as float on the quarry floor), the Farley exhibits a four foot zone of light grey, fossiliferous calcilutite containing abundant small brachiopods, lophophyllid corals, fusulinids, bryozoans, minor algal blades, and fine scale irregular argillaceous partings. Brachiopods show common sulfide replacement. This zone is capped by one foot of dark grey calcilutite that is poorly fossilferous. Separated from this basal section by a thin shale parting, the remaining 29 feet of Farley is a algal-brachiopod calcilutite, with Enteletes a common skeletal constituent. Brachiopods and algae shelter abundant void-filling calcite spar, and irregular, argillaceous partings separate thick beds. This locality is the southernmost measured section of the Wyandotte in the field area.

A thickened Wyandotte section is also described two miles to the northwest by BALL, BALL, and LAUGHLIN (1963, their location A13) at LA5. Although this outcrop is now

covered, based on their measured section and similar lithologic description at least 36.5 feet of Farley Limestone was exposed here (misidentified as Frisbie and Argentine; the unit they identified as Farley may actually be higher Merriam Limestone overlying the Bonner Springs Shale).

A medium to thinly bedded, ferruginous, sparry, algal-brachiopod calcilutite with a zone of robust fusulinids forms the westernmost measured section of probable Farley Limestone at GTNW1. Only six feet of section are exposed here, although an abandoned quarry less than a mile to the west (GTNW2) suggests that a significantly greater thickness is present.

Two additional outcrops in Johnson County are also of interest. At LE2, 6.2 feet of Farley skeletal calcilutite that is poor in phylloid algae but contains crinoids, Enteletes and other brachiopods, and small rugose corals are exposed between the overlying Bonner Springs and underlying Island Creek Shale. This outcrop is ferruginous at the base and calcarenitic at the top, and was the key outcrop in CROWLEY's (1969) interpretation of this area as an intermound channel in which all Wyandotte strata are generally thinner.

Lastly, O'CONNOR (1971, p.18) described an outcrop at GA1 along Little Bull Creek in southern Johnson County of 6

feet of oolitic and molluscan limestone, capping a basal silty limestone containing crinoids and brachiopod fragments. He proposed that this bed may be part of the Argentine, as demanded by the traditional correlation. In wells or outcrops in the immediate vicinity, he also recorded 80 to 100 feet of Lane Shale below this unit (O'CONNOR, 1971, p. 14, his Figure 6). These shale thicknesses, measured just to the north of thick type Lane Shale (108 feet at AN6), suggest that they also belong to the type Lane. This in turn suggests that the overlying limestone unit is most likely Farley. Attempts to locate this particular outcrop were in vain, although beds having coated grain calcarenite lithologies characteristic of (and mapped by O'Connor as) Merriam Limestone were identified higher in the section. In addition, at the same general locality, fusulinid calcarenites and fine-grained, argillaceous, skeletal limestones were described below the Bonner Springs Shale. Although O'CONNOR (1971, p.20) hesitated to ascribe these beds to either Farley or Argentine, they also probably belong to the Farley alone.

Discussion of Wyandotte stratigraphy and general relationship to model of cyclothemic deposition

An increased understanding of the relationship between eustatic rhythms, epicontinental marine circulation, and associated facies patterns has recognized the thin,

laterally extensive marine shale members of Upper Pennsylvanian Midcontinent limestone cycles as the deepest water deposits of each transgressive-regressive cycle (HECKEL, 1977). These core shales are the only ones to develop the black phosphatic facies, and are vertically embraced by carbonate facies deposited below effective wave base. Furthermore, the facies that develops in the stratigraphic position of the core shale is an indication of the relative extent of marine transgression (HECKEL, 1986). The presence of the black phosphatic facies signifies starved deposition under anoxic bottom water in a density-stratified sea. Such permanent stratification requires a minimum water depth estimated at 100 m (HECKEL, 1977, p.1057-58). In hierarchical fashion, cycles possessing the black, phosphatic, conodont-rich facies are described as major cycles (HECKEL, 1986). Intermediate cycles are those that lack the black phosphatic facies, but do preserve a conodont-rich interval at the position of the core shale. Intermediate cycles record a marine transgression that is perhaps of insufficient extent or duration to develop a permanent thermocline, and thus even the deepest-water sediments were deposited under relatively well mixed and oxygenated water. Minor cycles inundate only the lower shelf and lack conodont-rich horizons.

The original Wyandotte Limestone can be interpreted to represent two discrete eustatic marine cycles. The transgressive Frisbie Limestone Member, offshore Quindaro Shale Member, and regressive Argentine Limestone Member constitute the lower, intermediate cycle. As described in the previous section, the Argentine undergoes a transition from a thick, phylloid-algal-rich, shallow water carbonate to a deeper, offshore facies in central Miami County. Regressive Argentine carbonate deposition was terminated by an influx of deltaic clastics, sourced primarily from the southwest (type Lane Shale), with minor influx from the north (type Island Creek Shale Member). The sea was cleared upon subsequent eustatic sea-level rise and carbonate production was reestablished, forming the complex of shallow-water facies of the second, minor cycle: the overlying Farley Limestone Member. The Wyandotte can thus be cast against a framework of eustatic change, as is shown in Figure 2.27, taken from HECKEL (1985). This Wyandotte section, measured near Holliday in northern Johnson County, also shows the increasing influence of Island Creek Shale. HARRIS (1985, p. 42) argued that the middle Farley shale could be treated as a tongue of the Island Creek Shale, and that the lower Farley limestone, middle Farley shale, and Island Creek Shale were essentially correlative, reflecting the relative influence of clastic versus carbonate

sedimentation. The middle Farley shale is best represented in northern Johnson County, and cannot be recognized in any Farley exposures in Miami County.

Isopach mapping of the Liberty Memorial Shale below the entire Wyandotte (Figure 2.18) reveals at least two prodeltaic lobes encroaching on Miami County from the east and north, separated by an NE-SW trending area of reduced sediment thickness (represented by locality LE2/LE5 in Johnson County). As previously mentioned, CROWLEY (1969) interpreted this area as an interbank regime where the Liberty Memorial (as well as carbonate members of the overlying Wyandotte) thinned abruptly before regaining thickness to the southeast. Immediately to the northwest of this interbank area, Crowley described thickened Liberty Memorial Shale exposures (LE3 and LE4, his localities 18 and 31) of greater than 70 feet (his "Lane Shoal"). The correlation of the Liberty Memorial through this area in Johnson County may be in error, although this holds no serious ramifications for the overall pattern in Miami County. O'CONNOR (1971, p.12-13) mentions localities in east central Johnson County where a shale and limestone bed of as much as 3 and 5 feet, respectively, overlie the main bench of the Raytown Limestone along Tomahawk and Indian Creeks. This occurrence of a thin shale and limestone overlying the Raytown resembles that of PW11 or LA10 in

Miami County, and suggests the possibility that the thick shales described by Crowley's "Lane Shoal" may actually be Island Creek, with thin Liberty Memorial residing between the Raytown and overlying thin Argentine Limestone. Thin (0.1 foot) shales thought to be Island Creek at LE4 and LE3 would thus correlate with the middle Farley shale, oolites thought to be lower Farley would be upper Farley, and algal bank carbonates described as Argentine would be lower Farley. Attempts to unequivocally identify the Raytown Limestone along Tomahawk and Indian Creeks in this area of Johnson County were unsuccessful, and thus the identity of Crowley's "Lane Shoal" clastics remains somewhat problematic in this area.

By comparison, the transgressive Frisbie Limestone is found only as a distinctly recognizable bed where it is associated with thick underlying Liberty Memorial Shale, as is documented at Louisburg (LO1) and at other localities in Johnson County (at OL1 near Craig, OL2 near Olathe, and ED1 near Holliday; compare isopach maps, Figure 2.18 and 2.19). The Liberty Memorial Shale is not exposed at SP5, but by surface elevations is assumed to be relatively thick here as well. During the initial transgression, areas floored by thin Liberty Memorial may not have spent sufficient time in nonturbid, well-lit water free from waning prodeltaic influence to allow algal carbonate to form. In contrast, if

benthic algae first established themselves on the flanks of the delta slope (after delta abandonment and the return of clear water conditions), as may have been the case at SP5, they could have maintained an optimal position in the photic zone during continued eustatic rise both by mud production and simple upward growth as well as colonization of newly submerged delta platform. The thickened Frisbie sequence developed at SP5 may also have been a response to a preferred position close to the margin of the abandoned delta, that possibly afforded access to nutrients upwelled from deepening water.

The Quindaro Shale enjoys better lateral distribution than the Frisbie, as would be expected of a core shale deposited in deeper water. Even during the climax of the transgression, bottom topography appears to have influenced deposition, as the Quindaro is most conspicuously fossilferous where associated with thick sections of the Liberty Memorial Shale (LO1). This relationship could reflect either increased benthic productivity or preservation: bottom topography of the submerged delta platform may have enhanced bottom circulation and mixing, promoted surface primary productivity through increased upward nutrient fluxes (thus in turn increasing the flux of particulate organic matter to the bottom), or possibly influenced carbonate saturation state. Isopach mapping of

the Quindaro (Figure 2.20) suffers from sparse outcrop control, but the pattern also shows a generally positive relationship with that of the Liberty Memorial. In the western half of Miami County, as well as much of southern Johnson County, the Quindaro is probably 0.5 feet thick or less, but should still be recognizable from its abundant conodont fauna.

Isopach mapping of the Argentine (Figure 2.21) defines a broad, thickened platform having general NE-SW orientation, originating just to the east in southeastern Johnson and western Cass County, Missouri, with a thinning flank extending into central Miami County. Additional thickening of the Argentine is also seen in west central Johnson County, where it forms a prominent algal bank near Olathe (CROWLEY, 1969); however, this is regarded as a separate feature from the Stilwell-Wagstaff trend for reasons to be discussed shortly.

Although other depositional factors such as circulation undoubtedly influenced Argentine mounding, comparison of the position and strike of thick Liberty Memorial with that of the general trend of algal-rich, thickened Argentine again reveals that algal mounds were developed on the flank or crest of Liberty Memorial prodelta lobes (compare Figures 2.21 and 2.18). As this prodeltaic platform thins to the southwest, the overlying Argentine descends and thins

dramatically, suffering reduction in phylloid algae and associated carbonate mud, and ultimately approaching the top of the underlying Iola Limestone to the southwest, as revealed at localities PW11 and LA10. Here, beyond the distal margin of the prodelta, the Argentine is separated from the Raytown member of the Iola by only the thin (0.5 foot), conodont-rich Quindaro Shale. Further westward thinning of this shale interval would ultimately lead to a virtual superposition of the Raytown and Argentine Limestones with only a diastemic separation. The condensed Argentine section is distinguished by its flora of algal crusts, generally massive aspect, and thin shale horizon separating upper and lower limestone sections. CROWLEY (1969) identified similar carbonate lithologies in Johnson County only at the base of the Argentine in the Kansas City area (and within the Frisbie Limestone north of his interbank area). Although the thin shale horizon just mentioned is laterally continuous, this shale lacks marine fossils and does not correlate with the conodont-rich Quindaro Shale identified at the base of the lower carbonate at PW11 and LA10.

In the Stilwell-Wagstaff trend, the Argentine is typically a wavy bedded algal-skeletal calcilutite, with beds separated by thin cherty or argillaceous partings. These partings may represent short-lived influxes of clastic

material, most likely shed from the encroaching Lane delta. These partings are absent in the condensed Argentine found in western Miami County, suggesting that Argentine carbonate deposition was overwhelmed in western Miami County, while algal mound growth continued in the northeast, ultimately curtailed more by dropping sea level than by clastic influx. The molluscan fauna that dominates the capping Argentine calcarenite at LO3 and BU6 may simply indicate the increasing restriction and variability in temperature, salinity, etc., typical of very shallow water environments.

Structural dips in the area around North Wea Creek just north of Somerset (PE1; see map inset, Figure 2.26) were measured in some detail by MILLER (1966), who concluded this area to be a small, slumped or downdropped block of the Wyandotte, separated from the rest of the platform by minor faults that affect the underlying section as well. Just to the west and southwest of PE1 at PE3 and PE17, respectively (west of North Wea Creek), cross-bedded skeletal calcarenites of the Dewey Limestone (identified through conodont faunas of the underlying Quivira Shale at PE17) crop out in the approximate structural position of the Wyandotte. These localities must represent an upthrown block to the west of the small graben described by MILLER (1966). Because of lack of field evidence that would suggest pre- or syndepositional faulting, it is assumed that

the activity which gave rise to present day structural disposition postdated deposition of the Wyandotte Limestone. Field and subsurface data of greater detail and density might afford a determination as to whether any precursor of this structure is manifest in the Wyandotte. Isopach mapping of the Argentine has characterized this area as slightly thinner than the section represented at SP5, but this is mostly conjecture.

This control of carbonate thickness by an underlying deltaic platform was reversed during deposition of the Lane Shale-Island Creek clastics. As demonstrated by the exposures at PE8 and LA10, the stratigraphic position of the type Lane Shale between Argentine and Farley Limestones demonstrates its correlation with the Island Creek Shale. Isopach mapping (Figure 2.22) of the Lane-Island Creek interval reveals a delta lobe that dominates western Miami County and stretches northeastward into Johnson County where it occupies the interbank area described by CROWLEY (1969). As suggested by comparison of Lane-Island Creek Shale and Argentine Limestone isopach maps (Figures 2.22 and 2.21), northeast migration of the Lane delta front was confined to areas of thin underlying Argentine, notably in the SW-NE oriented channel that separates the Stilwell-Wagstaff trend of thick Argentine from mounds developed to the northwest

and north in Johnson County near Olathe and Kansas City (described by CROWLEY, 1969).

In previous mapping of the distribution of the Island Creek in Johnson and adjacent Counties, CROWLEY (1969, p. 14, his Figure 10) measured a maximum thickness of Island Creek Shale in northwestern Wyandotte County (43 feet). His mapping shows a lobe extending south into Johnson County. It is instead possible to argue that the clastic interval separating the Argentine from the Farley in Miami County and southern Johnson County represents material supplied primarily from southern (Lane) source areas, and influence from Island Creek clastics, sourced from the north, was minor and not felt here until perhaps fairly late in the regression (this of course assumes that the thick shales at LE3 and LE4 indeed belong to the Liberty Memorial). There is little evidence that overall carbonate production was greatly fouled by clastic influx in the Stilwell-Louisburg area, as the Island Creek in this areas is thin and conspicuously fossiliferous. Thus the middle Farley, representing a later, minor clastic influx from the northern, Island Creek source area, is not found to the south in Miami County, where carbonate deposition continues without interruption through the entire Farley cycle.

It is assumed that the steep front defined by the abrupt change in thickness of Island Creek sections exposed

at SP5 and PE8 persists to the northeast into Johnson County. This gradient may also be characterize the delta margin in the southern Miami County, but detail is lacking there due to poor outcrop control. Where data is available on a sufficiently fine scale in Paola West quadrangle, the Lane delta margin is resolved as a complex of interdistributary bays and prodelta lobes.

Depositional topography atop the Lane-Island Creek deltaic complex in turn governed bathymetry during subsequent carbonate deposition, and thus controlled the distribution of ooid shoals, calcarenites, and algal mounds of the Farley Limestone. The Farley isopach map (Figure 2.23) depicts a series of mounds developed in the Farley around Lane, northwest of Paola, and possibly southeast of Gardner (local thinning of the Bonner Springs Shale recorded by O'CONNOR (1971) can be used as indirect evidence of Farley thickening in the Gardner area). The control of Farley mound development can be seen through comparison of its orientation with that of the underlying Lane deltaic complex. Although the thickness of the underlying Lane-Island Creek Shale is unknown at LA8 in Linn County, it is assumed that the mound development here was controlled by thickening of the underlying section. As mound growth would have been self-limiting along the crest of the underlying deltaic platform, the steep margins of the delta front may

actually have been preferred sites of mounding, as these would have offered both access to sunlight and renewal of nutrients from deeper water, in addition to room for both lateral and vertical growth. This same relationship can also be seen between the Argentine and the Liberty Memorial at Stilwell, where maximum mound thickness occurs off the crest of the underlying delta platform, which lies to the southeast (compare Figures 2.21 and 2.18).

Oolites developed in the basal Farley represent shoals developed during the Farley transgression. As water deepened, current agitation and carbonate saturation increased, and siliciclastic detritus from the abandoned delta served as nuclei for ooid growth. The morphology of the underlying platform also undoubtedly influenced current direction, and thus the orientation of the ooid shoal as well.

East of the Lane-Island Creek delta margin in Miami County, the Argentine assumes the role of providing a suitable platform for Farley mound development. This is clearly expressed at Stilwell, where the pattern of Farley thickening essentially mimics that of the underlying Argentine Limestone. (The same pattern, albeit more mildly manifest, can also be seen west of the delta margin near Olathe).

Thus there are three related aspects that are central to Wyandotte stratigraphy in Miami County and the surrounding area, illustrated in the two cross sections A-A' and B-B' (Figures 2.24 and 2.25). First, delta/prodelta platforms (Liberty Memorial, Lane-Island Creek) formed during eustatic low stands strongly influenced the facies and thickness of the overlying marine carbonate deposits, both during the initial transgressive (Frisbie/Quindaro, lower Farley) and later regressive (Argentine, upper Farley) phases of a given cycle. Algal carbonate banks and mounds favored topographically elevated areas afforded by the underlying shale platform, often in an off-axis position close to a break in slope that may have offered well-lit, quiet water and access to nutrients (e.g., the Argentine in the east half of A-A' and B-B'; the Farley at PW4, A-A' and at LA8, B-B'). Mounds also formed over carbonate topography inherited from a previous cycle, as is the case west of Olathe and at Stilwell (Farley at ST6 on B-B'), perhaps with a minor shift in locus. Second, areas beyond the distal margin of the prodelta acquired only thin carbonates during the marine regression (e.g., the Argentine in the west half of both cross sections), with essentially diastemic horizons formed during the preceding transgression. Lastly, these lower areas then become the path of access for the prograding delta formed during the low stand, as can clearly

be seen in both cross sections with the confinement of the Lane delta by thick Argentine to the east (and to the north in Johnson County, near Olathe).

The various lithologies that comprise the Wyandotte have been touched upon only briefly here. The following chapter will organize them in a facies framework based on petrographic examination.

Figure 2.1. Index map, showing general area of thesis study in Miami, Johnson, and Franklin Counties, east central Kansas. Wyandotte Limestone outcrop belt generally coincides with distribution of open and closed circles: closed circles indicate Wyandotte outcrops measured or studied, open circles are localities compiled from sources cited in text (in Miami County these are generally no longer accessible). Lines of stratigraphic cross sections A-A' and B-B' are presented in Figures 2.24 and 2.25, respectively. Locality abbreviations are referenced in text. Inset frame is boundary of enlarged view in Figure 2.26. Note that map is not an equal area projection: one degree latitude equals one degree longitude, thus generating approximately 25% horizontal exaggeration.

Figure 2.1.

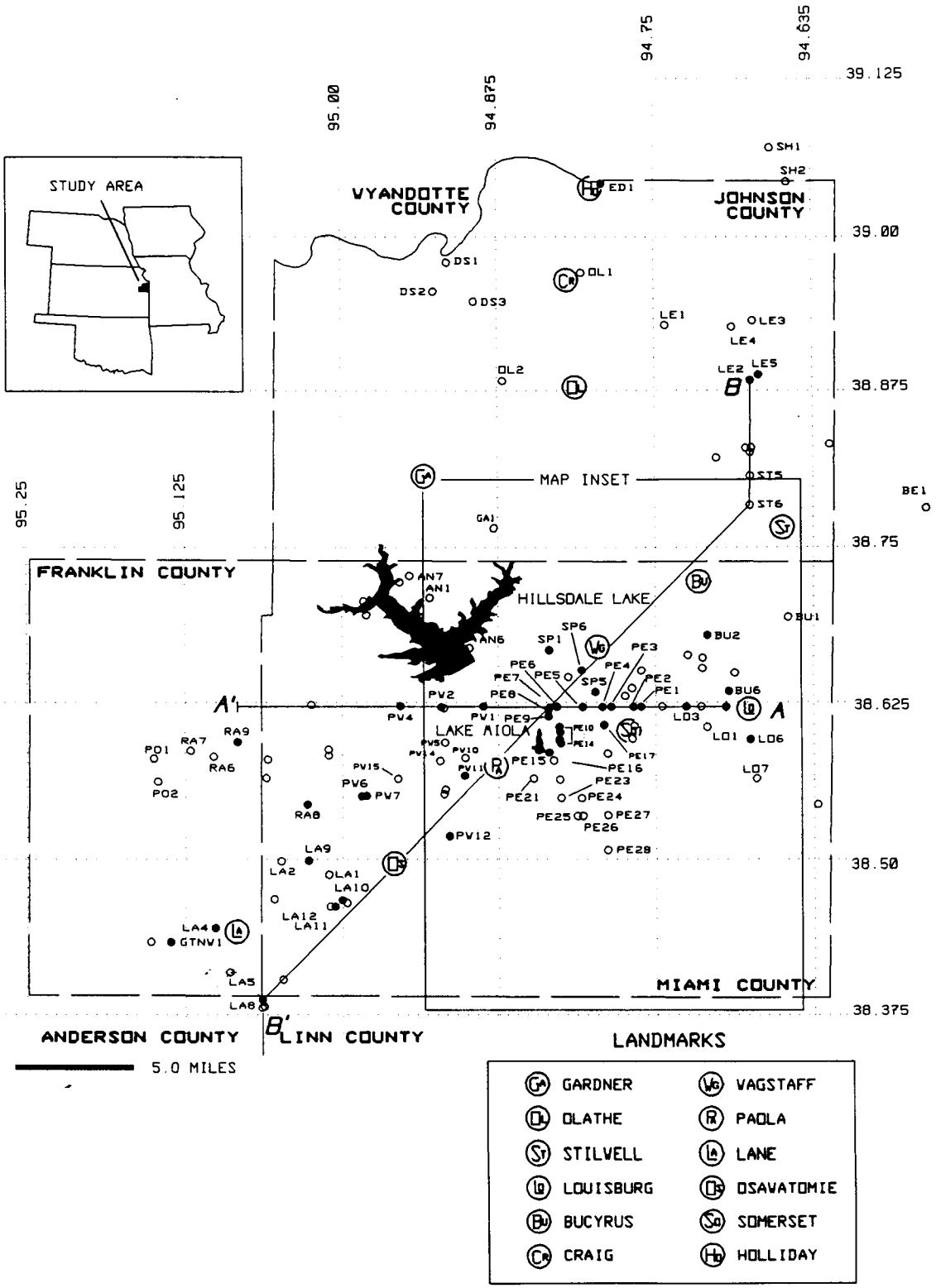
STUDY AREA
WYANDOTTE COUNTY
JOHNSON COUNTY
FRANKLIN COUNTY
MIAMI COUNTY
ANDERSON COUNTY
LINN COUNTY
MAP INSET
HILLSDALE LAKE
LAKE MIOLA
94.75
94.635
95.00
94.875
95.25
95.125
39.125
39.00
38.875
38.75
38.625
38.50
38.375
5.0 MILES
LANDMARKS
GARDNER
OLATHE
STILWELL
LOUISBURG
BUCYRUS
CRAIG
VAGSTAFF
PAOLA
LANE
OSAWATOMIE
SOMERSET
HOLLIDAY

Figure 2.2. General reference section, Wyandotte Limestone. Generalized section is typical of Johnson County exposures. The Wyandotte is seen fully exposed only at one locality in Miami County (SP5). Note that this figure includes the revised correlation of HECKEL (in review), which revives the name Liberty Memorial for sub-Wyandotte clastics (previously miscorrelated with the Lane Shale in the Kansas City area), and incorporates the Island Creek Shale, Farley Limestone (both previously Wyandotte members), and Bonner Springs Shale as members of the Lane Shale. The division of the Farley Limestone into two limestones and an intervening shale bed is best exposed in northern Johnson County, and is not seen in Miami County.

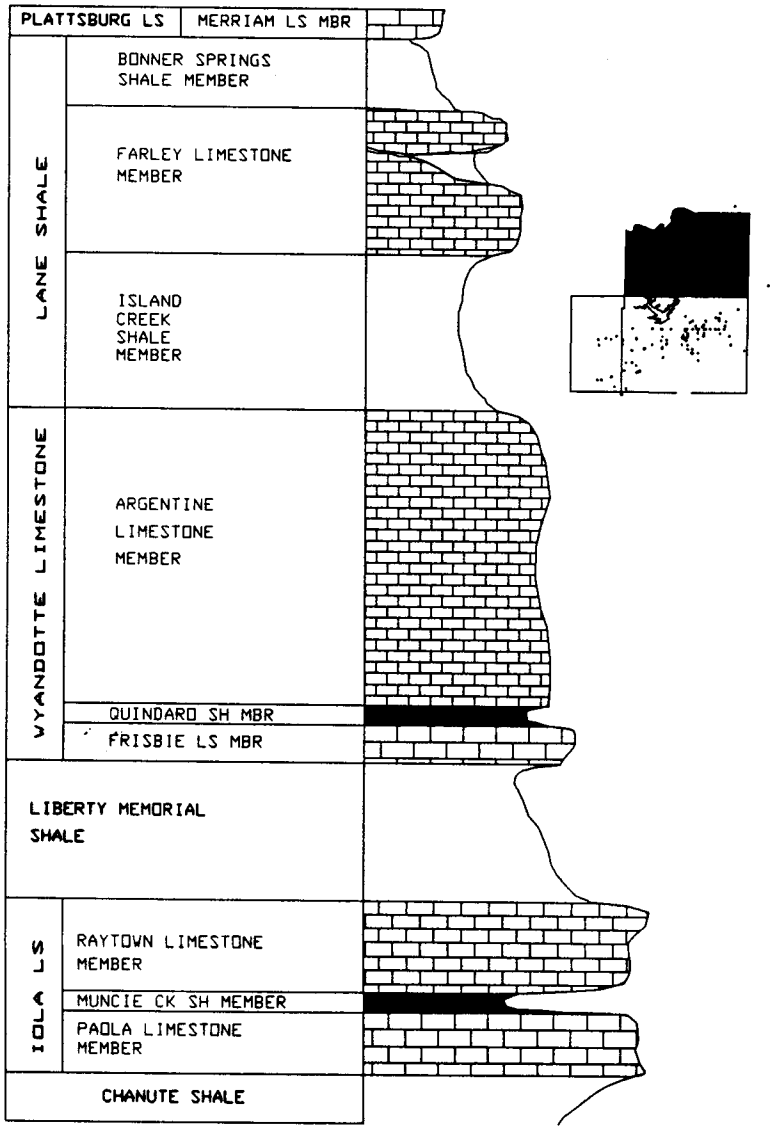

Figure 2.3. Measured section at locality PE15, U.S. Highway 169-K7, just east of Lake Miola, Miami County (C 11 T16S R23E). Lower part of Liberty Memorial Shale section is covered. A slightly greater thickness of Liberty Memorial (38 feet) was measured by NEWELL (1935) immediately to the east at PE16. Note that the Frisbie Limestone is absent, and the Quindaro Shale is identified by conodont faunas. The Argentine Limestone still contains abundant phylloid algal debris, and this locality marks the southwestern margin of phylloid algal mounds within this unit.

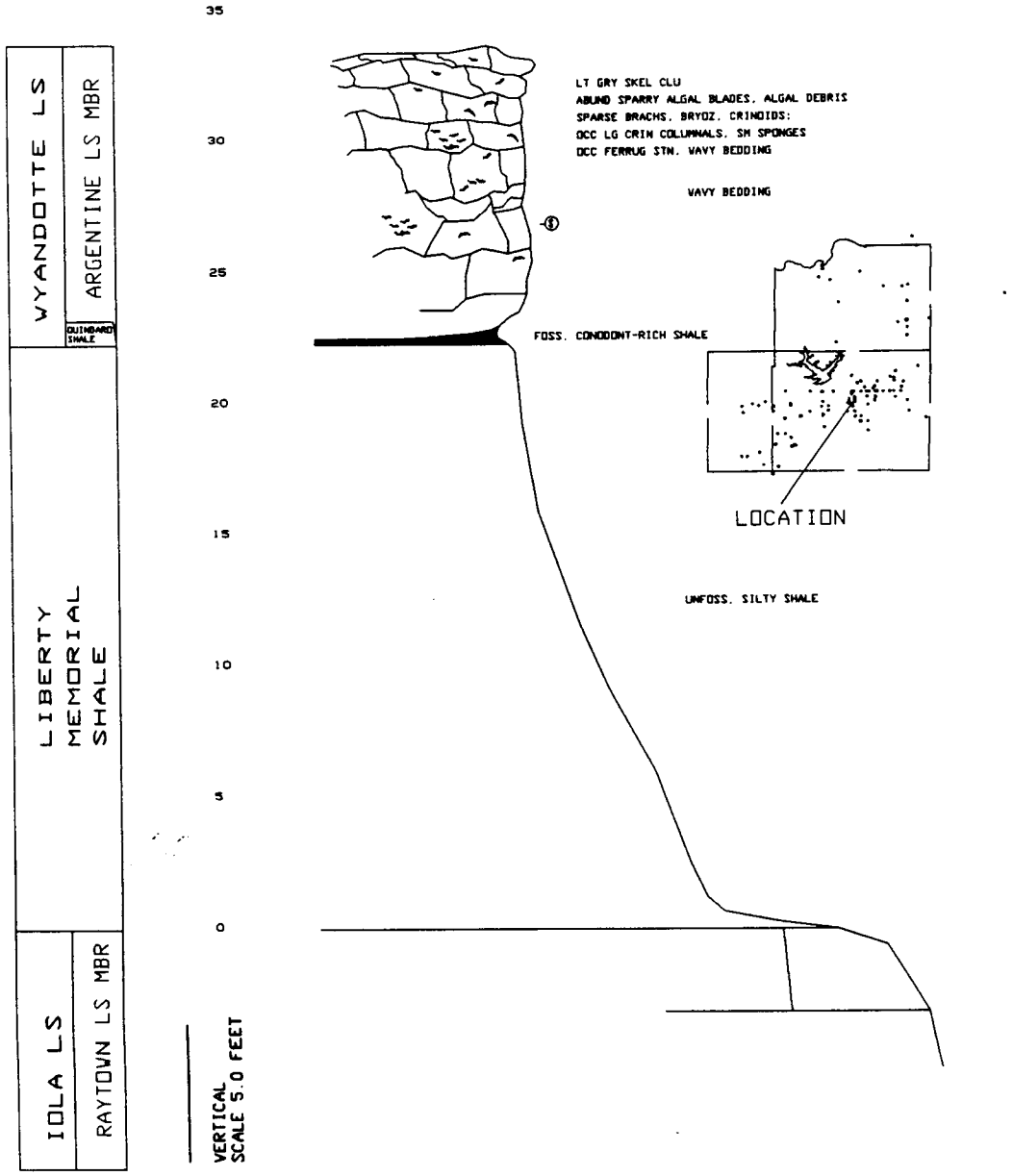

Figure 2.4. U.S. Highway 169-K7 roadcut exposure at locality PE15, Lake Miola, Miami County (C 11 T16S R23E). Argentine Limestone exposed over Liberty Memorial Shale (Quindaro Shale is thin and largely covered, Frisbie Limestone is absent). Note wavy, medium-bedded character of phylloid algal wackestone facies typical of the Argentine in eastern Miami County.

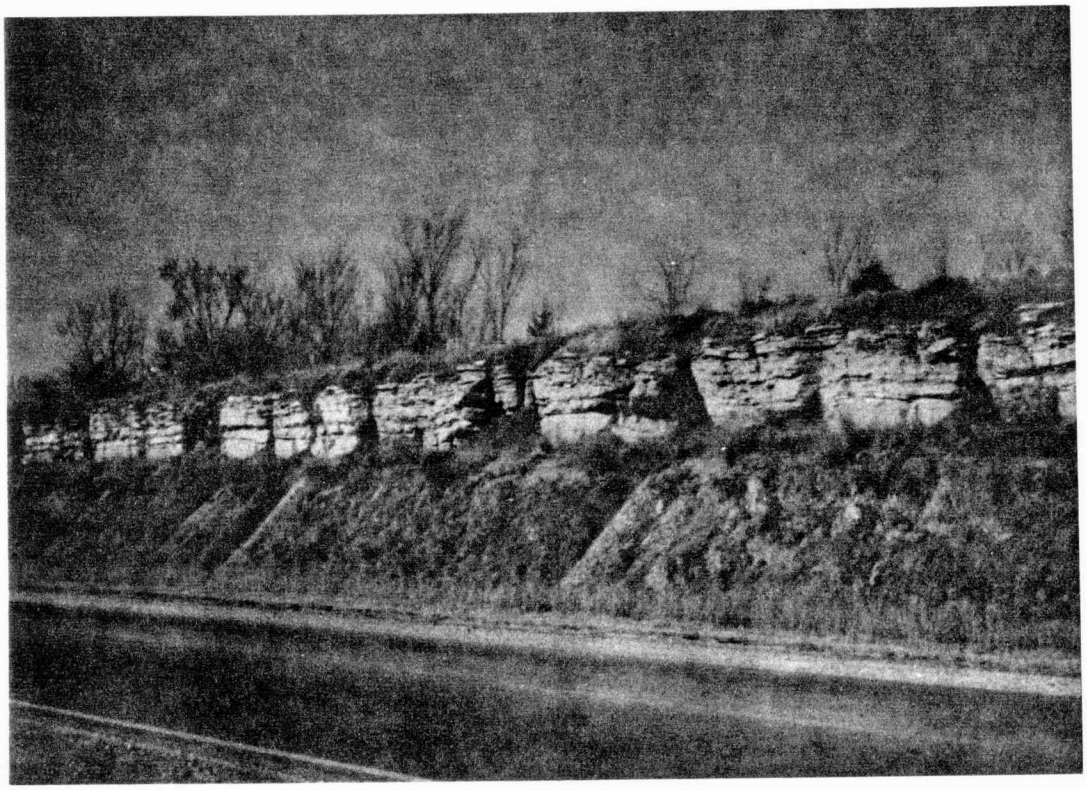

Figure 2.5. Measured section at locality PW11, quarry exposure west of Paola, Miami County (C SW SE SE 18 T17S R23E). Note six foot section of thickly bedded Argentine over Liberty Memorial Shale. Quindaro Shale identified through conodont faunas reported by MITCHELL (1981), Frisbie Limestone is absent. Contact with overlying type Lane Shale is covered.

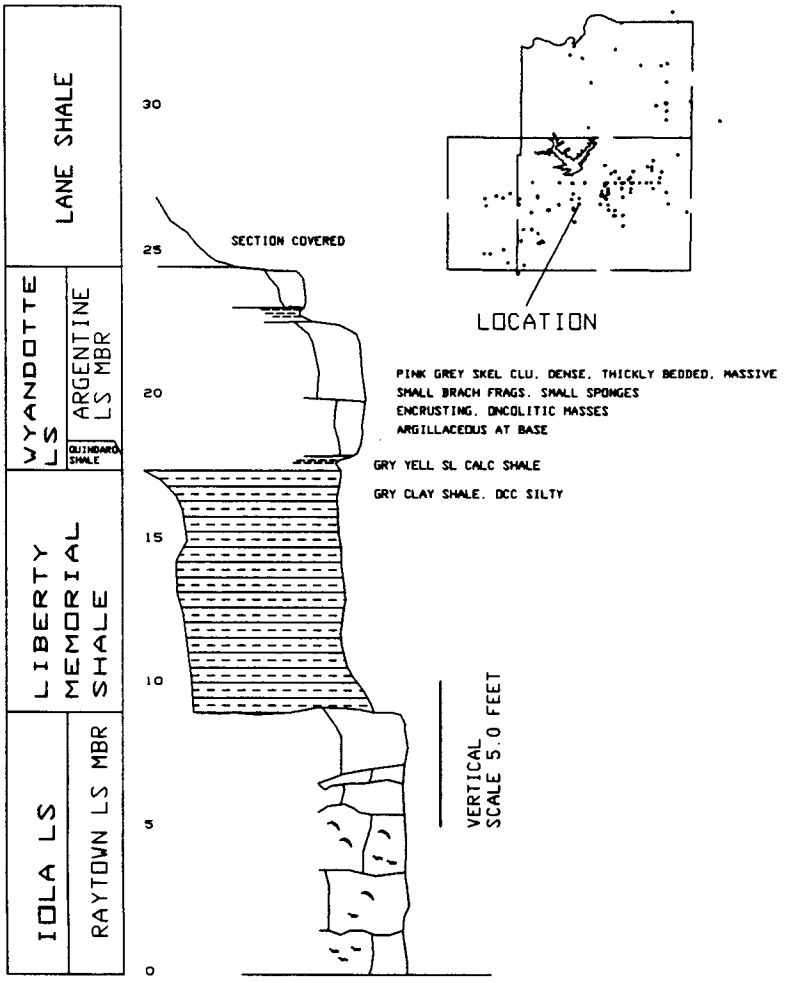

Figure 2.6. Quarry exposure at locality PW11, west of Paola, Miami County (C SW SE SE 18 T17S R23E). Base of type Lane Creek Shale (LSh) at top, covered, over conspicuous bed of Argentine Limestone (Ag), recessed grey Liberty Memorial Shale (LMSh), and light grey Raytown Limestone (Rtn). Argentine Limestone here was mistakenly included as part of the Raytown by MILLER (1966) and MITCHELL (1981), although abundant conodonts, now recognized as identifying the Quindaro Shale, were reported from a fossiliferous shale horizon just below the basal Argentine ledge.

Figure 2.7. Composite measured section of Farley Limestone and Island Creek-Lane Shale (locality PE8) and Argentine Limestone (locality PE9), east and south, respectively, of intersection of Kansas State Highway K68 and U.S. Highway 169-K7, Miami County (W/2 NW NE 35 T16S R23E and C 35 T16S R23E, respectively).

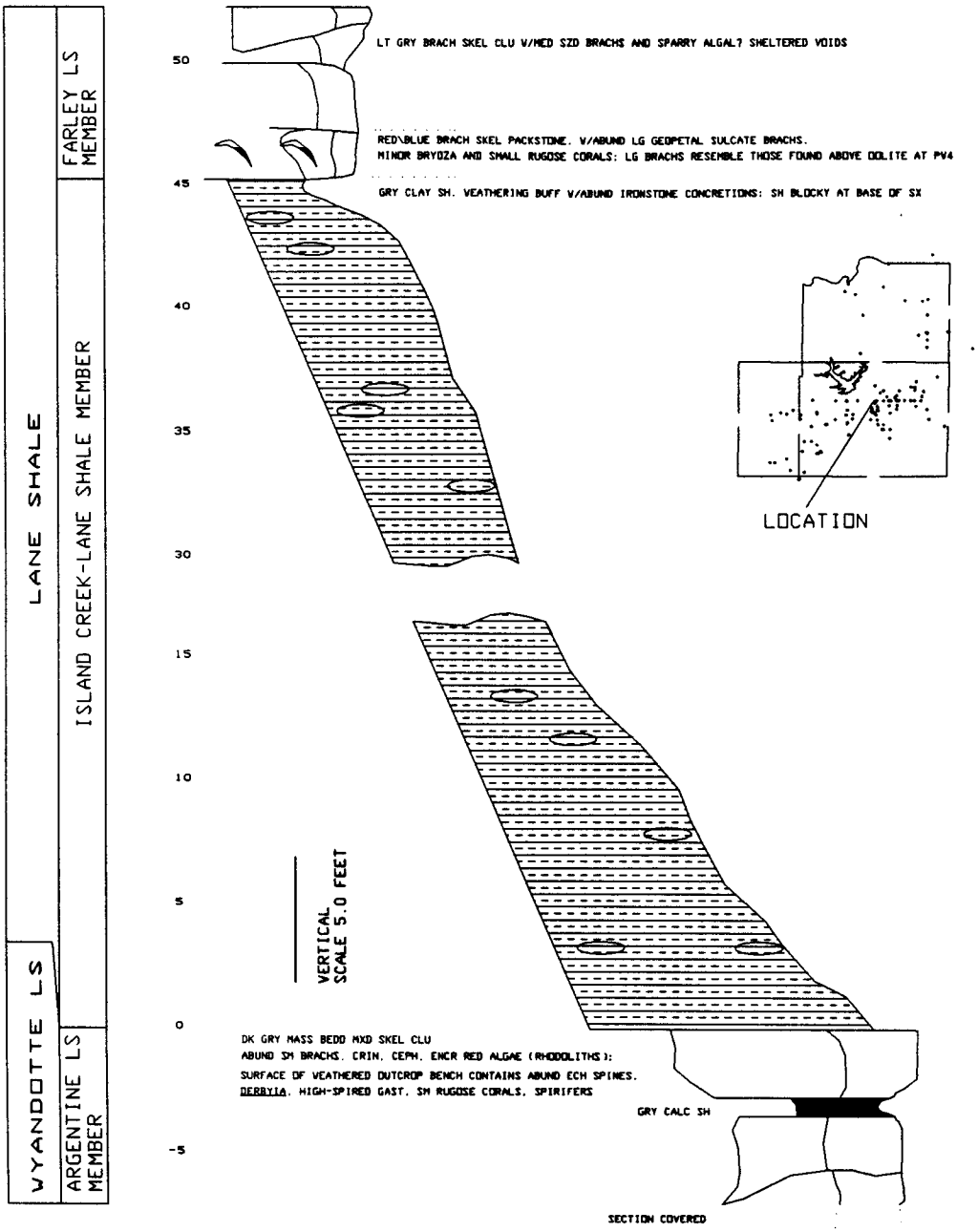

Figure 2.8. Roadcut exposure of top of Argentine Limestone at locality PE9, Miami County (C 35 T16S R23E). Thick bedding, onkoid structures, and bands of Fe staining are identical to the Argentine at quarry west of Paola (locality PW11; see Figures 2.5 and 2.6).

Figure 2.9. Composite measured section at localities LA10 (Raytown, Argentine) and LA11 (Farley), southwest of Osawatomie, Miami County (C NW SE 20 T18S R22E and C SL W/2 20 T18S R22E, respectively). Upper contact of type Lane Shale and basal Farley Limestone is covered. Lower section (Raytown through Argentine) exposed in working quarry. Fissile, black shale of the Muncie Creek Member, Iola Limestone is locally exposed on quarry floor. The thin shale exposed in the upper Argentine section is also seen at PW11 and PE9, and the overall lithology of the Argentine is identical as well.

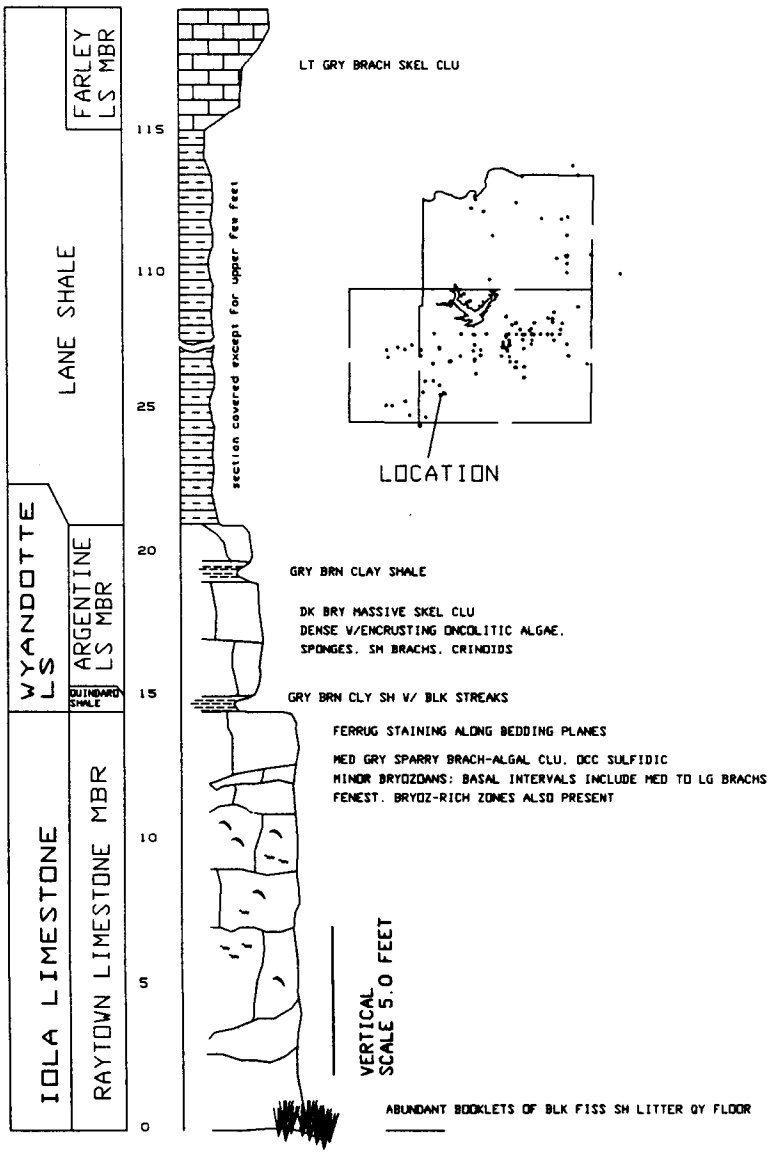

Figure 2.10. Argentine Limestone at LA10, SW of Osawatomie, Miami County (C NW SE 20 T18S R22E). **TOP:** Quarry exposure of Argentine (Ag) over Raytown Limestone (Rtn), separated by Quindaro Shale (reentrant at Qu above five foot staff). Frisbie Limestone and Liberty Memorial Shale are essentially absent. Argentine contact with overlying Lane Shale is covered. **BOTTOM:** Detail showing onkoid structures and Fe staining of Argentine, identical to PE9 and PW11.

Figure 2.11. Measured section at SP5, quarry south of Wagstaff, Miami County (W/2 NW NE 30 T16S R24E). This is the most complete exposure of the Wyandotte at a single locality in Miami County. Thickened Frisbie Limestone represents carbonate-mud-rich algal mound, the base of which is not exposed. Note increase in argillaceous material towards top of Argentine section.

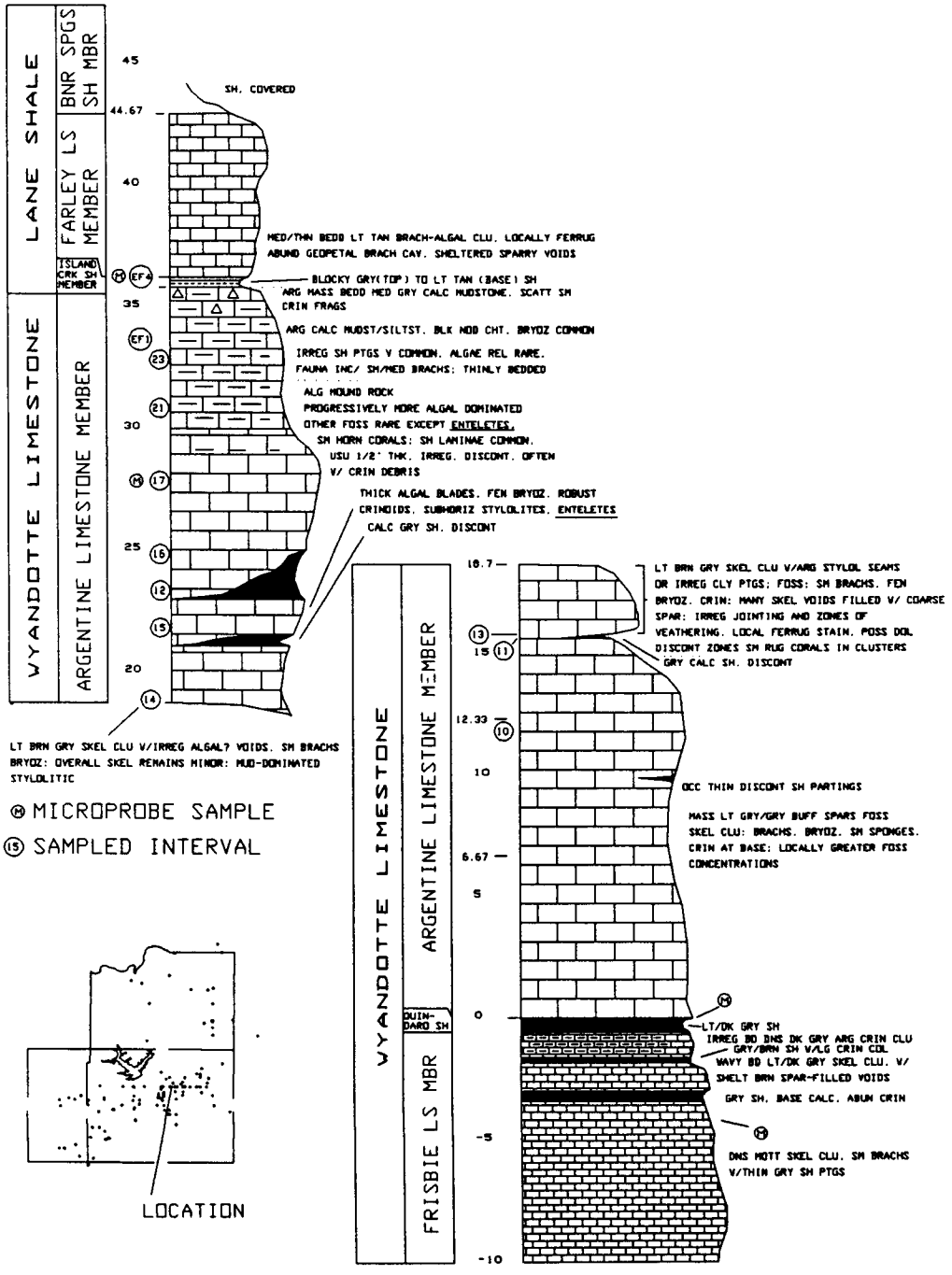

Figure 2.12. Wyandotte exposure at SP5 quarry, Miami County (W/2 NW NE 30 T16S R24E). Basal Frisbie Limestone (Fb; note thickness) is characterized by shale interbeds, and is separated from overlying, light grey Argentine Limestone (Ag) by thin, conodont-rich Quindaro Shale (Qu). Top of exposed section consists of more thinly bedded, Fe-stained Farley Limestone (Fa), separated from the Argentine by thin Island Creek-Lane Shale (IC). Quindaro and Island Creek-Lane Shales are well-exposed but too thin to be visible from this distance. Total exposed thickness is approximately 45 feet. Section is dipping slightly to the left of the photo (NW).

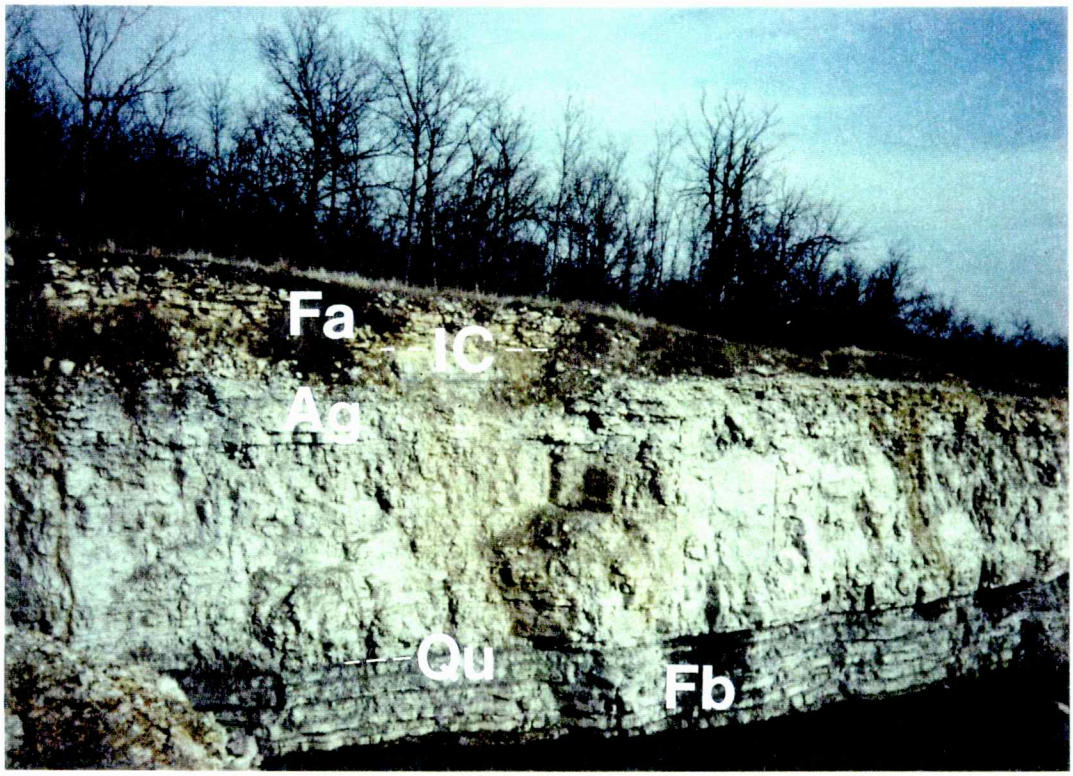

Figure 2.13. Measured section of Farley Limestone at LA8, northwestern Linn County (C NW NW 23 T19S R21E). Circles are sample points. Basal Farley is characterized by thin, discontinuous, shale partings, and an open marine fauna. Thick upper section is dominated by phylloid algae and small, spar-filled brachiopods (Enteletes). Although the underlying Lane Shale contact is not exposed, shale float probably belonging to the Lane is present on the quarry floor.

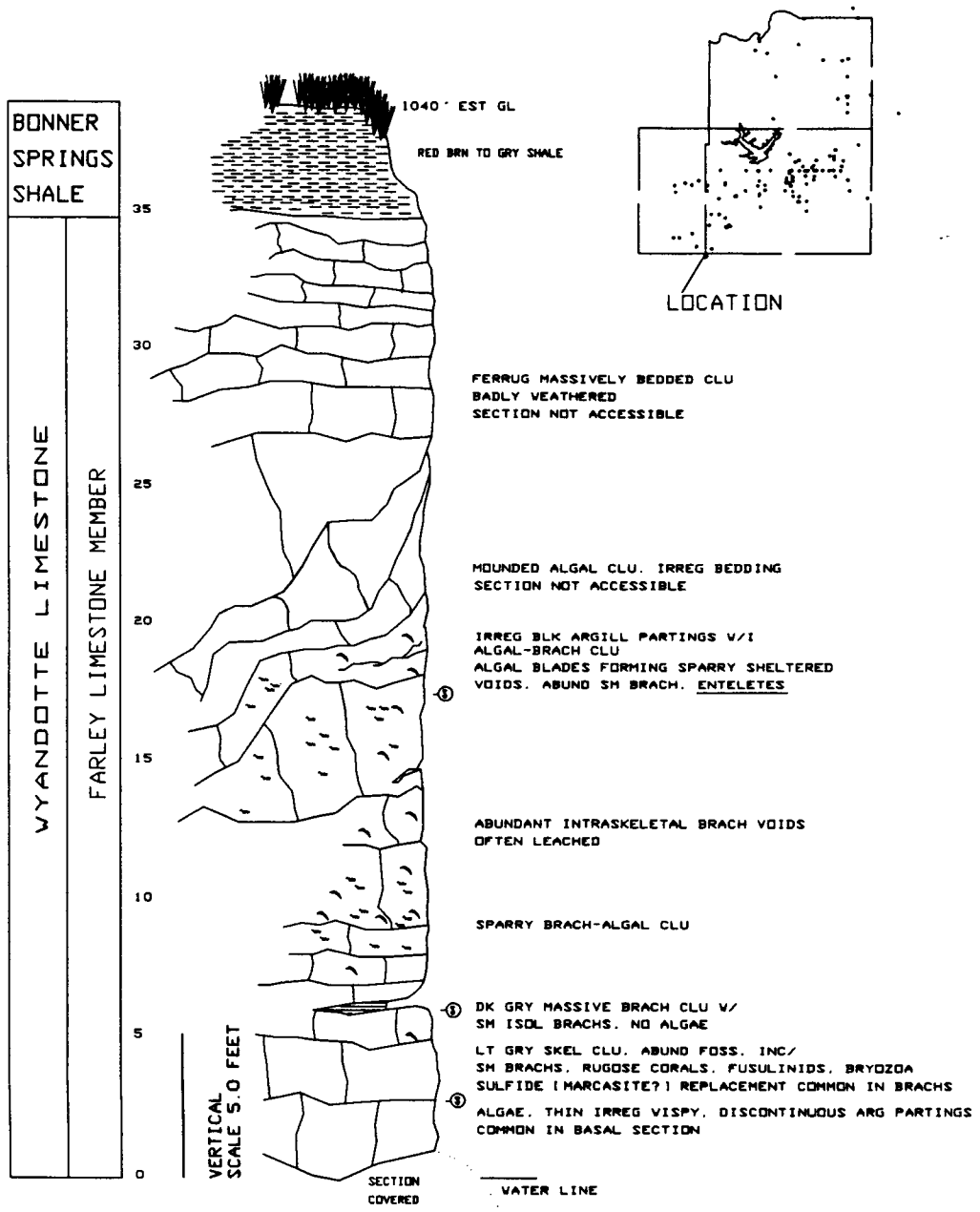

Figure 2.14. Farley Limestone quarry exposure at LA8, Linn County (C NW NW 23 T19S R21E). Note visible mound structures developed in algal-brachiopod calcilutite. Staff is 5 feet in length.

Figure 2.15. Roadcut exposure of lower Wyandotte section at LO1 just west of Louisburg, Miami County (SE corner, 30 T16S R25E). Basal Frisbie Limestone (Fb) and Quindaro Shale (Qu) are highly fossilferous. Overlying buff Argentine Limestone (Ag) is 20 feet thick here, and shows typical wavy-bedded aspect, with thin interbeds of nodular chert.

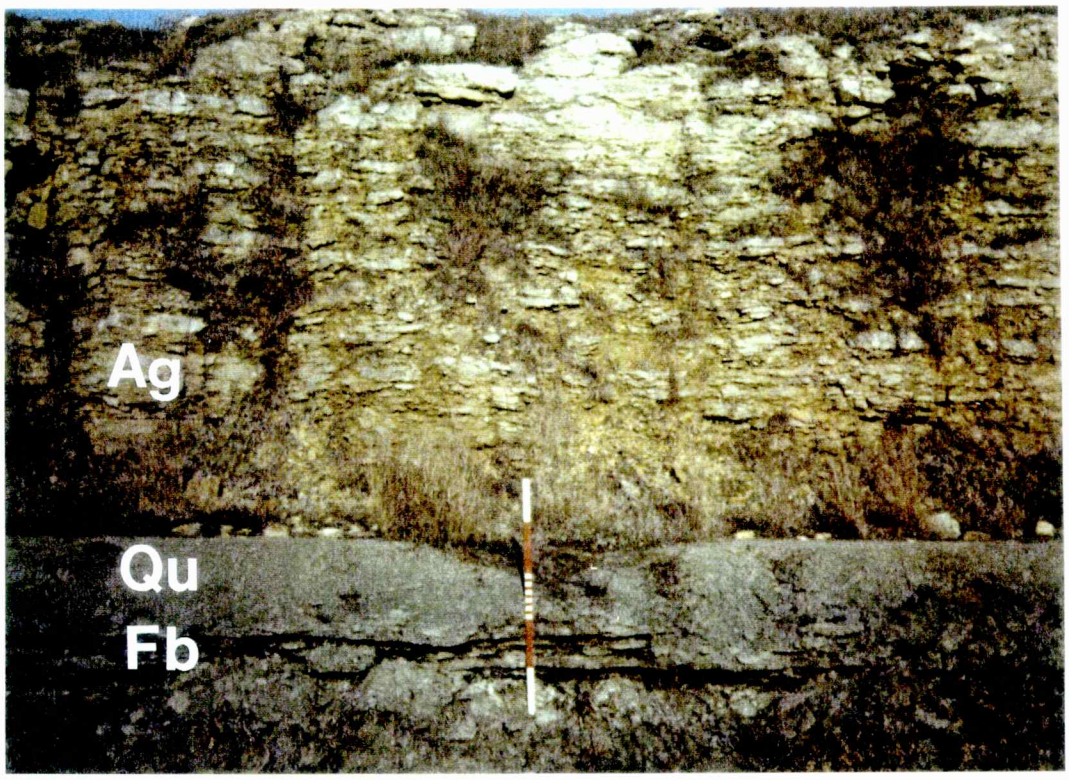

Figure 2.16. Roadcut exposure of Argentine Limestone at PW1, west of Bull Creek on State Highway K68, Miami County (C SL SE 29 T17S R22E). Argentine (Ag) is separated from the underlying Raytown Limestone (Rtn) by conodont-rich Quindaro Shale (Qu). The Liberty Memorial Shale is essentially absent by pinch out.

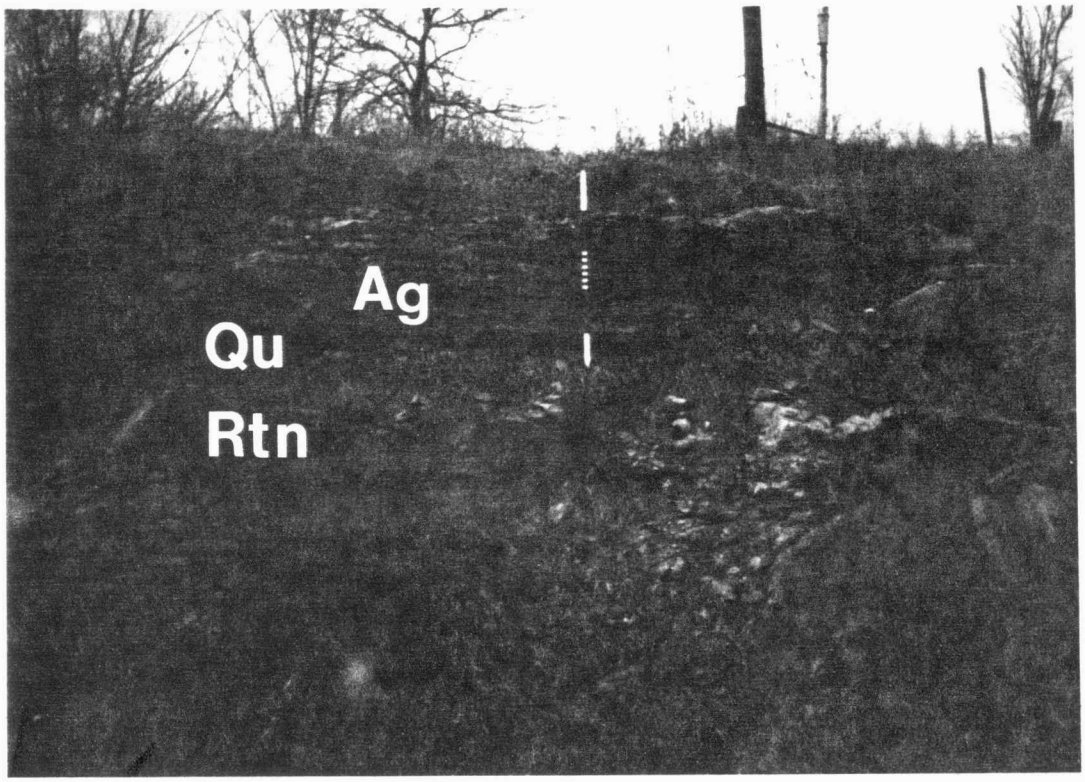

Figure 2.17. Roadcut exposure of Farley Limestone at RA9, Franklin County (WL NW NW 10 T17S R21E). This outcrop of algal-brachiopod calcilutite is sandy at the base where it overlies the Lane Shale, and is typical of the Farley in much of western Miami and eastern Franklin County. Limestone bedding is enhanced by horizons of solution cavities (SC).

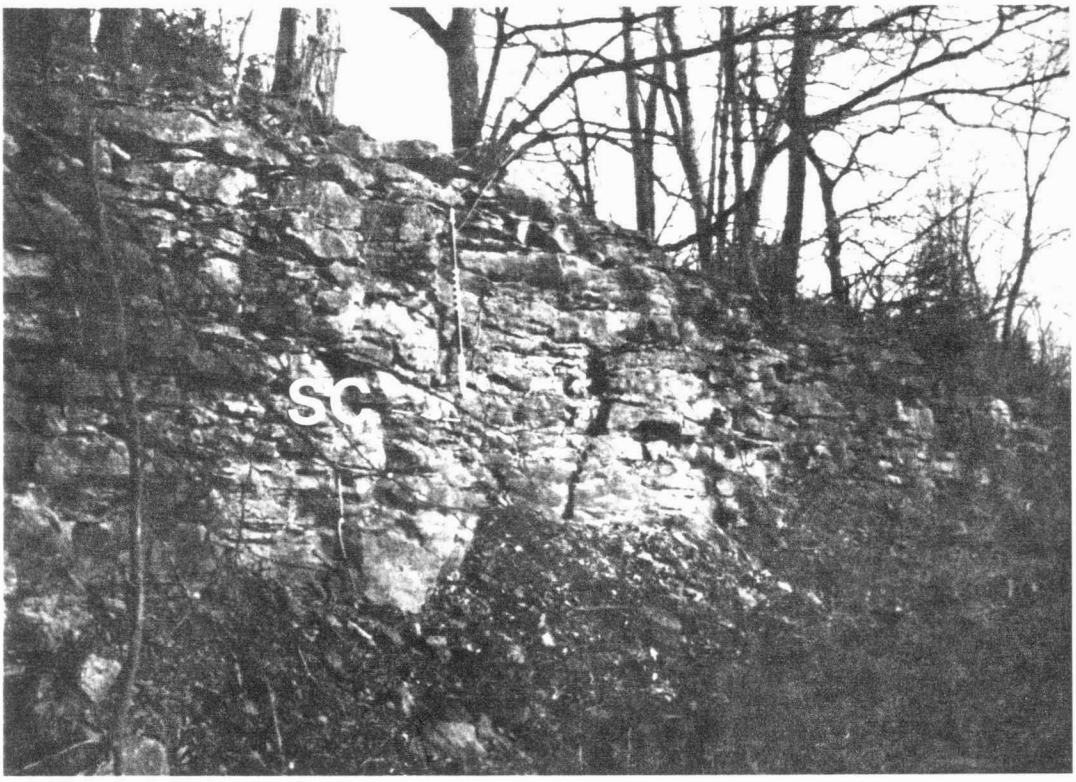

Figure 2.18. Isopach map, Liberty Memorial Shale. Measured thicknesses at data points are given in feet. Note variable contour interval. "INTERBANK AREA" and "LANE SHOAL" refer to features described by CROWLEY (1969).

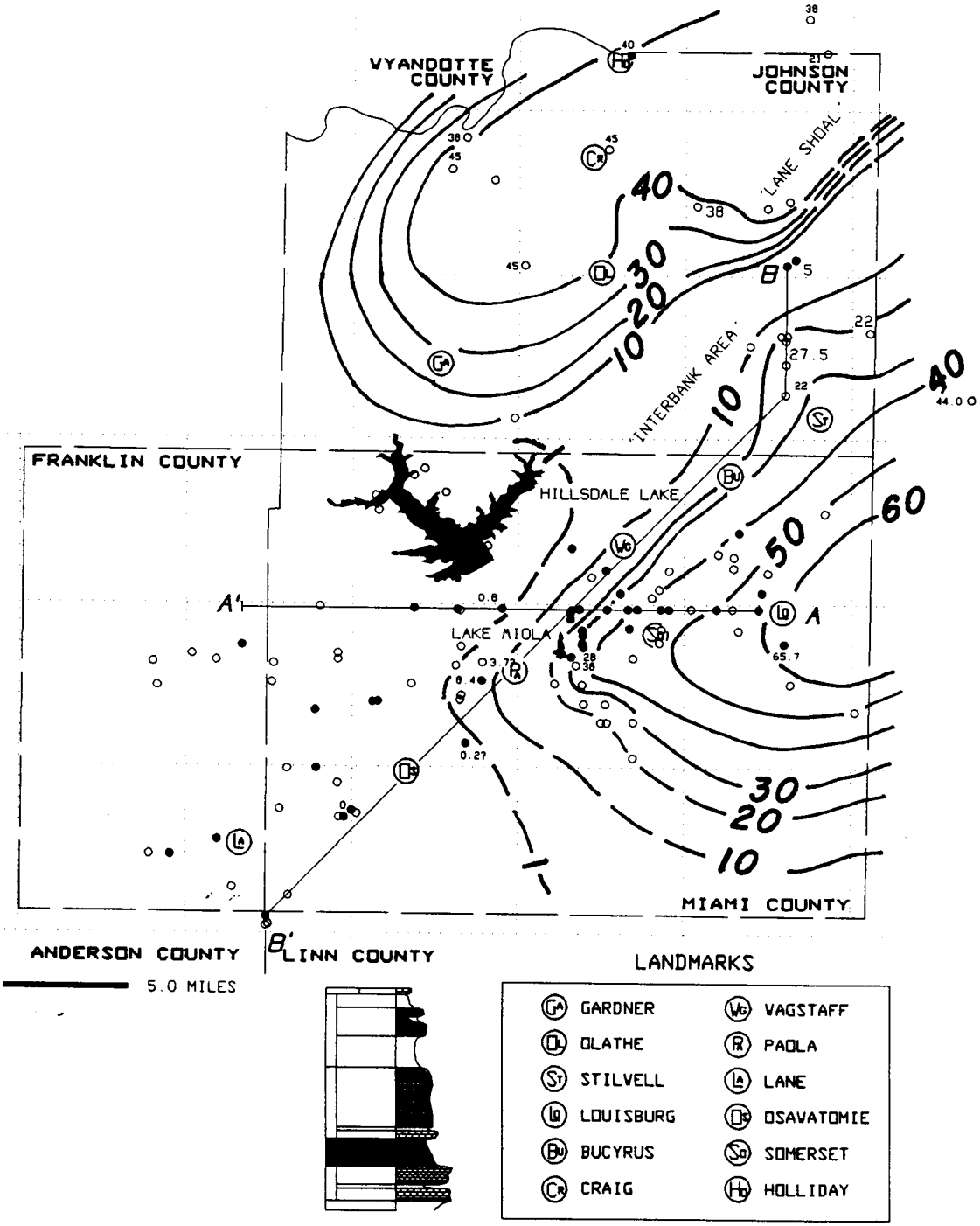

Figure 2.19. Isopach map, Frisbie Limestone. Measured thicknesses at data points are given in feet. Contour interval 5 feet.

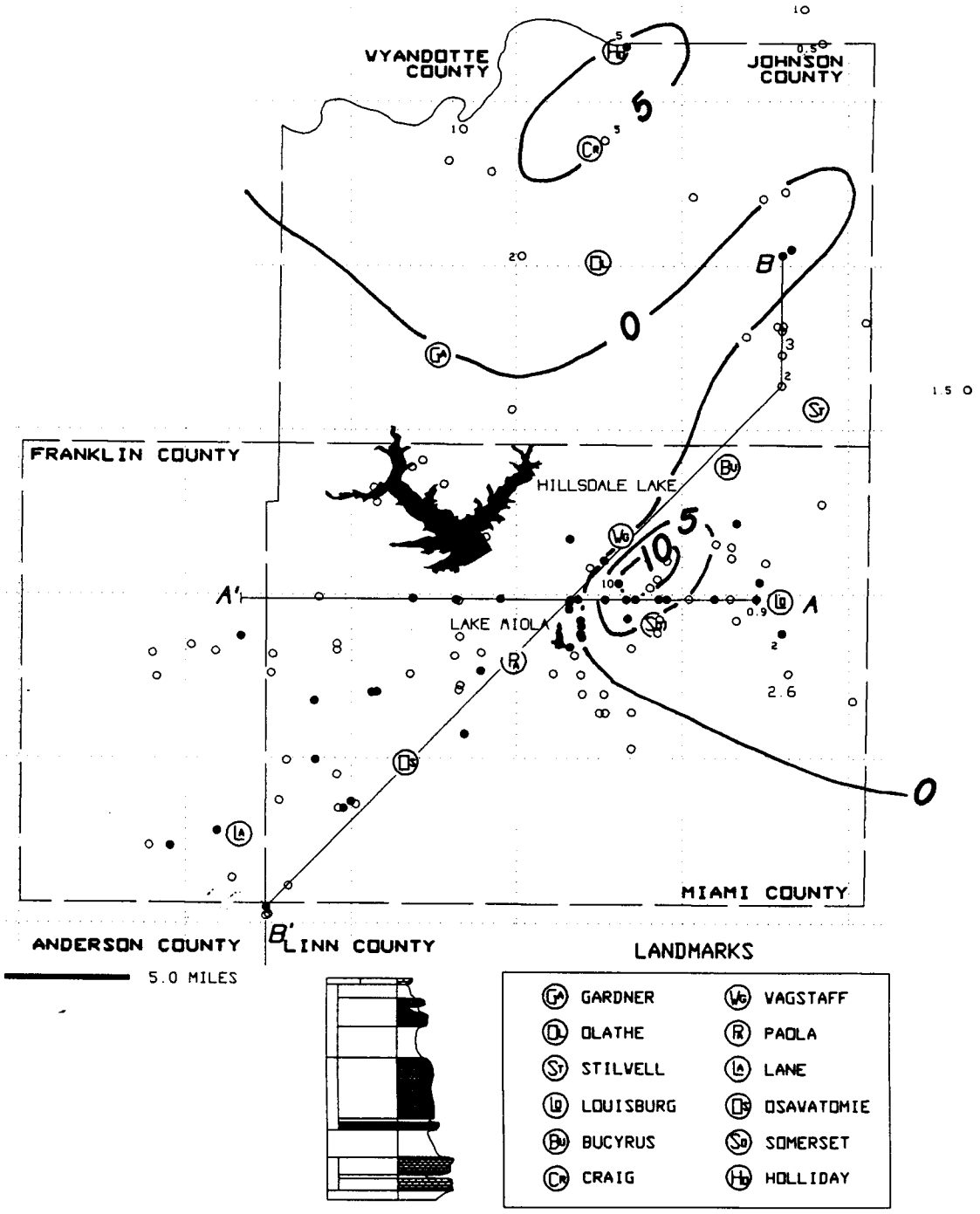

Figure 2.20. Isopach map, Quindaro Shale. Measured thicknesses at data points are given in feet.

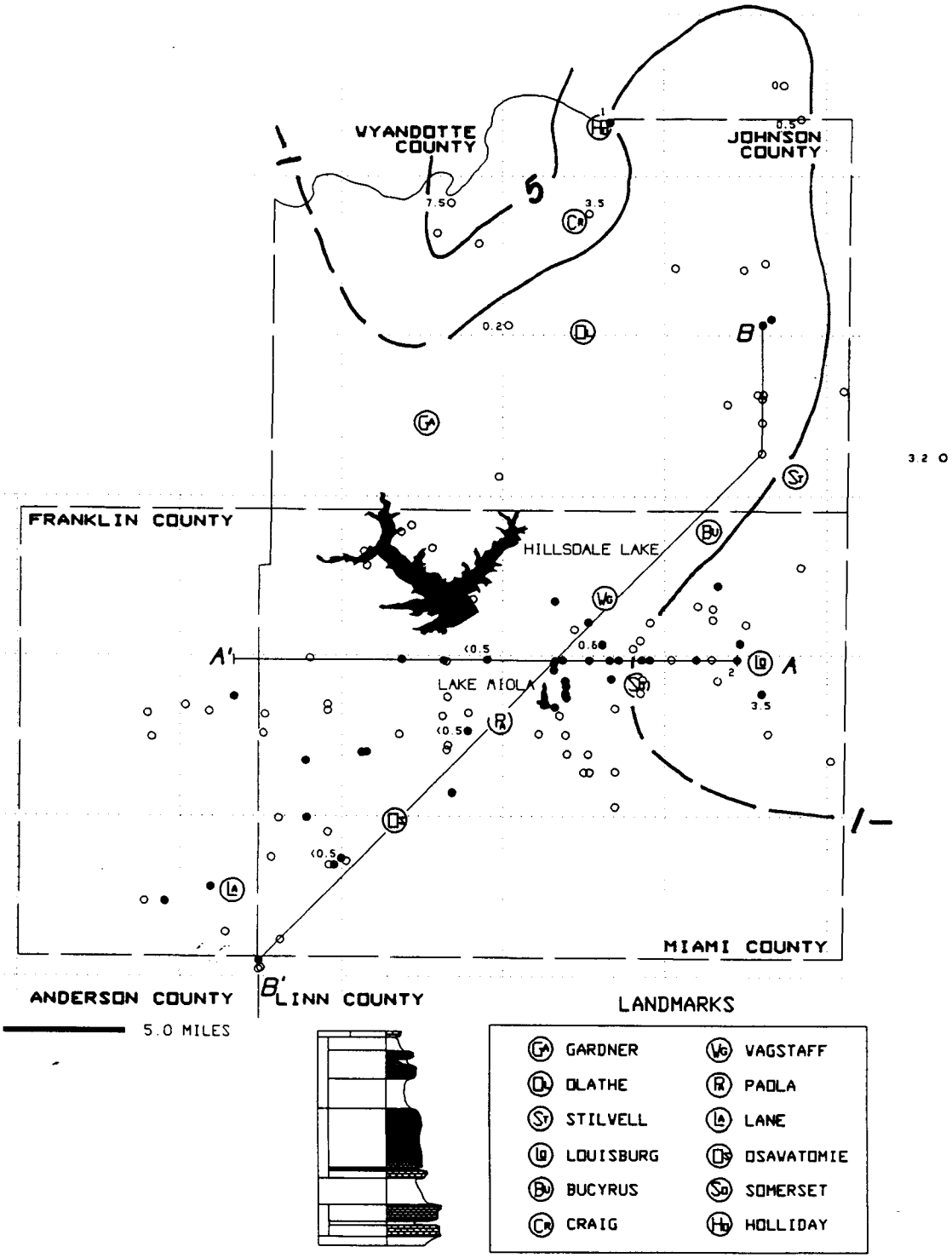

Figure 2.21. Isopach map, Argentine Limestone. Measured thicknesses at data points are given in feet. Note variable contour interval.

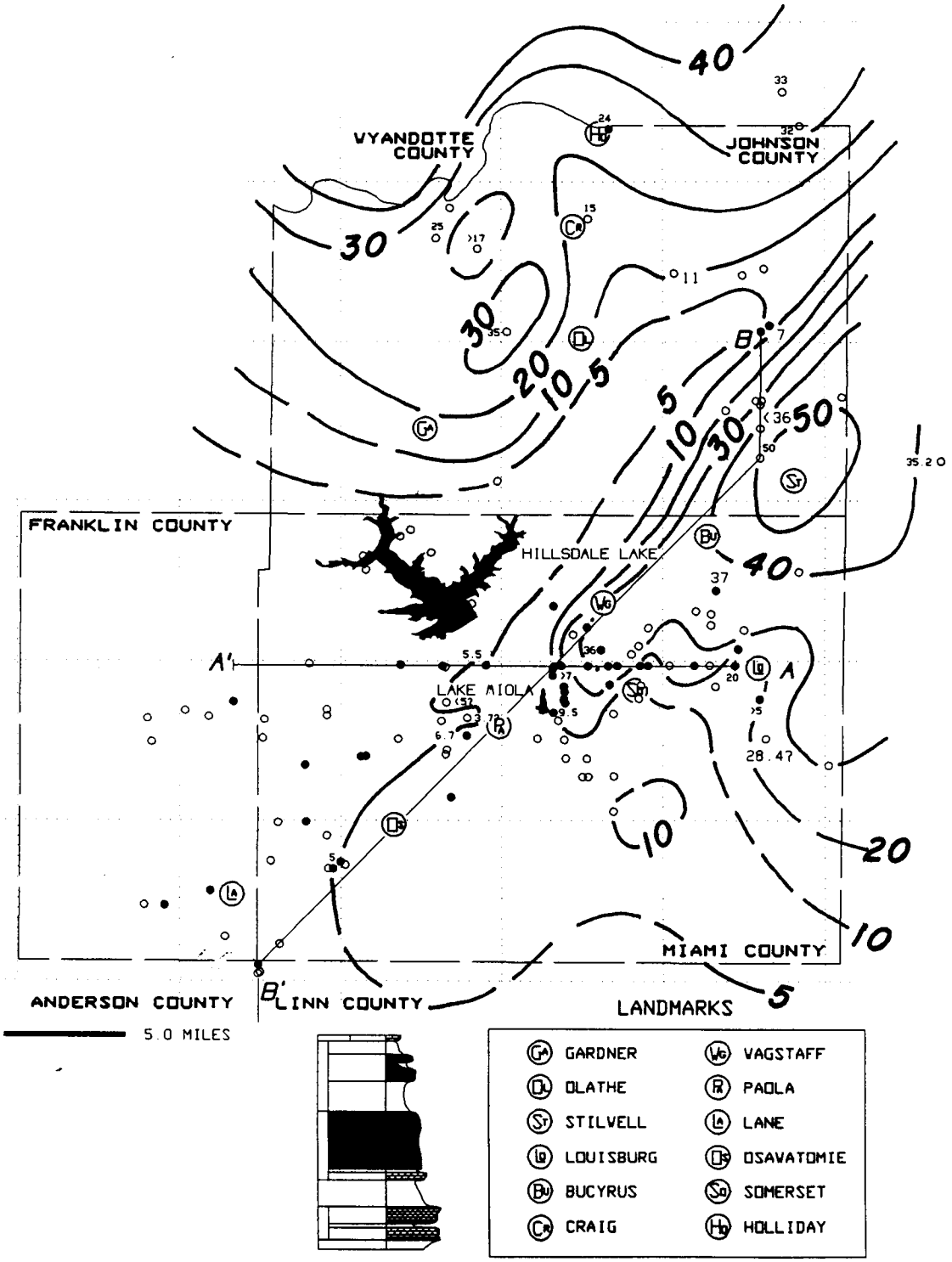

Figure 2.22. Isopach map, type Lane-Island Creek Shale. Measured thicknesses at data points are given in feet. Note variable contour interval.

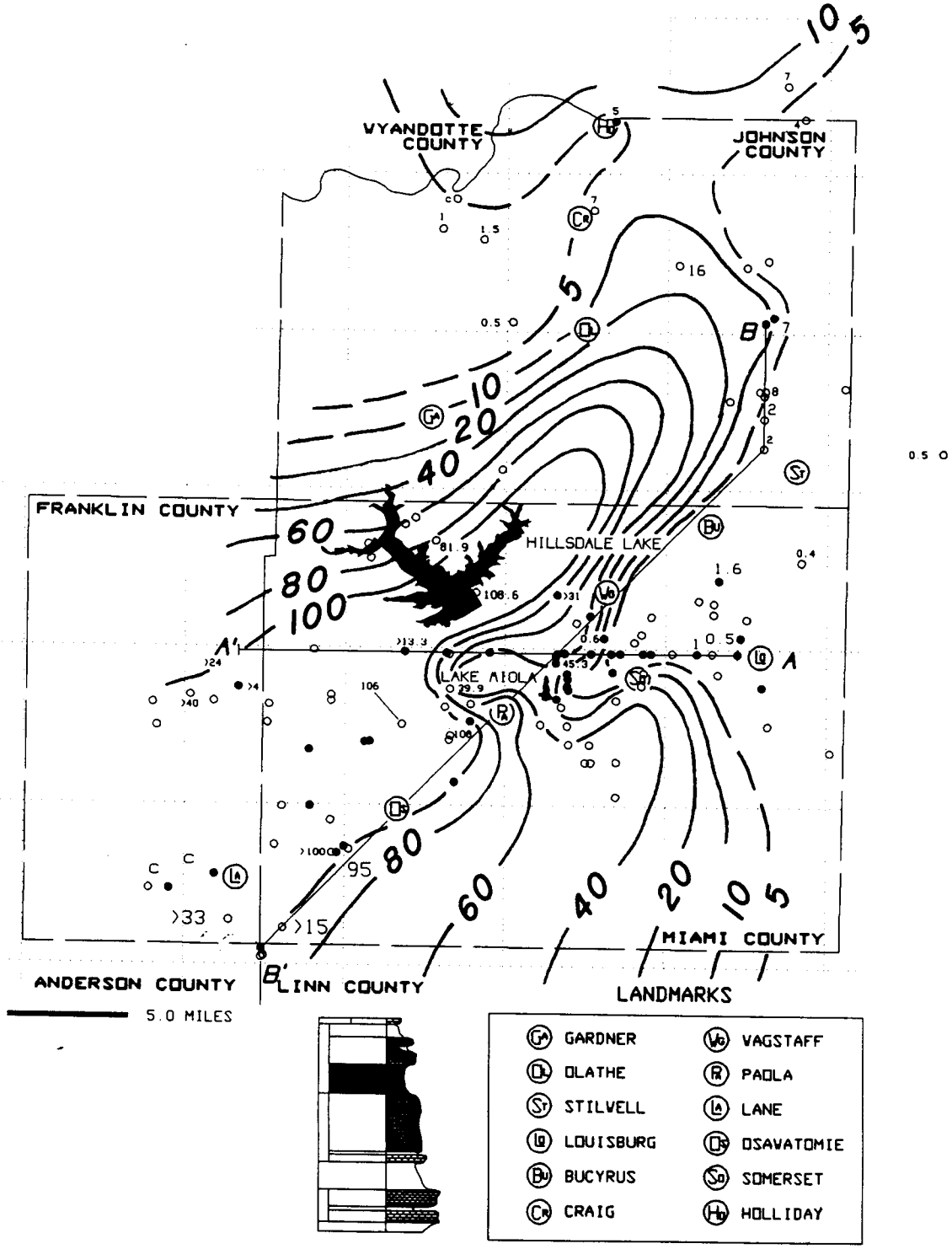

Figure 2.23. Isopach map, Farley Limestone. Measured thicknesses at data points are given in feet. Note variable contour interval.

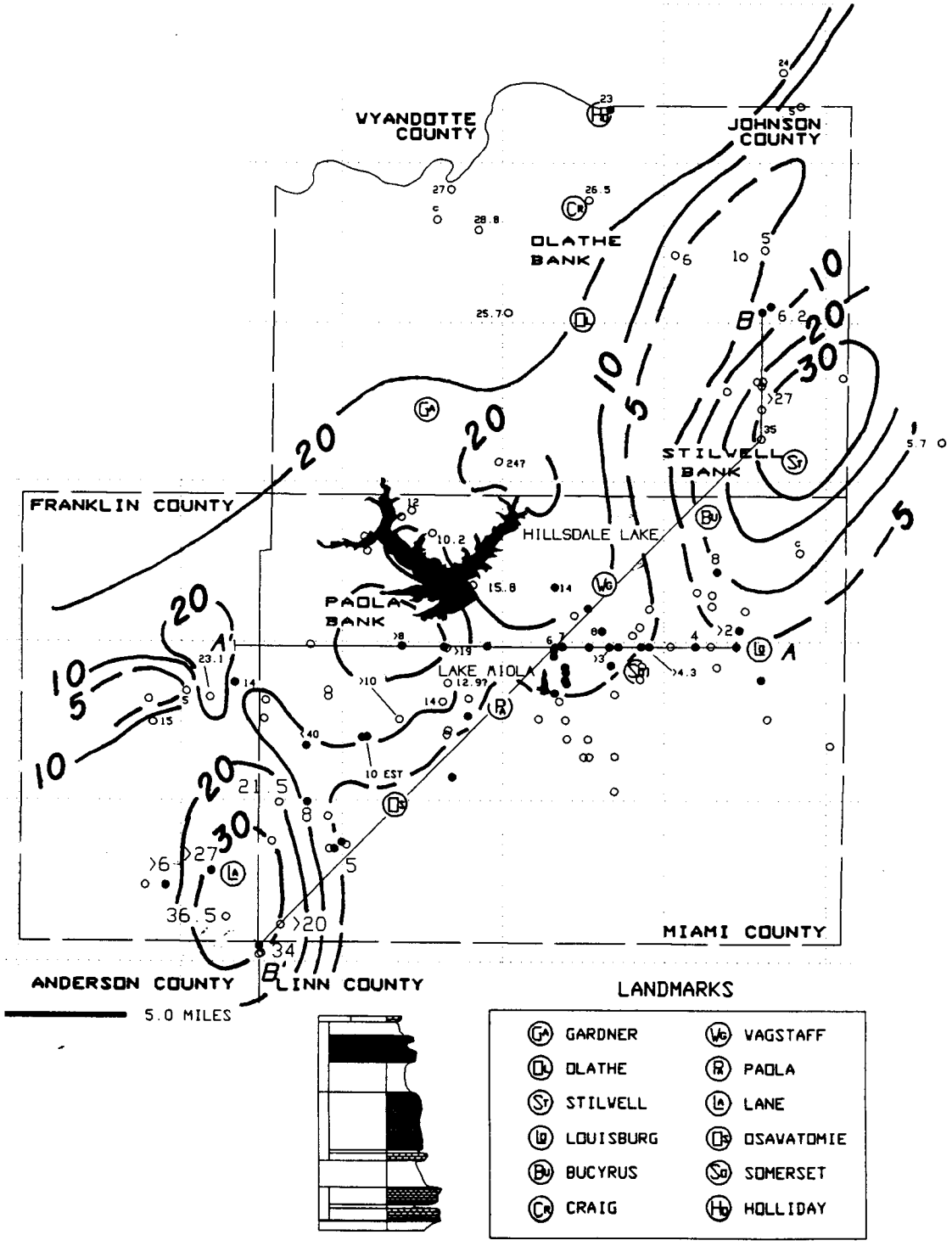

Figure 2.24. Stratigraphic cross section A-A'.

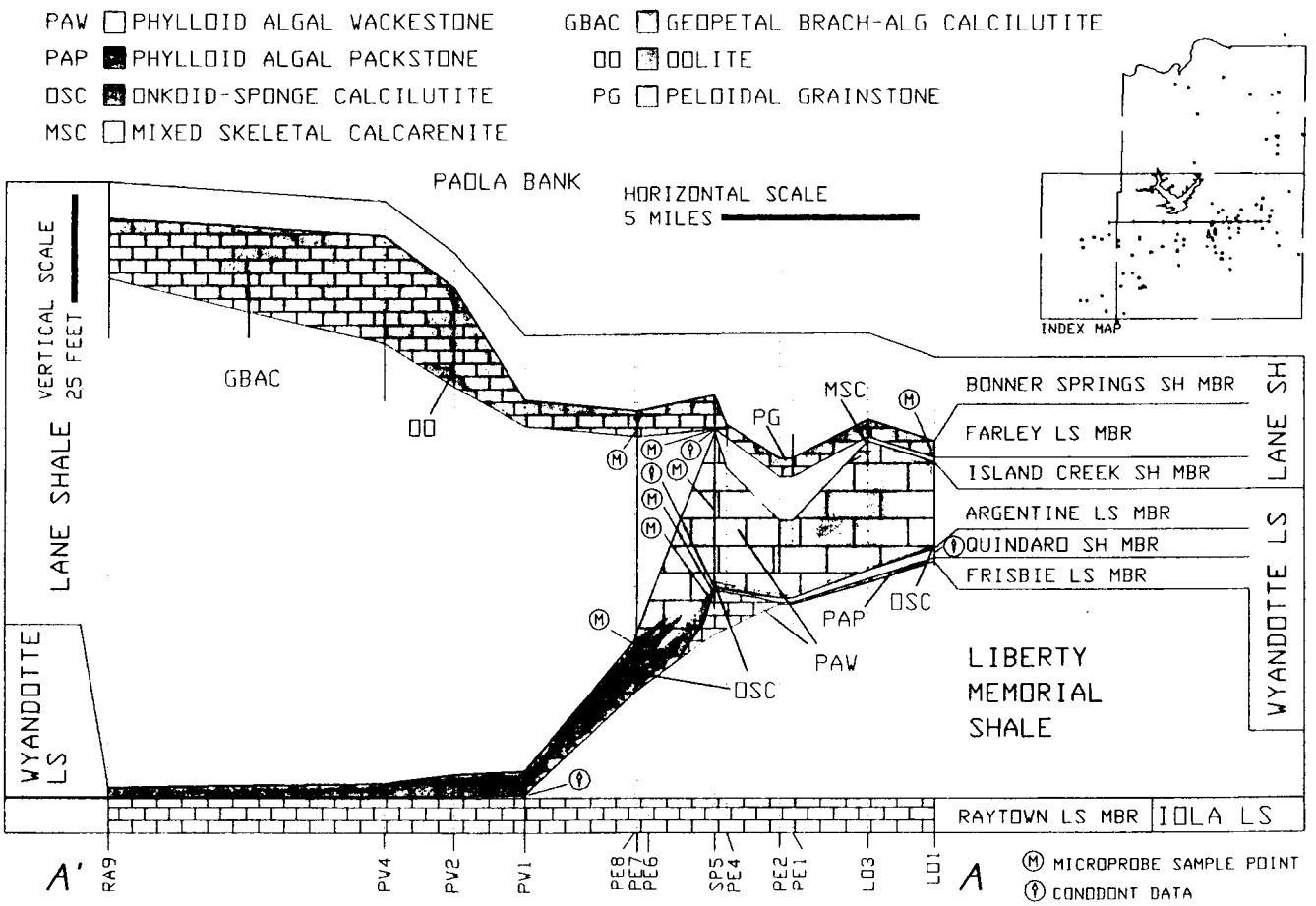

Figure 2.25. Stratigraphic cross section B-B'.

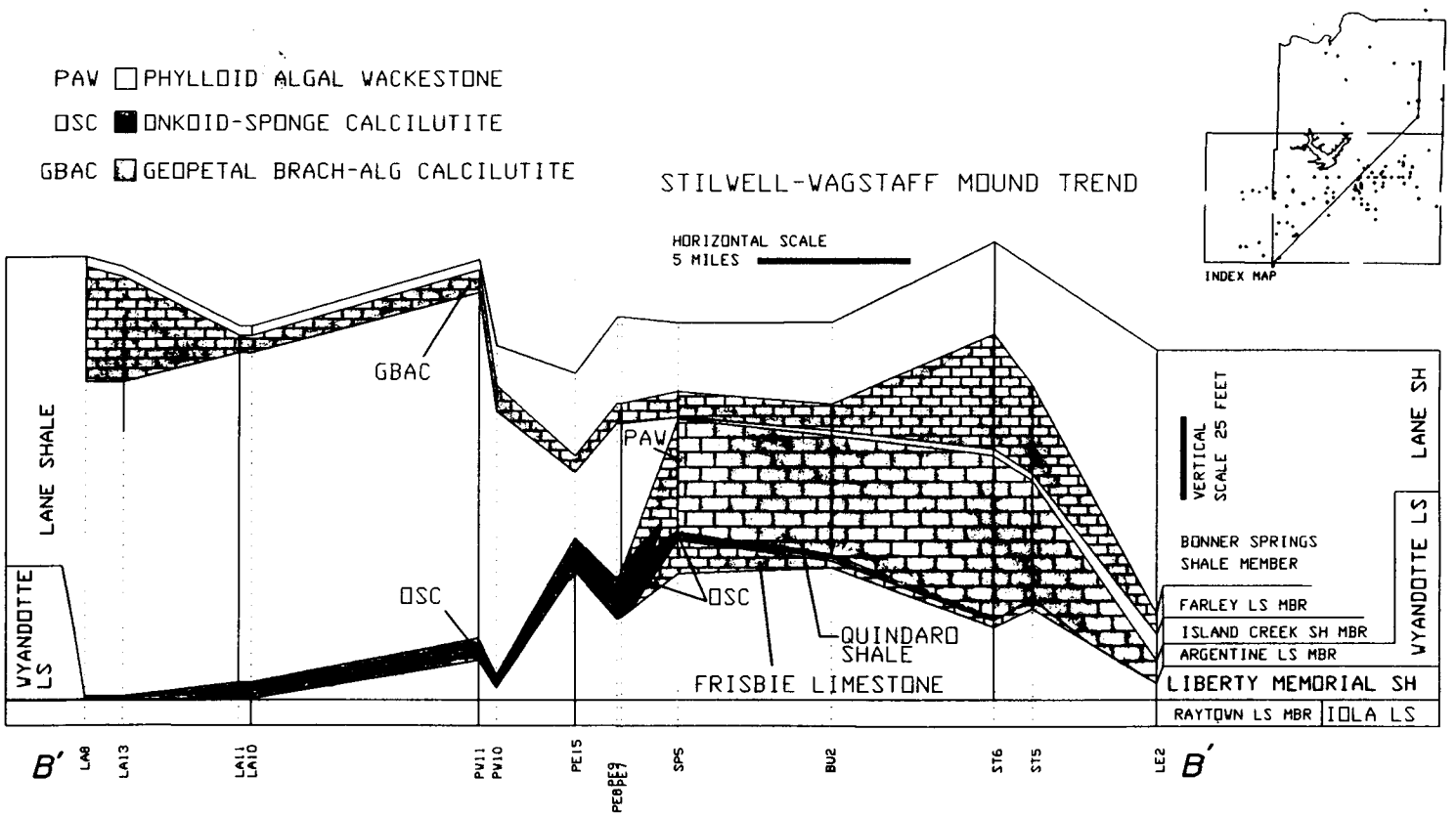

Figure 2.26. Detailed map of southern margin of Stilwell-Wagstaff algal mound trend, showing Argentine Limestone isopach, eastern Miami County. NW flank of mound is defined by trend of thin Argentine, connecting to the NE with the "interbank area" of CROWLEY (1969). Small sinus in mound flank NNE of Somerset honors the strike of a possible structural precursor to the post-depositional displacement observed in this area. Argentine is poorly exposed in the southern half of Paola East quadrangle, but earlier work (NEWELL, 1935) indicates probable outliers.

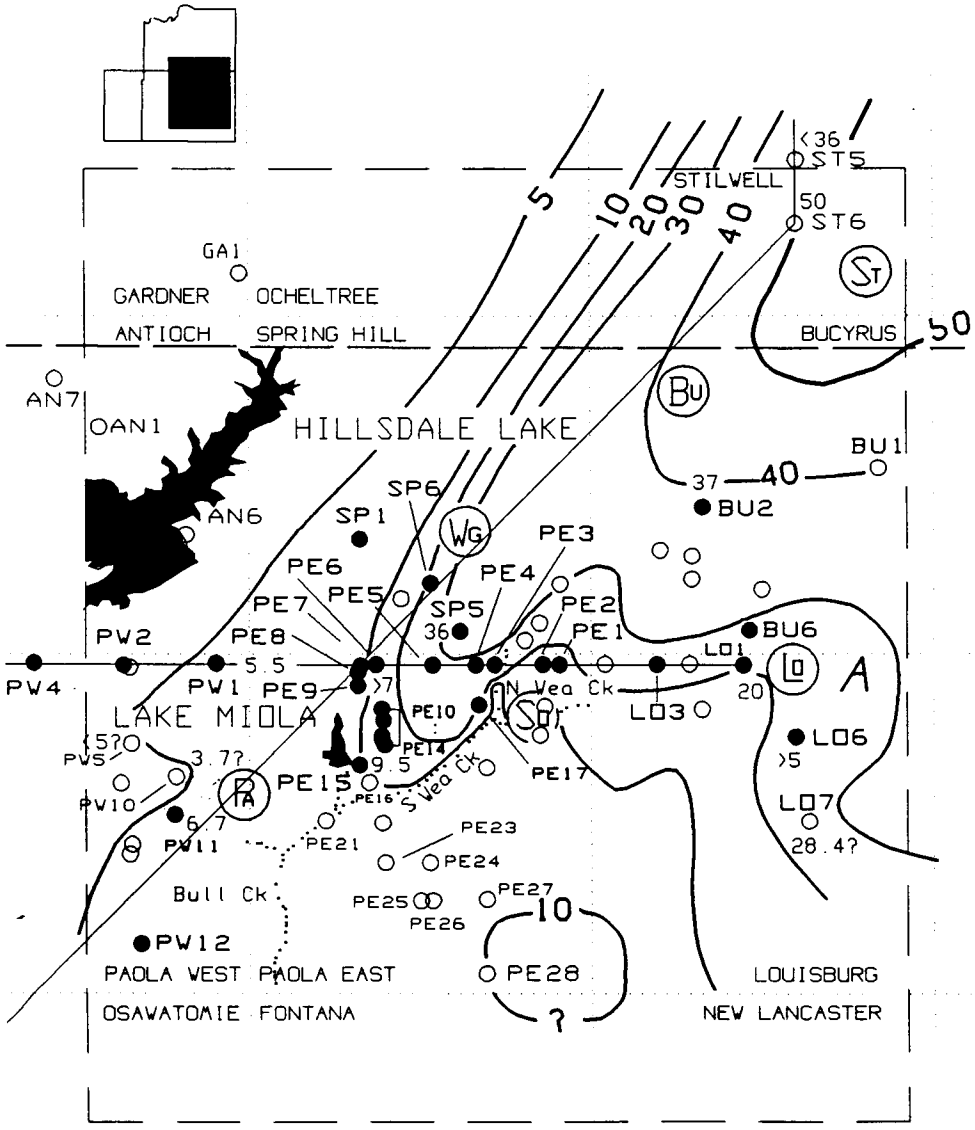

Figure 2.27. Measured section of Wyandotte and Iola Limestone, exposed at I-435 Holliday Road exit ramp, Johnson County (locality ED1, C NE NW 6 T12S R24E). Stratigraphic names reflect the traditional correlation which is currently under revision (HECKEL, in review). HARRIS (1985) argued that the middle Farley Shale was essentially a tongue of the Island Creek Shale, and thus the lower Farley in northern Johnson County reflects a minor transgression within an otherwise shallow water, clastic-dominated regime. Basinward to the south, Miami County was out of reach of middle Farley Shale clastics. Thus this interval is not represented in Miami County, where Farley Limestone reflects essentially uninterrupted carbonate deposition. Taken from HECKEL (1985).

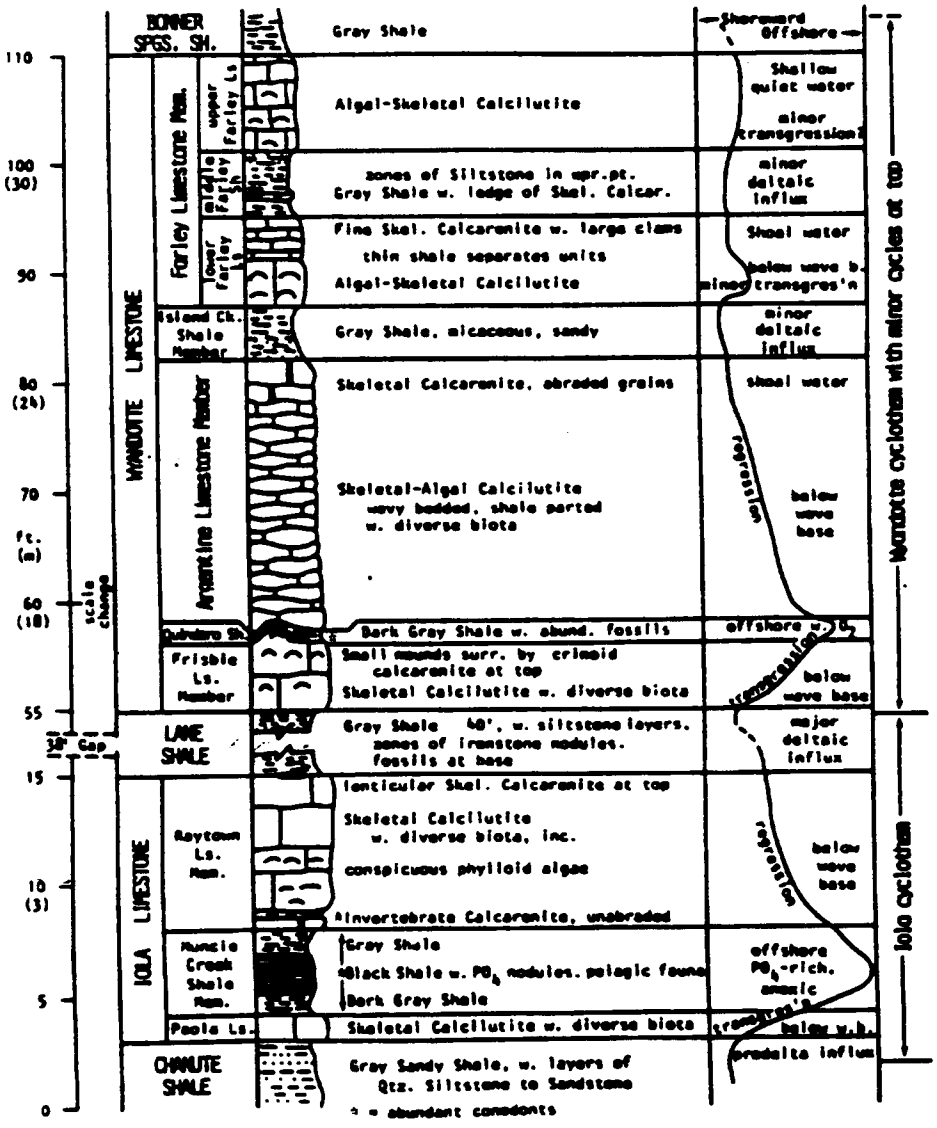

CHAPTER III

LITHOFACIES AND CARBONATE PETROGRAPHY

Description of carbonate microfacies

The Wyandotte Limestone can be profitably organized into seven basic lithofacies: phylloid algal wackestone, phylloid algal packstone, geopetal brachiopod-algal calcilutite, onkoid-sponge calcilutite, oolite, peloidal grainstone, and mixed skeletal calcarenite. Their distribution is shown in Figures 2.24 and 2.25, and their petrography is described in detail below. This is followed by a discussion of petrographic aspects that bear specifically on diagenesis of the Wyandotte Limestone as a whole, thus setting the stage for presentation in the following chapter of trace element data, whose relationship to diagenesis are necessarily more theoretical. This chapter concludes with mapping of the facies' vertical and areal distribution, and a brief interpretation of depositional environments.

Phylloid algal wackestone facies

This facies is expressed in various localities in all carbonate members of the Wyandotte Limestone, although in

Miami County it is best exposed at the quarry south of Wagstaff (SP5). Phylloid algae are the dominant skeletal constituent. An associated open marine fauna, consisting of small rugose corals, brachiopods, gastropods, and bryozoans is sparsely distributed through this facies, and these tend to occur as isolated individuals. The ratio of phylloid algae to other skeletal material typically increases upsection in this facies. On outcrop the rock is light grey in color, and medium to thinly bedded, with beds separated by thin chert or shale partings commonly rich in crinoid debris. As mentioned in the previous chapter, these shale partings also become increasingly numerous towards the top of this facies at SP5. Algae are found in states of preservation that vary on the scale of outcrop to thin section. In many samples, this facies is composed entirely of micrite and blocky, spar-filled voids, whose characteristic outline identifies them as algal blade molds (see Figure 3.1). Elsewhere, the cellular microstructure of the hypothallus and perithallus are relict but clearly visible, and the alga can be identified as Archaeolithophyllum (WRAY, 1964). Visible algal microstructure is common only in the Frisbie and basal Argentine at SP5, and near the top of the algal wackestone facies at LO3 and BU6, where the mound is capped by mixed skeletal calcarenite.

Within the interior of the algal bank at SP5, micrite is the dominant component, and often exhibits a disturbed or intraclastic fabric. Micrite can also assume a softly clotted or pelletal appearance close to the margin of a sheltered or geopetal void fill, with small clots having diffuse margins floating in sparry calcite. This texture tends to disappear with increased packing density of the clots away from the margin of the void.

Early, fibrous marine cements are relatively rare, but are found near the base of the facies at SP5 as relict phases in small voids sheltered by algal blades, or throughout the algal mound in body cavities of gastropods (which are themselves replaced by blocky calcite), rugose corals, and brachiopods. Large, open voids or fractures are typically filled with euhedral calcite. No early marine cement is seen in these latter features, and the void-filling calcite is typically clear, low relief, inclusion-free, occasionally poikilotopic, and exhibits an even, moderate to dull luminescence that lacks any visible growth zonation (with the exception of sector zoning). This calcite becomes the principal cement phase towards the top of this facies at SP5. Coarsely crystalline, zoned, strained (saddle) dolomite is a relatively minor, late cement phase that both replaces micrite and fills open voids towards the top of this facies. This dolomite is also

followed by clear, blocky calcite (Figure 3.2). Cryptocrystalline quartz is also a late, void-filling phase, but is found only as a trace component.

Certain areas within the algal bank at SP5 also exhibit a calcite spar consisting of cloudy, subhedral to euhedral crystals, whose boundaries are lined with opaque material that may be an oxide or other insoluble phase. These calcite crystals commonly exhibit a range in diameters, and can often be seen to grade with decreasing size directly into micrite, and with increasing size into euhedral, void-filling spar, although the latter transition is more abrupt. (This feature is not confined to the algal wackestone facies, but is found throughout the Wyandotte: see Figure 3.15). Under CL, these crystals emit a blotchy luminescence that reveals no obvious crystal growth sequence. Lastly, close to the base of the Argentine at SP5, the basal margin of algal blade voids filled with calcite spar is lined with a thin rim of sulfide, probably pyrite. Similar occurrences of sulfide rims are also seen in like facies of the Frisbie at the same locality.

Phylloid algal packstone facies

This facies is not widespread in the Wyandotte, and is found best represented at the base of the Frisbie Limestone south of Louisburg at LO6, and to a much lesser extent at the top of the Argentine algal bank to the north at BU6. On

outcrop it is dark to bluish grey, dense, and massive or thickly bedded. As in the algal wackestone facies, phylloid algae is the dominant skeletal component, and other fossils include brachiopods and sponges. Micrite is a minor constituent. It is distinguished from the algal wackestone facies by the close, subhorizontal packing of algal blades (probably belonging to Archaeolithophyllum, see Figure 3.3). Blade microstructure is occasionally recognizable, although strongly overprinted with euhedral, slightly ferroan calcite that may also be slightly dolomitic (the results of potassium ferricyanide staining were equivocal here). Packed blades are often broken and fractured and have fallen into the remaining void space, with the associated micrite and cement cut coherently by the same fracture (Figure 3.4).

Two basic types of cement exist: fibrous and blocky. The first is a highly fibrous, early marine cement, probably aragonite or possibly magnesian calcite. It exhibits great variety in style of preservation, from distinct, essentially unaltered needles to highly neomorphosed botryoids. This cement is found either in sheltered voids between algal blades, or in what may have been conceptacle pore spaces. Many of these acicular crystals are notable in being crystallographically distinct, having blunt terminations, and being optically distinguishable from enclosing blocky calcites (Figure 3.5). Although an independent means of

verifying their mineralogy was not used, they are the morphologic equivalent of modern, fibrous, marine cements. Neomorphosed, radiating, fan-like masses of cement are also found both in sheltered void cavities and apparently growing into the micrite matrix (Figure 3.5). These botryoidal fans have a dark, blotchy appearance and a blocky calcite overprint. Masses of this cement commonly exhibit breakage and fracturing that is healed by later calcite.

Where they occur in sheltered void fills, the above cements are postdated by the second cement type consisting of large, unstrained, blocky, very clear calcite euhedra whose crystal diameters rival that of the pore space they occupy. This type also fills fractures that clearly postdate growth of the earlier cements. No distinct growth zonation is visible under CL in any of these cements, and both the skeletal remains and cements as a whole exhibit at best a dull luminescence.

Geopetal brachiopod-algal calcilutite facies

This facies is best represented in the Farley Limestone, and is found at virtually every exposure of this unit. Principal skeletal constituents are small to medium brachiopods (commonly Enteletes), whose abundance distinguish this facies from the previous two, and whose intact valve cavities are typically filled with geopetal micrite and blocky calcite spar. Phylloid algae are also

present, although in less relative abundance than in the algal wackestone facies. Other skeletal constituents include fusulinids, small sponges, small rugose corals, trilobites, bryozoans, crinoids, and encrusting algae (Figure 3.6). Micrite is the common matrix component, often developing similar clotted or pelletal fabrics to those described in the algal wackestone facies. In certain areas skeletal grains and micrite intraclasts appear to float essentially unsupported in blocky calcite spar, which is the dominant cement type. In general, early marine cements are present in minor quantity only as thin, relict rims of inclusion-rich fibrous cement lining skeletal cavities, although locally these isopachous rims are quite well-developed. There is abundant evidence of dissolution of earlier cement generations, in which corroded boundaries of an early, cloudy, inclusion-rich, relatively fine-grained calcite are in contact with a later generation of clear, coarsely crystalline (often poikilotopic) calcite that completes the void-filling sequence. The opaque-lined calcite spars described earlier are found here as well.

Euhedral quartz is also a late void-filling cement, clearly postdating earlier blocky calcite. Cryptocrystalline quartz also locally replaces brachiopod valves, although this is not a pervasive feature.

Onkoid-sponge calcilutite facies

This facies is found in the Argentine Limestone throughout the western half of Miami County, at the very base of the Argentine at SP5, and in the upper half of the Frisbie Limestone in the Louisburg area. It is distingished by the unique occurrence of onkoid coatings on skeletal grains, and a general dearth of the phylloid algae so characteristic of the phylloid algal wackestone facies. Usually dense and dark grey on outcrop, this facies also contains an abundant, open marine fauna of small brachiopods, crinoids, cephalopods, gastropods, small sponges, small rugose corals, and bryozoans. This facies is termed a calcilutite as it consists of intergrading wackestone to packstone fabrics, and these locally intercalate with lenses of the mixed skeletal calcarenite facies described below. Skeletal grains occasionally show minor abrasion, and breakage of brachiopod and cephalopod valves is common in packstone intervals. Red algae are a minor constituent only, in great contrast to the facies described above. They are most common in this facies at PE8/9 (Argentine), .i.e, still relatively close to the margin of the Wagstaff-Stilwell algal mound complex, where their microstructure is overprinted by blocky calcite but still quite visible. West and south of this point they are quite rare.

This facies is also distinguished by the common encrustation of skeletal grains by cm-thick crinkly-laminated crusts or mats termed onkoids (see Figure 3.7). Concentrically laminated crusts are seen enveloping skeletal grains entirely or covering only the top surface of a grain. No microstructure that would identify these structures as algal in origin is visible. Mats appear to have initially nucleated on skeletal grains, with growth proceeding thereafter both upward and laterally, producing laminated structures subparallel to bedding. These may also shelter spar-filled voids at their base. Other encrusting fauna, such as small foraminifera and fistuliporid bryozoans, are incorporated in the crust as well.

Fibrous, early marine cement is common in this facies, lining sheltered cavities and body cavities of corals, brachiopods, and cephalopods. This cement is represented by a thin, relict, inclusion-rich, isopachous fringe which is invariably followed by blocky calcite spar. At PE8/9 and SP5, these voids host a complex sequence of cement zones under cathodoluminescence, and share in common a brightly luminescent, early calcite lining the void wall. The zoned sequences are described in detail in the following chapter. In addition, areas of inclusion-rich spar occur in contact with these blocky cements. Although relatively finely crystalline, these spars are organized into larger domains

having a fan-like gross morphology, and in which lines of solid inclusions are crudely oriented in a radiating fashion. These resemble aragonite botryoids in outline, although save for the orientation of inclusions, no relict fibrous structure is visible (Figure 3.8).

Oolite facies

As described in Chapter II, oolites are found solely at the base of the Farley Limestone in a belt close to the margin of the underlying Lane-Island Creek delta. The boundary with underlying sandstone of the Lane Shale at PW6 is sharp. Oolite intraclasts several centimeters in size are found within the brachiopod-algal calcilutite facies where it overlies the oolite in gradational contact at PW2. Ooids are approximately 0.5 mm in diameter, are closely packed but not overpacked (Figure 3.9), are relatively uniform in shape and texture, and have well-formed cortices possessing faint concentric but no radial structure. No skeletal grains are present. Nuclei consist of well-sorted, silt-sized, angular to subangular quartz grains. A faint fibrous fringe that is probably a relict early marine cement is visible along some ooid grain boundaries. Interparticle porosity is filled by blocky calcite cement. In samples taken directly from the base of facies, where it overlies clastics of the Lane Shale, ooids are more recrystallized than those from higher in the section. These do not retain

any concentric structure, but display a coarsened, microspar texture that overprints both the ooid and the surrounding cement (see Figure 3.9). All of the oolite samples display a moderate luminescence, with no difference in intensity between grain and cement, and no visible growth zonation visible in the latter.

Peloidal grainstone facies

This facies is found only at one locality (PE1) capping the Farley Limestone, but its unique nature warrants its distinction as a separate group. Grains are well-sorted, subspherical, homogeneous, micritic masses 0.3-0.5 mm in diameter, and have sharp boundaries in face contact. Locally, relict skeletal grains can be identified by their shape and faint internal structure, and appear to be in a state of transition to structureless, rounded grains (Figure 3.10). Interparticle cement is clear, blocky calcite, but early marine cement is not present.

Mixed skeletal calcarenite facies

Calcarenites are represented by a fairly diverse group of lithologies whose skeletal composition and texture varies according to their stratigraphic position within the Wyandotte Limestone, but whose overall limited distribution does not justify division into more than one facies type. Not surprisingly, they typically occur at the top or base of

a given limestone unit. Where it caps thick algal wackestones of the Argentine Limestone at LO3 and BU6, this facies is 0.5 feet thick, ferruginous, poorly sorted, and composed of conspicuously large bivalves and calcisponges, crinoids, encrusting foraminfera, bryozoans, trilobites, small gastropods, and algal blades (Archaeolithophyllum sp.; see Figure 3.11). Many of the grains are coated with mm-thick algal coatings. The large bivalves are completely replaced with a coarse, blocky spar, and the interiors of sponges are filled with the same material. Grains show varying degrees of abrasion, but all show mechanical wear. Matrix is micrite or microspar.

At the base of the Farley Limestone at LO3 and BU6 this facies appears as a fusulinid packstone to grainstone. Fusulinids are robust, abraded, and slightly coated. They are associated with bryozoans, small bivalves and crinoids, and phylloid algae. This facies grades directly into overlying phylloid-algal wackestone. Matrix spar is fine granular to microspar in texture, and no fibrous early marine cement is present. A two foot thick packstone to grainstone interval also caps the Farley Limestone at LE2, composed of abraded bryozoans, brachiopods, crinoids, and small rugose corals. Where interparticle sparry cement is present, it forms a blocky mosaic, with crinoids showing syntaxial overgrowths. No CL zonation is present in these

cements, and the rock shows an overall dull, even luminescence under CL.

Calcarenites are also present a few feet from and at the base of the Argentine Limestone at PW11 and PW1, respectively. Here the facies grades from a dense skeletal packstone to grainstone and is composed of large crinoids, micrite intraclasts, bryozoans, sponges, and small brachiopods. Skeletal grains show no significant abrasion. Sparry cement is a fine-grained, granular mosaic, and crinoid grains lack any syntaxial overgrowths. Lastly, a dense crinoidal calcarenite composed almost entirely of columnals in sutured contact is present in the Frisbie Limestone at LO1.

Summary of depositional environments

Eustatic changes during deposition of the Wyandotte Limestone were responsible for the distribution of the facies described above. To guide the reader in the following review, facies have been mapped in vertical profile and appear on the two cross sections A-A', B-B' (Figures 2.24 and 2.25).

Deposition of the Wyandotte Limestone began with the marine transgression that stymied the Liberty Memorial delta, thus stranding prodelta lobes in Johnson and Miami County. As the sea deepened and cleared, optimal conditions for benthic algae along more elevated, well-lit portions of

the seafloor supported by the underlying shale platform gave rise to algal mud banks of the Frisbie Limestone, exposed at SP5 and LO6. The temporal relationship of the basal algal packstone facies at LO6 and the algal wackestones that compose most of the Frisbie at SP5 is not certain. The dearth of micrite in the former suggests either possible late stage winnowing by currents, or nonproduction (or dissolution) of mud. The vigorous circulation of sea water necessary to precipitate the conspicuous marine cements of the algal packstone facies is consistent with the former explanation. The seafloor at LO6 was also probably higher than that at SP5, owing to a greater thickness of underlying Liberty Memorial Shale. Thus if banks at the two localities were coeval, carbonate mud deposition at the latter could have continued below wave base, as algal proliferation kept pace with rising water, while residence in the zone of wave activity prevented mud from accumulating in the former. Note that the <u>top</u> of Frisbie at LO6 is composed of onkoid-sponge facies: here a micrite matrix and lack of phylloid algae suggests deposition below wave base and below or at the lower reaches of the photic zone. This facies is absent from the top of the Frisbie at SP5, and this in concert with the above relationships suggest that the unit is somewhat time-transgressive, with younger sediments present at the top of the Frisbie at LO6.

Maximum transgression increased the depth of the seafloor below the limit of lime mud accumulation, giving rise to the Quindaro Shale. This interval hosts a more diverse and abundant open marine fauna in areas where the seafloor was elevated by the underlying thick Liberty Memorial Shale, in contrast to deeper areas of the seafloor where the Quindaro is represented by a more diastemic, sediment-poor, but conodont-rich horizon.

Deposition of the Argentine Limestone during the following regression also responded to bottom topography inherited from the underlying shale platform. The onkoid-sponge facies, representing deposition in deeper, quiet, open marine water probably at low light levels, was distributed as only a thin veneer over elevated areas, which then became the locus for deposition of thick mounds of the algal wackestone facies. In contrast, off- or inter-mound areas received onkoid-sponge facies only. Material shed from the emerging mounds also accumulated in these areas as well. As the regression continued, progradation of the Lane delta terminated carbonate deposition west of the mound complex. Growth of the algal mounds continued however, with influxes of detritus shed from the advancing delta front represented by shale partings in the upper Argentine at SP5.

During the late stages of regression, clastics of the Lane delta advanced to the mound flanks and were shunted

along intermound channels. Growth of the mounds probably slowed as carbonate mud was winnowed from mound tops in depths above wave base, and reworked skeletal sands dominated by large clams and sponges were deposited in the shallowing water. An influx of clastics of the Island Creek delta probably records minimum water depths, although abundant fusulinids and bryozoans in this interval indicate that carbonate sedimentation was not totally quenched.

The following Farley transgression brought local deposition of ooid sands, in restricted areas atop the Lane-Island Creek delta front whose flooding afforded the requisite conditions of abundant nuclei in contact with supersaturated, agitated water. Further deepening established an open marine, shallow water environment, and renewed deposition of algal-skeletal carbonates. Mound development in the Farley was again controlled by bottom topography of the Lane-Island Creek delta, as well as that inherited from mounds developed in the Argentine. In Miami County, this topography was more modest than that available to the earlier marine cycle, hence the Farley is relatively homogeneous and shows less variation in lithic character between mound and off-mound settings. Phylloid algae and an abundant brachiopod fauna proliferated in areas that offered good circulation and sufficient water depth to afford upward growth. More lithic variability is seen in the Farley,

particularly the basal section, to the north in Johnson County, probably as a result of either shallower water conditions, or increased proximity to the Island Creek delta of northern derivation. Carbonate deposition was terminated during regression by the clastic influx that deposited the Bonner Springs Shale.

Petrographic evidence for diagenesis

Heckel (1983) related general petrographic features of cyclothemic sequences to their transit through meteoric (vadose; under-, active-, and stagnant-saturated phreatic), marine (vadose; active and stagnant phreatic), mixing, or burial environments. In this model, original cement mineralogy, uniformity of early cement rims, degree of compaction, ferroan cements, neomorphism, and pervasive leaching are criteria in the recognition of particular diagenetic environments.

Diagenesis of the Wyandotte Limestone includes six basic features (not necessarily in order of occurrence):

1) local cementation by early, fibrous marine cements;

2) dissolution of early marine and meteoric spars;

3) multistage calcite cementation in a shallow meteoric environment;

4) neomorphic overprint of metastable carbonate grains, particularly phylloid algae, and early marine cements;

5) crystal coarsening or ripening of micrite;

6) late emplacement of limpid, homogeneous, calcite cements, in addition to precipitation of dolomite and quartz, all probably under burial conditions.

The occurrence of marine cements is limited in the Wyandotte, and confined in all members to sheltered voids and interior skeletal walls of brachiopods, corals, sponges, and cephalopods. Algal blade voids lack early fibrous cements. In the Argentine, marine cements are most common towards the base of the unit. Most typically, these cements have been overprinted by a mosaic of blocky calcite, and are represented only as a relict, inclusion-rich fringe. With the possible exception of the basal Farley oolites, none of the grainstone facies of the Wyandotte preserve any early marine cements.

Highly neomorphosed aragonite botryoids are present in the onkoid-sponge facies of the Argentine at PE8. Abundant fibrous marine cement, probably aragonite or possibly magnesian calcite, is best represented, although variably preserved, in the algal packstone facies of the Frisbie at LO6. This variability in preservation style could reflect different generations of cement. Early aragonite botryoids would have supported algal blades, and thus maintained permeability and sea water access for later generations for marine cement to precipitate. Alternatively, cements precipitated in pore shelters of overlapping algal blades

may have been subject to greater lithostatic stress during compaction than those precipitated in rigid, intraskeletal voids such as conceptacles. This difference is stress could have rendered the former more susceptible to later neomorphism. If near-saturation with respect to aragonite was maintained during transit from the marine phreatic to a deeper burial regime, small differences in free energy and solubility due to strain, surface area, or the presence of organic matter may have led to neomorphism of algal grains and some cement, leaving other cements unaffected. CL microscopy showed only a dull, uneven luminescence in all these cements. A far more complete understanding of these cements and their burial history could be attained through selective sampling of stable isotope and trace element geochemistries.

Although HECKEL (1983) noted that early marine cements are relatively rare within transgressive limestones, he described similar relict, inclusion-rich aragonite botryoids in sparite facies of another transgressive algal mound in a later cycle (Captain Creek Limestone Member, Stanton cycle). This similarity extends to the overall fabric as well, as he noted the breakage of algal blades and collapse of material into remaining void spaces, a feature shared by the Frisbie at LO6. He attributed these features to maintenance of early permeability by aragonite botryoids within the marine

phreatic, with later partial collapse, final cementation, and aragonite neomorphism occurring during descent into the deeper-burial connate regime.

Thus with the exception of the Frisbie algal packstone facies, pervasive early marine cementation is not preserved in the Wyandotte. The fact that early marine cements are preserved in protected skeletal body cavities of stable mineralogy (e.g., brachiopods) suggests that they may have been more extensive, but have suffered either dissolution or such intense neomorphism as to render them unrecognizable during subsequent meteoric diagenesis.

Although evidence for the dissolution of early meteoric spars can be seen under transmitted light, it is more systematically revealed under CL. Figure 3.12 shows part of a void-filling sequence from the basal Farley Limestone at BU6, in which the younger margins of poorly luminescent, early spars reside in corrosional contact with later, brightly luminescent cements. The nucleation patterns of the later cements are disjunct relative to the earlier phases, and thus did not exploit earlier crystal orientations for growth. Examples of dissolution of early cements are common throughout the Farley Limestone, and in the Argentine are best seen in the upper reaches of the Wagstaff algal mound at SP5. There is no evidence in the Wyandotte of vadose cements or paleocaliche fabrics.

Cementation by blocky calcite is ubiquitous in the Wyandotte Limestone. In all void filling sequences, blocky ferroan or nonferroan calcites were the last cement to have precipitated, and obviously postdated earlier marine cements. CL petrography permits distinction of early cements precipitated in a relatively shallow, meteoric environment versus a deeper, burial setting. Void fills in the Wagstaff quarry mound at SP5, that preserve some vestige of early marine cements, if only as relics, also host luminescent-zoned calcite. This zonation is primary evidence of a fluctuating pore water chemistry responding to perturbations induced at the surface, and thus demands residence in a relatively shallow diagenetic environment. In contrast, deep-seated burial environments, by their very isolation, are relatively free from such perturbation. Limpid, inclusion-free, poikilotopic, moderately luminescent, void-filling spars having no CL zonation were thus most likely formed in a deeper, burial setting. These cements dominate voids fills in the upper section of the algal mound sequence at SP5 (Farley and upper Argentine), and are never found in contact with relict early marine cement. Luminescent-zoned calcites, by contrast, are more typical of void fills in the Frisbie and lower Argentine at this location, and can be seen in contact with relict marine cements.

Dolomite and quartz cements, characteristic of the Farley and upper Argentine at SP5, were minor, late diagenetic constituents, and were probably also precipitated in the burial environment. Dolomite cements seen in the Wyandotte are composed of large, well-formed crystals whose size indicates slow growth in a setting free from fluctuation, and thus these probably did not form in a mixing zone environment.

CL petrography also reveals details of the process of neomorphism of algal blades. Overprinting of algal microstructure by a blocky calcite mosaic is common in the Argentine at PE8, in the basal Argentine (onkoid sponge/algal wackestone facies) at SP5, and in the Frisbie at LO6 (basal section only) and SP5. Figures 3.13, 3.14, and 3.15 capture cement sequences in algal grains and associated voids in the Argentine at PE8 as transmitted/CL light pairs. Figure 3.13 shows a typical thallus with blocky calcite overprint. Although the entire blade is overprinted, the CL counterpart clearly resembles a void-filling growth sequence. This begins with an early, moderately luminescent cement infiltrating much of the blade fabric, followed by brightly luminescent and poorly luminescent zones, respectively, which precipitated from the margins of the thallus inward. Preservation of relict microstructure indicates that no wholesale leaching of the

thallus took place, and thus the distinction as to whether this represents void-filling or neomorphism is somewhat arbitrary. These relationships signify a diagenetic regime in which incongruent dissolution operated on a sufficiently small scale to maintain fine structures, and that neomorphic replacement in this case proceeded in much the same fashion as cementation of truly open voids elsewhere in the rock.

Figure 3.14 compares the cementation sequence of what clearly was an open void with that of a neighboring Archaeolithophyllum grain. Although the void fill to the right contains a more complete record of finely subzoned, interior cement, the essential order in both is identical, and the last cement to fill both sequences is moderately luminescent and lacks subzoning. Although the relationship of this final cement to the earlier subzoned phases is preserved in this example, Figure 3.15 illustrates void fills that are more typical of the Argentine in the upper reaches of the algal mound. Algal thalli here have been partially leached, and the resulting void space is filled with clear, nonzoned cement. Inspection of the CL counterpart clearly illustrates that preservation of part of the algal grain allowed it to host early luminescent cement. Where it was leached, only late cement, probably precipitated in a deeper burial setting for the reasons

discussed above, is visible. This is also further evidence of dissolution of early phases.

The last feature of diagenetic importance is more enigmatic. Throughout all members of the Wyandotte, sparry areas are observed in which there is a range of crystal diameters, grading from micritic to several hundred microns, with crystal faces lined with masses of opaque material of unknown composition (Figure 3.16). Although impossible to substantiate by petrographic evidence alone, this fabric may be the product of crystal coarsening of a micritic carbonate. Given a distribution of small crystal sizes, Ostwald ripening theory (described in MORSE and CASEY, 1988) predicts a gradual increase in crystal size with time. Crystals in equilibrium with a solution of given supersaturation have a critical radius, and those larger than this radius will continue to grow, while those smaller will dissolve. With time, the coarsening ensemble's mean crystal size and critical radius continue to increase, while the number of crystals decreases. As mass is transferred in this process, new crystal growth will have cleansed itself of impurities and insoluble material, which are left behind as residues. The observation that such fabrics are seen grading into micrite suggests that a process akin to Ostwald ripening may be responsible. Under CL these areas lack any growth zonation, which also suggests that the crystal grew

an environment of relative stasis, and thus probably in a burial regime.

Features described in the Wyandotte are in general agreement with diagenetic trends predicted for individual cyclothem members by HECKEL (1983). He argued that transgressive calcilutites show early marine cements primarily in organic buildups, and that their otherwise dark, dense character reflects increasing compaction without early marine cementation during oxygen consumption. This predicted trend is certainly well-expressed in the Frisbie at LO6 and LO1. At SP5 however, the mud-rich Frisbie does not display significant compaction of algal void spaces, but contains patchy relict marine cements, neomorphosed algal grains, and blocky calcite cement, features shared by the overlying basal Argentine Limestone. The luminescent characteristics of early calcite cement are the primary evidence of meteoric diagenesis here, and are described in detail in the following chapter.

The Lane-Island Creek Shale interval separating the Argentine and Farley Limestones is thin along the Wagstaff-Stilwell mound trend in eastern Miami County, and contains a restricted, albeit still marine, fauna. It seems doubtful that truly fresh water would have had much long term, direct access to the Argentine Limestone in eastern Miami County prior to re-submergence of the carbonate platform during the

Farley transgression. Extensive meteoric diagenesis would thus probably have been postponed until the next low stand marked by the Bonner Springs Shale.

In contrast, the thick, sandy Lane Shale could have allowed a sizable freshwater lens to become established, possibly permitting fresh water access to the top of the thin or transitional Argentine that characterizes western Miami County. However, the Argentine at PE8/9 contains relict marine cements, neomorphosed skeletal grains, and ferroan blocky calcites, features that do not suggest such a lens had access to this extent.

With the possible exception of the Frisbie at LO6, all members of the Wyandotte underwent extensive meteoric stabilization and cementation in the meteoric phreatic environment. Questions that cannot be answered here concern the extent of interaction with meteoric water. For example, skeletal voids of stable mineralogy near the top of the Argentine mound at SP5 do preserve a history of early marine and meteoric phreatic cementation. Is this early history comparable to that expressed in voids fills at the base of the mound? How does the cement sequence expressed in sheltered voids in the onkoid-sponge facies of the Argentine at PE8 differ from that of the algal mound?

Leached and collapsed algal voids of the Farley Limestone are filled with clear, blocky calcite, and lack

early marine cement. Geopetal brachiopod skeletal voids do, however, preserve an early history of marine followed by meteoric phreatic cementation. Common late infilling by euhedral quartz and local silicification of brachiopods probably occurred during deeper burial. Fresh water would have first had access to the Farley during deposition of the overlying Bonner Springs Shale. Based on similarity of depositional setting, one would not expect dramatic differences in diagenetic history recorded by void-filling cements of the Farley at SP5 and those to the east at BU6. Although the morphology of blocky calcite is identical at both localities, is there in fact a genuine cement stratigraphy that can be correlated between the two? How does this history compare to that recorded in the underlying Argentine Limestone? These questions are the task of the following chapter.

Figure 3.1. Phylloid algal wackestone petrography. Algal blade voids with collapsed micrite envelopes preserve no early marine cement. Argentine Limestone 16 feet above base at SP5. Scale bar 670 microns, PPL.

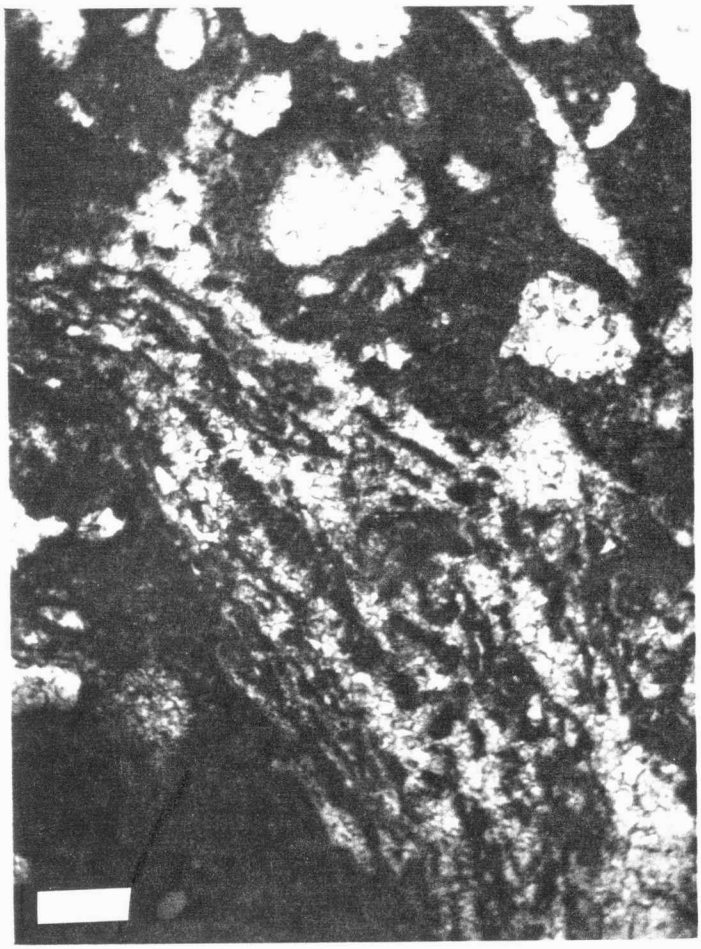

Figure 3.2. Late cements in the phylloid algal wackestone facies. Clear, euhedral calcite (C) is replacing zoned, saddle dolomite cement. Micrite (M) has been incorporated into dolomite crystal (D); however both dolomite and micrite are truncated by later calcite (C). Argentine Limestone, 16 feet above base, SP5. Scale bar 670 microns, PL.

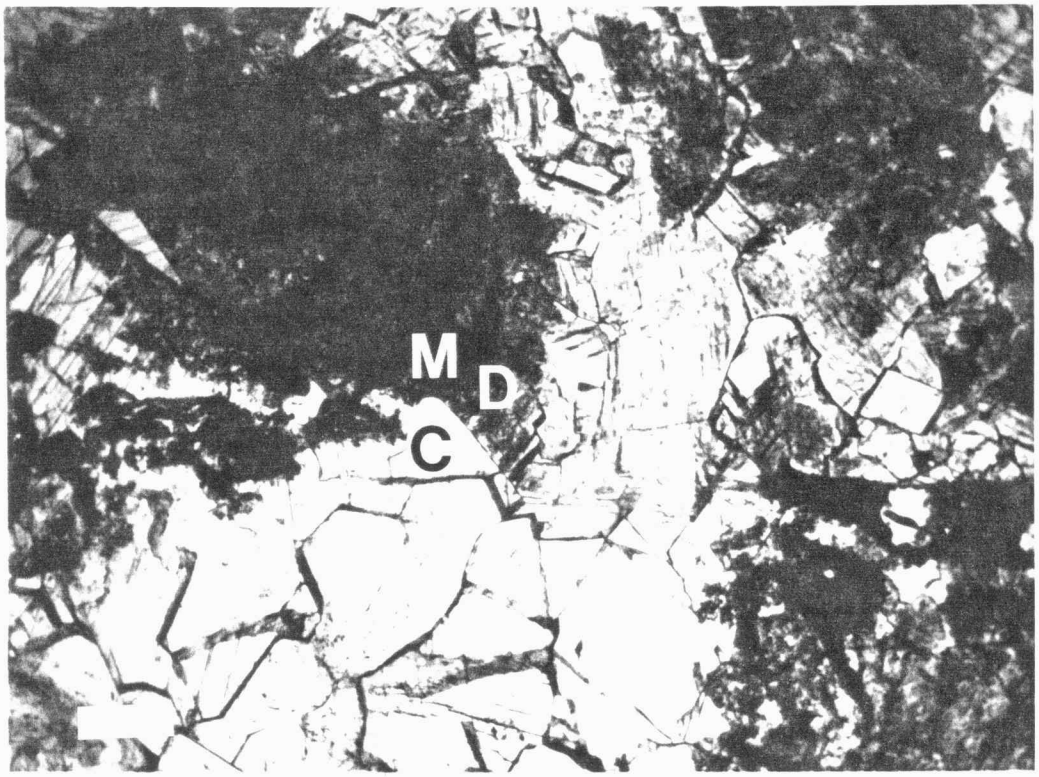

Figure 3.3. Phylloid algal packstone petrography. Base of Frisbie Limestone, LO6. TOP: Note fracture and collapse of recrystallized algal blades (B), dark botryoidal aragonite fans (A), final clear calcite cement (C). Scale bar 670 microns, PPL. BOTTOM: Detail of algal blade. Note relict, cellular microstructure of thallus, marginal fibrous cement, overprint of calcite mosaic. Scale bar 200 microns, PPL.

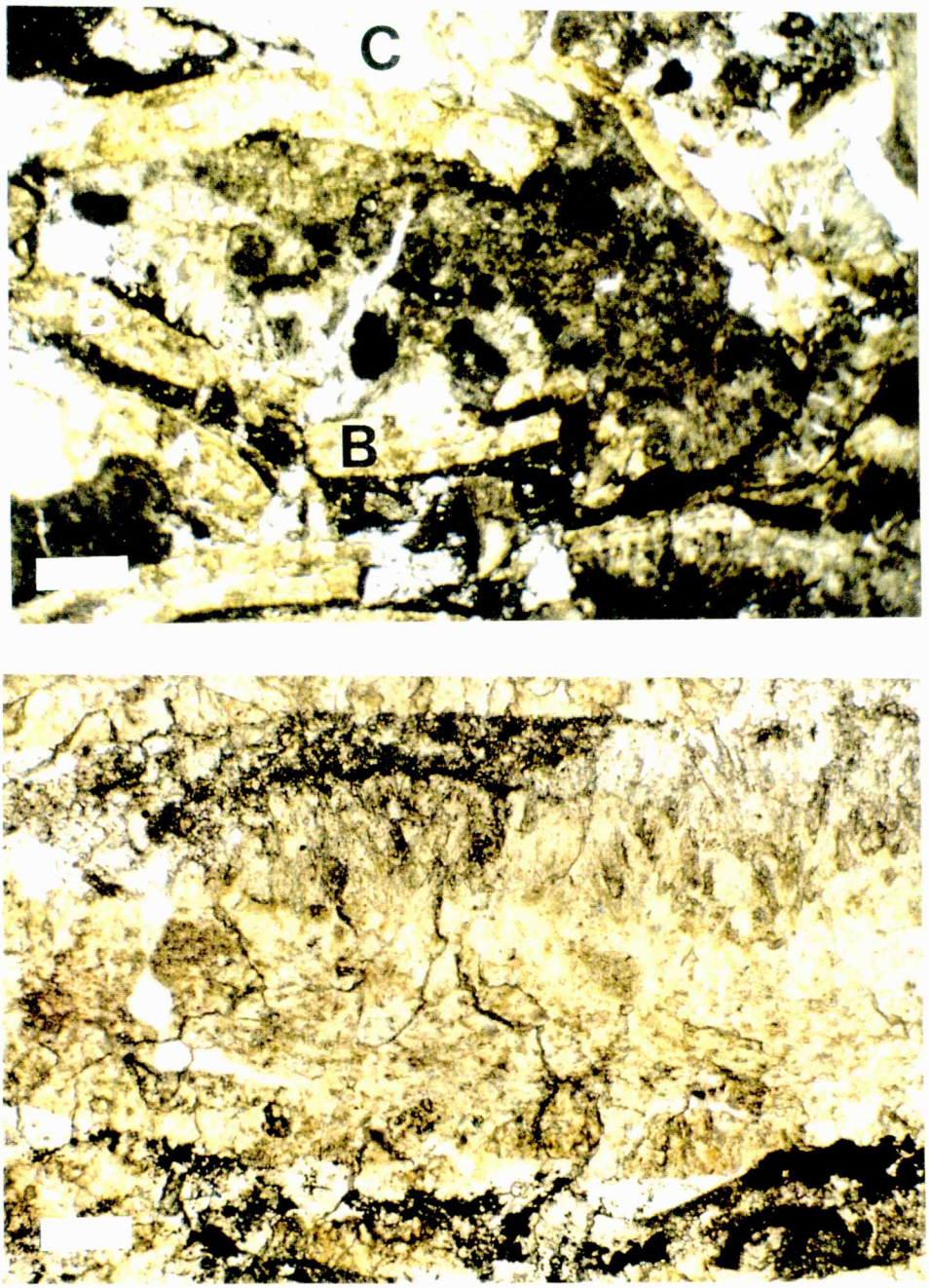

Figure 3.4. Fracturing and collapse of early marine cement and algal grains, phylloid algal packstone facies. Note that dark fibrous cement fan (A) and algal blade (B) substrate share a common fracture surface (F), healed (suggesting void-filling origin) and overprinted (suggesting neomorphism) by later, clear calcite (C). Scale bar 200 microns. Base of Frisbie Limestone, LO6.

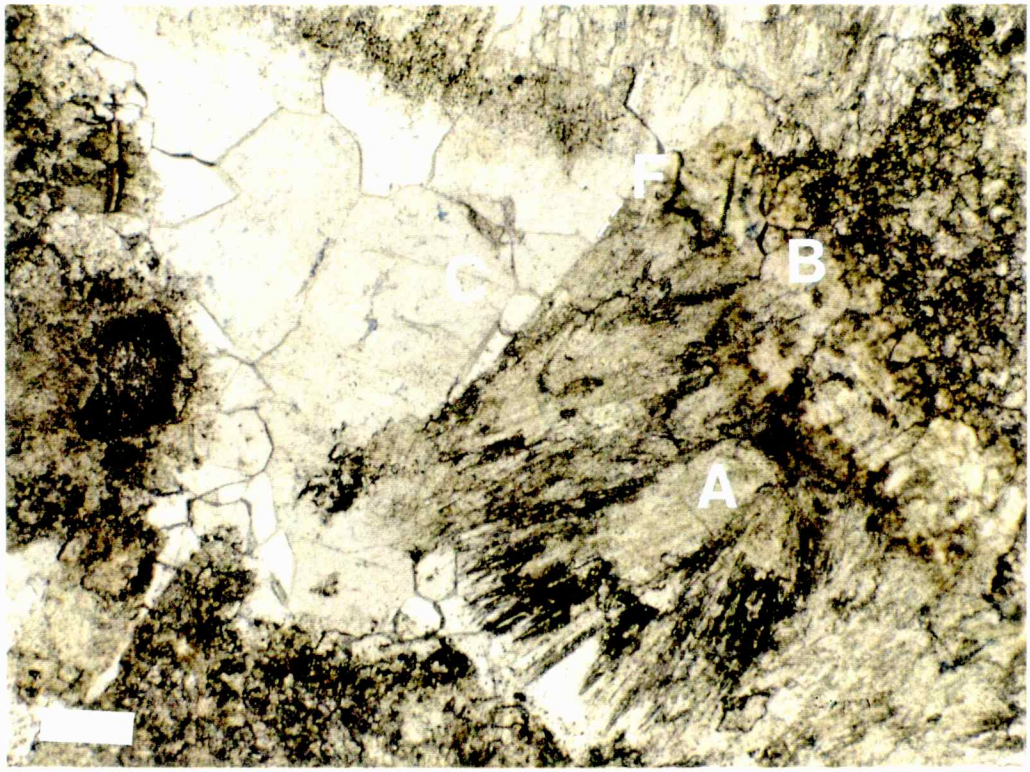

Figure 3.5. Early marine cements of phylloid algal packstone facies. Scale bar 200 microns, XPL. Base of Frisbie Limestone, LO6. TOP: Intact fibrous marine cement lining algal conceptacle. Note that despite overprint of neomorphic mosaic, acicular crystals are crystallographically intact. BOTTOM: Mollusc valve replaced by blocky calcite, in contact with dark, blotchy, recrystallized aragonite? fan.

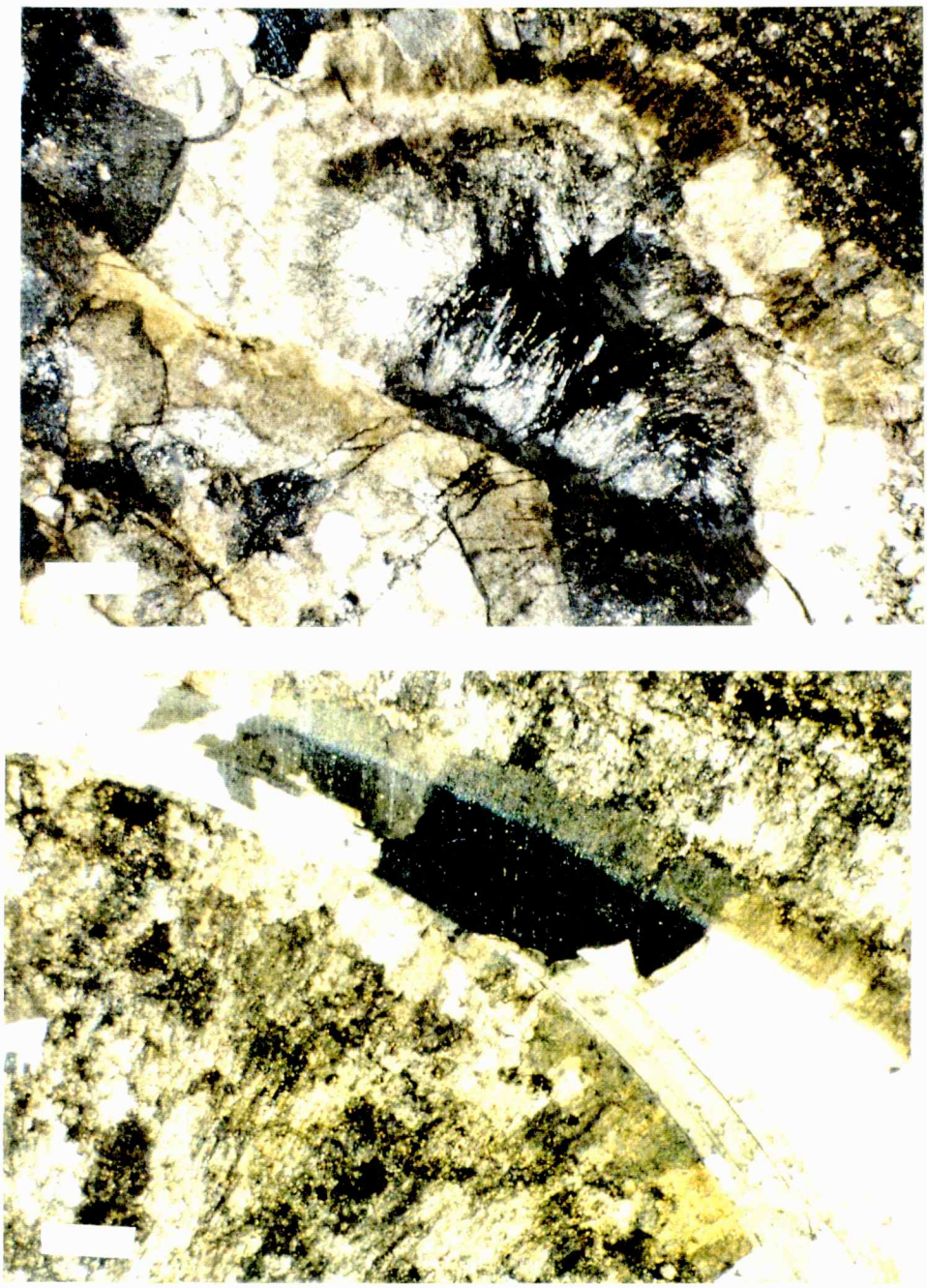

Figure 3.6. Geopetal brachiopod-algal calcilutite facies. Note abundance of brachiopod debris, thin, relict marine cements, and later blocky calcite. Fusulinids are characteristic near base of Farley. Base of Farley, SP5, scale bar 670 microns, PL.

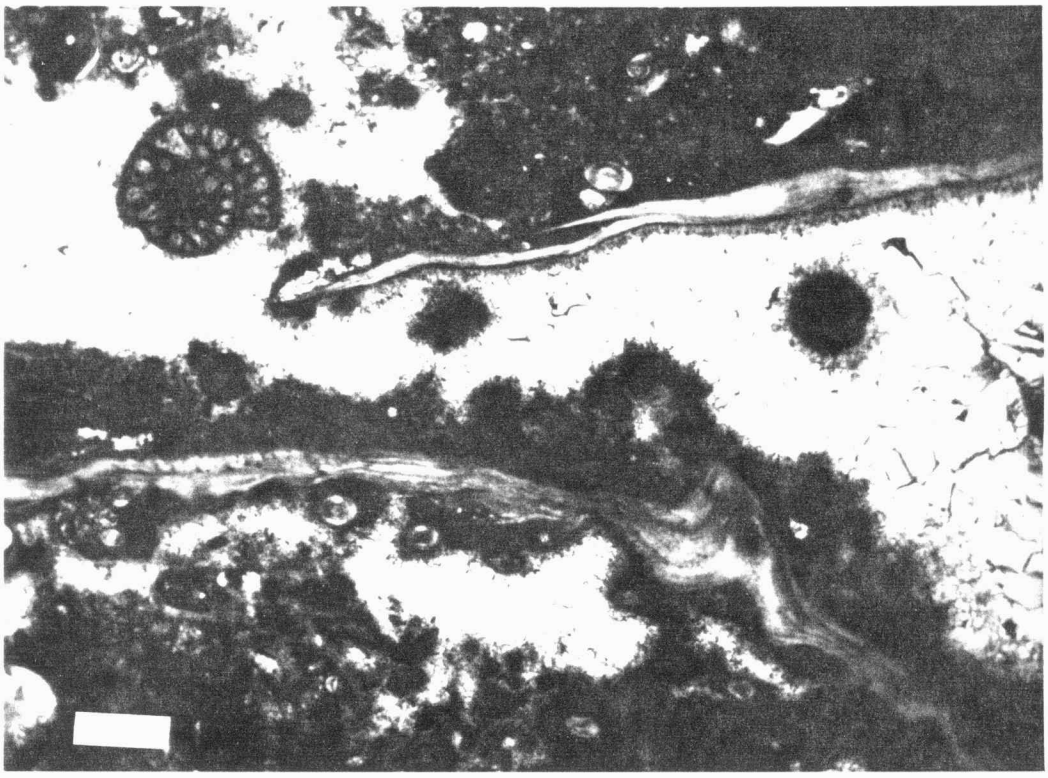

Figure 3.7. Onkoid-sponge calcilutite facies petrography. Scale bar 670 microns, PL. TOP: Laminated, encrusting organisms, probably algae, and encrusting bryozoans (B). Top Argentine, PE8. BOTTOM: Brachiopod debris completely coated with thick organic mat, possibly algal in origin. Near base of Argentine, PW11.

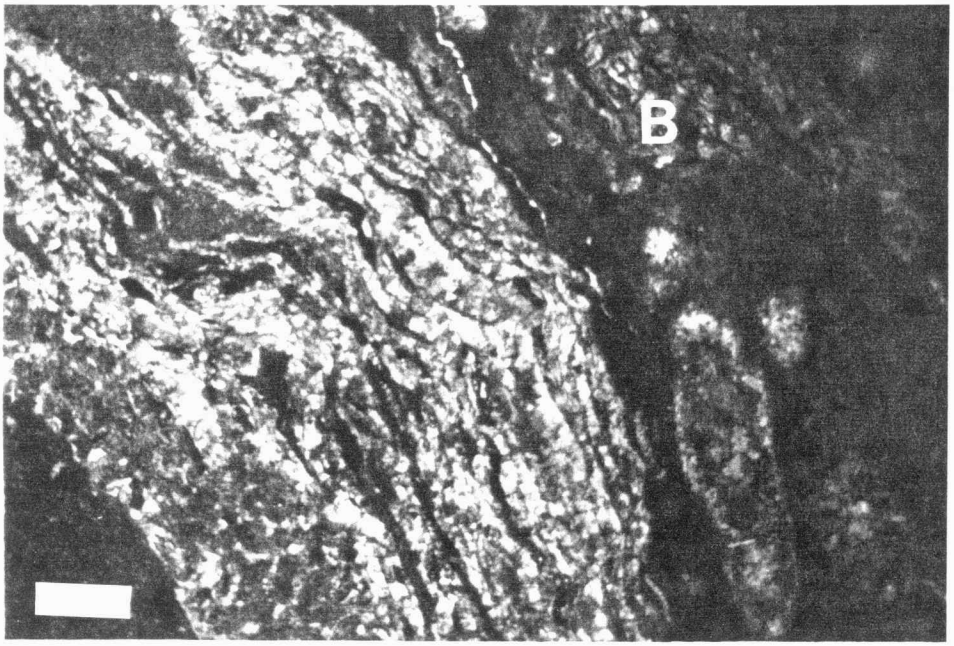

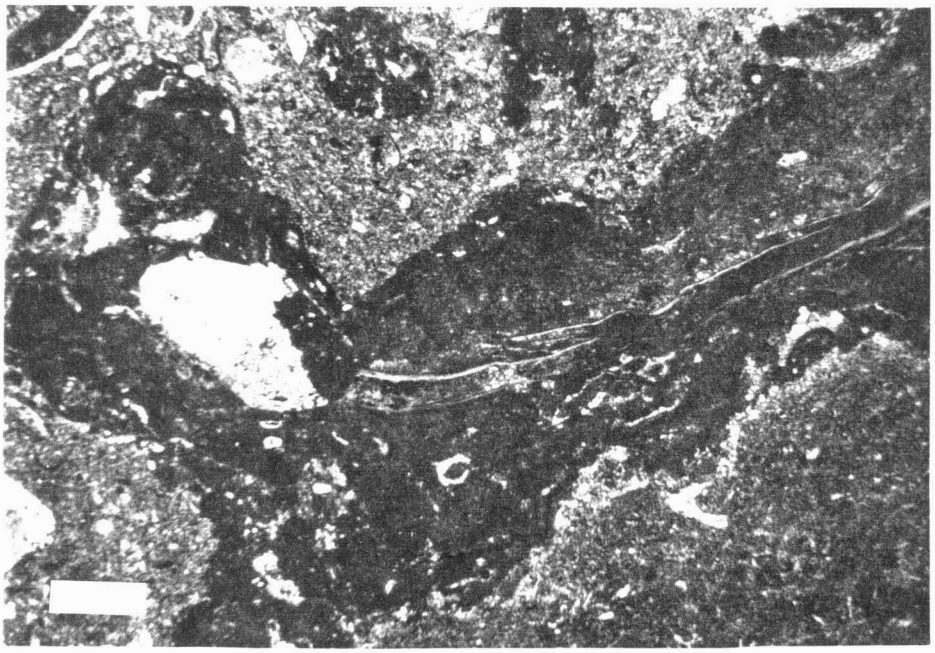

Figure 3.8. Relict botryoidal aragonite, onkoid-sponge calcilutite facies. TOP: Inclusion-rich domains show corroded margins, fibrous fabric. Discoloration of epoxy is from CL beam oxidation. Note early fibrous cement lining gastropod cavity. Top of Argentine, PE8, scale bar 670 microns, PPL. BOTTOM: Relict fibrous texture within inclusion-rich, irregular spar crystals. Base of Argentine, PW1, scale bar 200 microns, PPL.

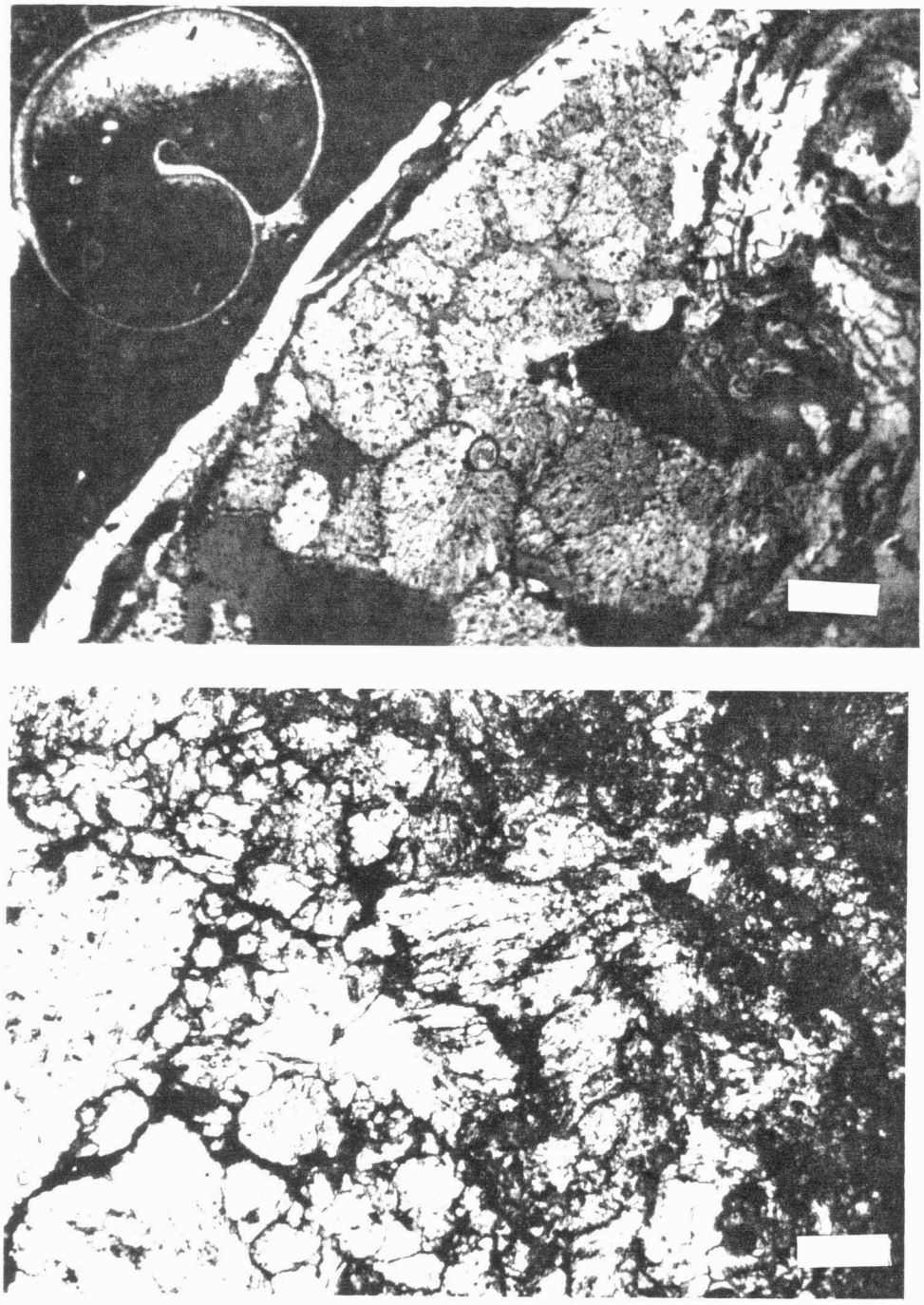

Figure 3.9. Oolite facies petrography. From base of Farley, PW6. Note relict concentric structure, neomorphic overprint of blocky calcite. Scale bar 200 microns, PPL.

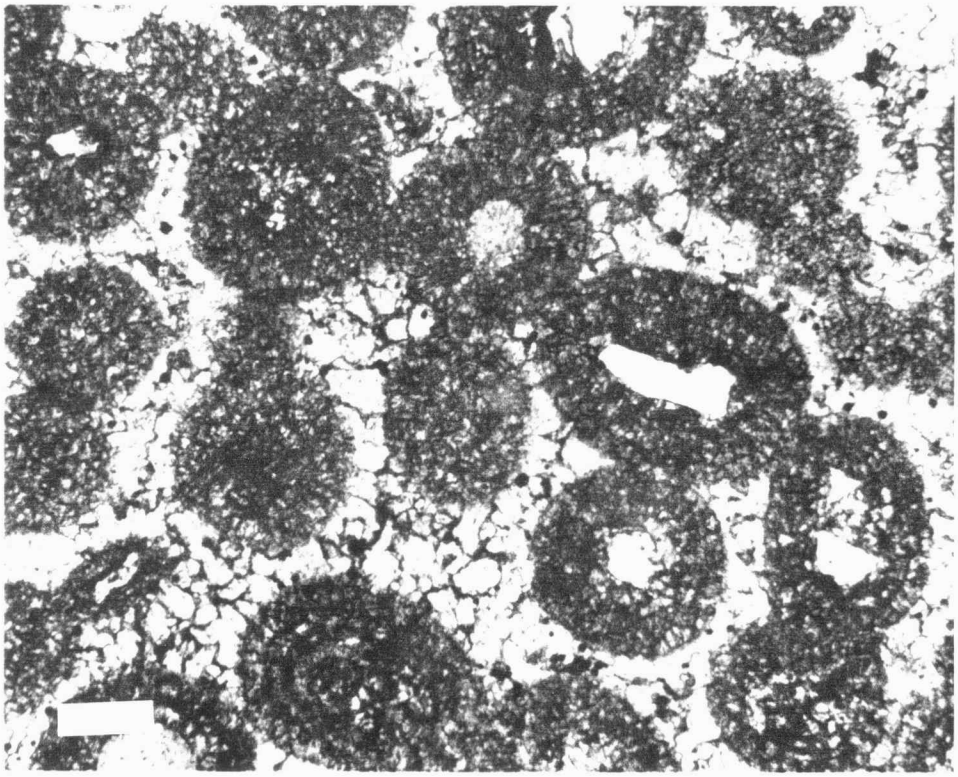

Figure 3.10. Peloidal grainstone facies. Note variety of grain types, ranging from those having a probable skeletal origin (that have suffered micritization and loss of structural detail), to structureless, micritic masses. Interparticle cement is blocky calcite spar. Top of Farley Limestone at PE1. Scale bar 200 microns, PPL.

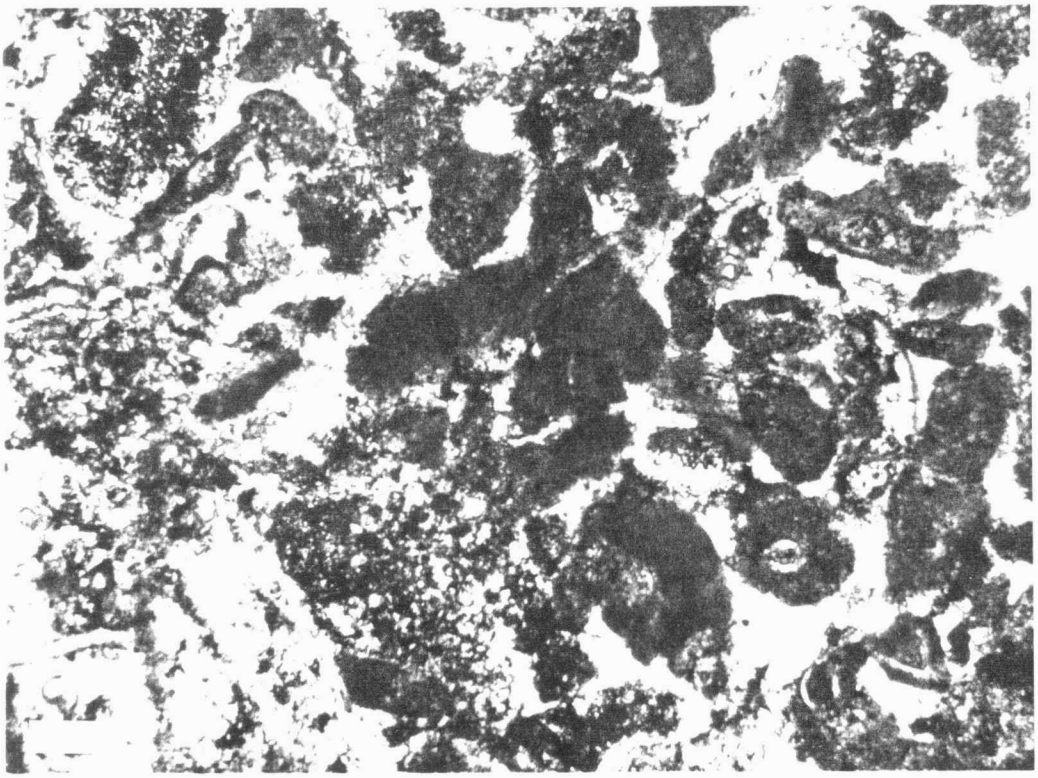

Figure 3.11. Mixed skeletal calcarenite facies petrography. Top of Argentine at BU6, scale bar 670 microns, PPL. TOP: Algal, brachiopod, trilobite, crinoid, bryozoan debris in micrite matrix. BOTTOM: Note preservation of algal microstructure.

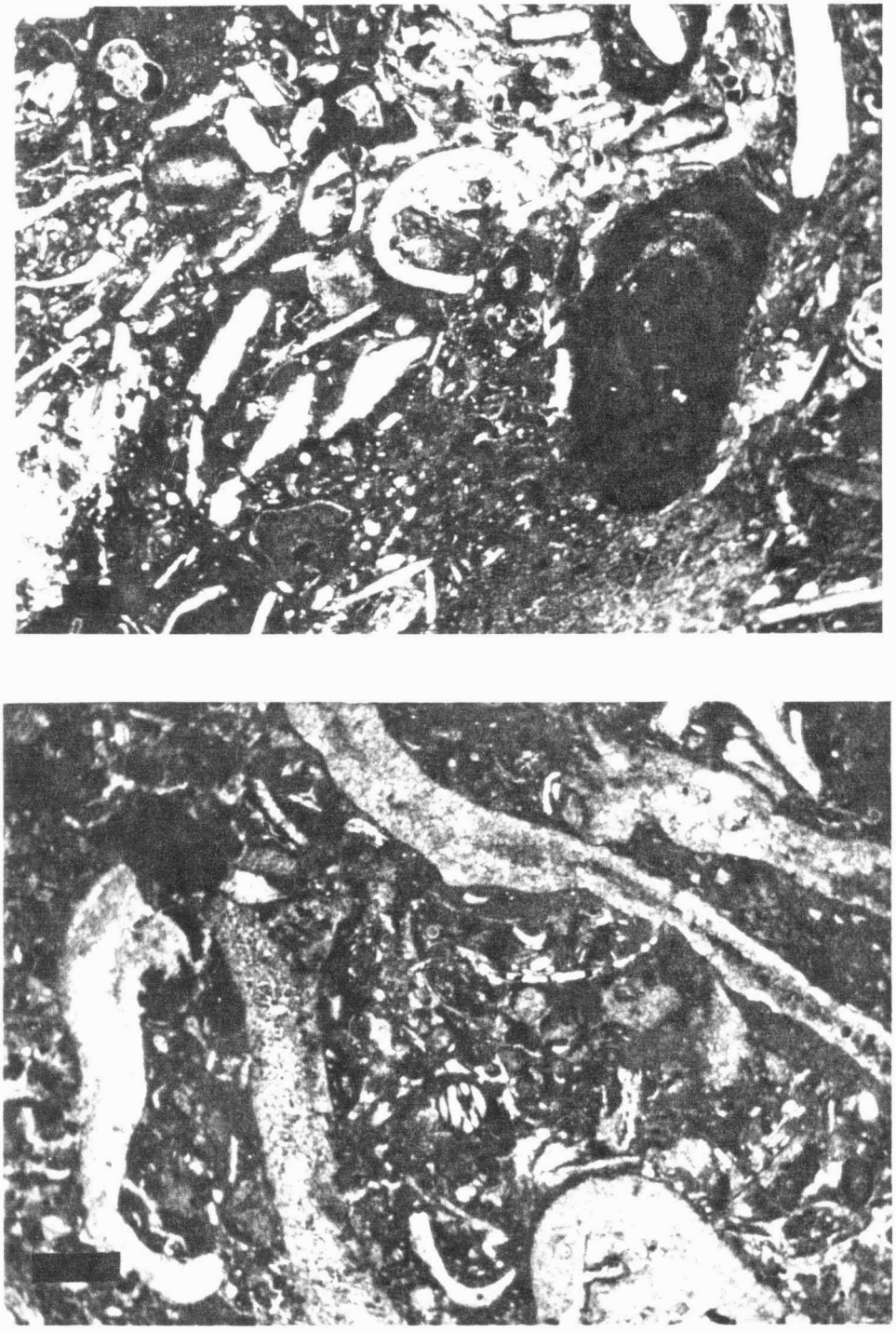

Figure 3.12. Evidence for dissolution of early meteoric spars. Note ragged boundaries and terminations (B) of early, poorly to non-luminescent spar, in contact but not in crystallographic continuity with later luminescent cement (C). Microprobed section, base of Farley, BU6, scale bar 50 microns, CL.

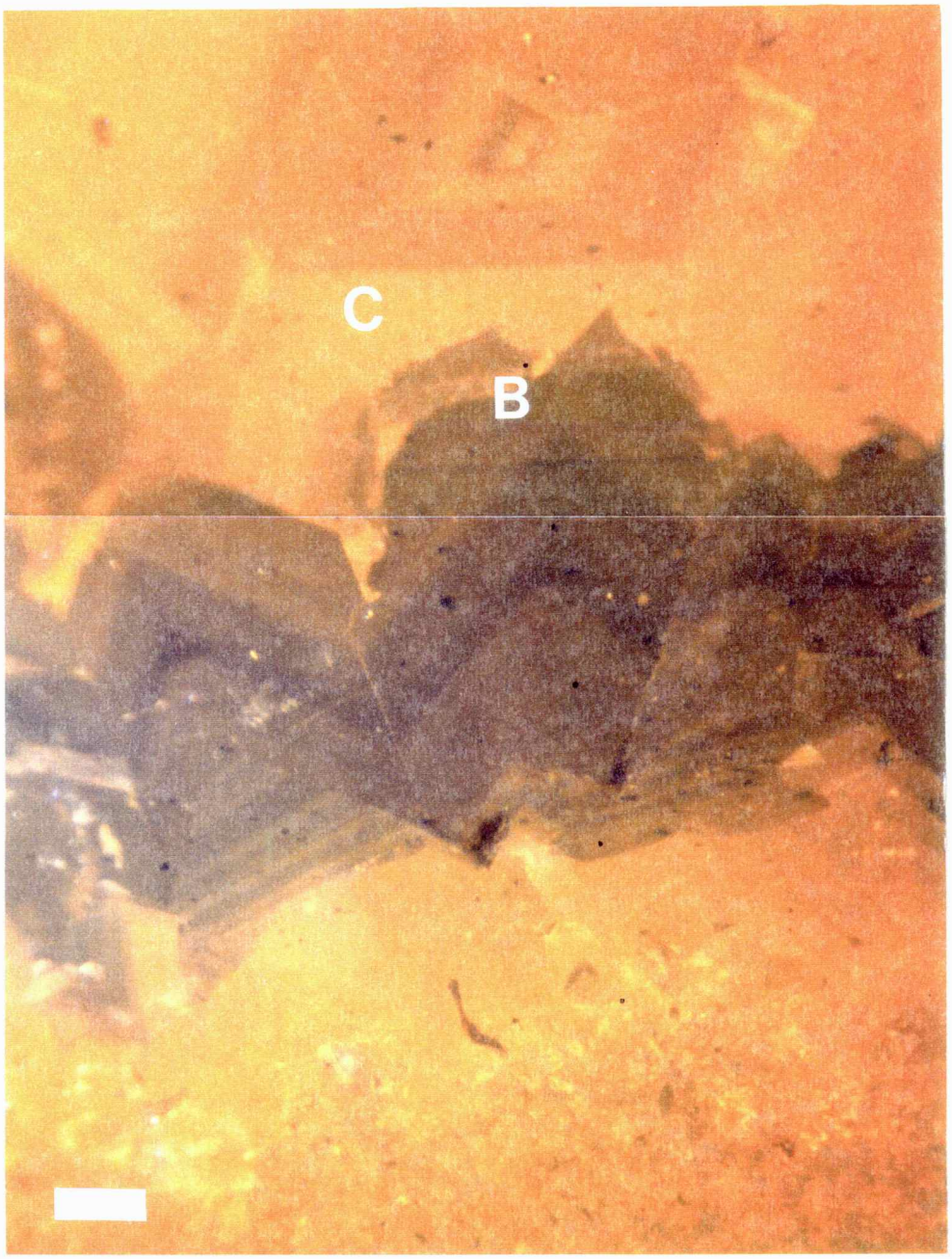

Figure 3.13. Neomorphic preservation of algal microstructure. Scale bar 100 microns. Top of Argentine at PE8. TOP: PPL. BOTTOM: CL.

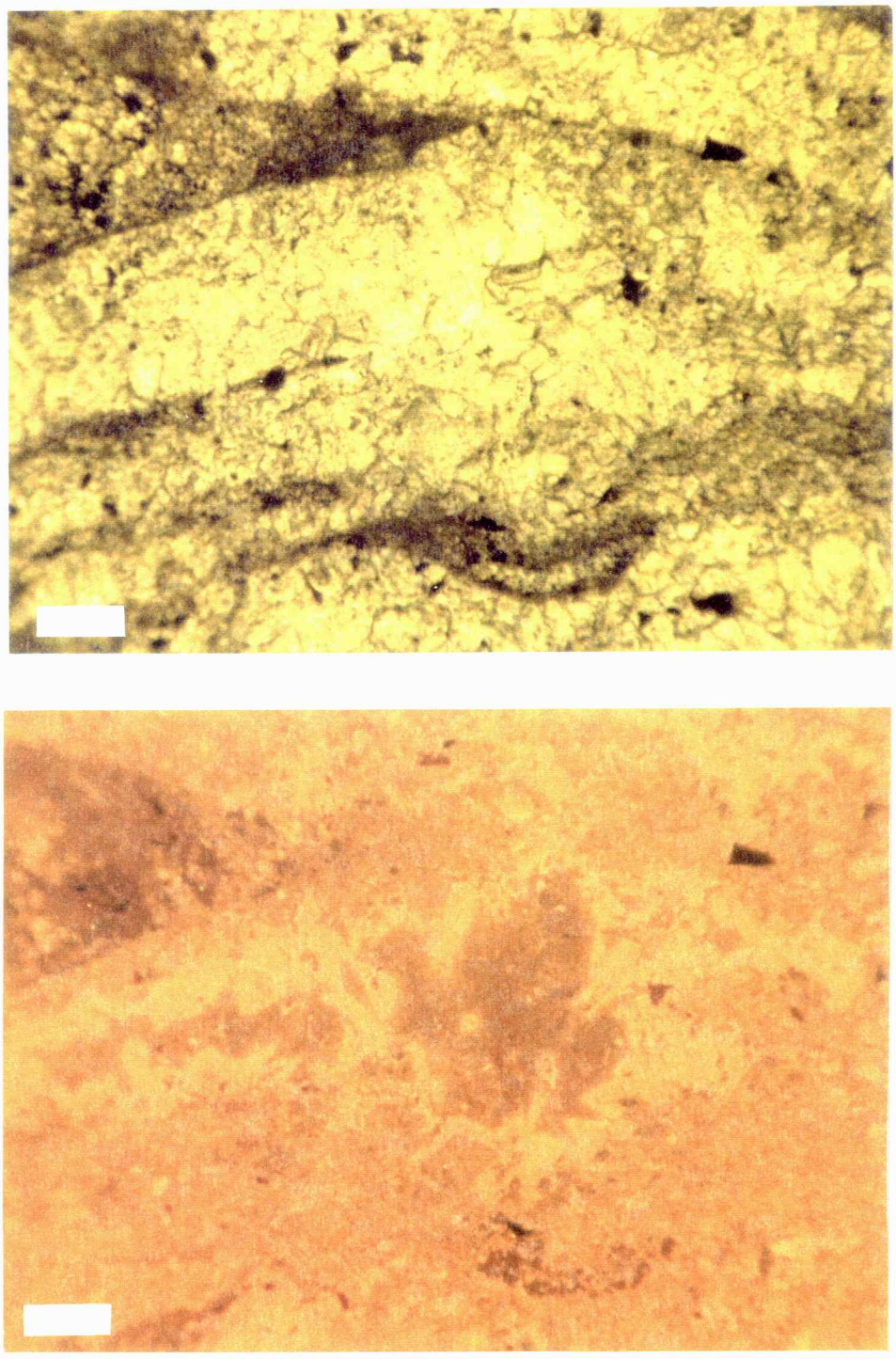

Figure 3.14. Comparison of neomorphic fabrics, partial dissolution, cementation. Scale bar 50 microns. Top of Argentine at PE8. TOP: PPL. BOTTOM: CL.

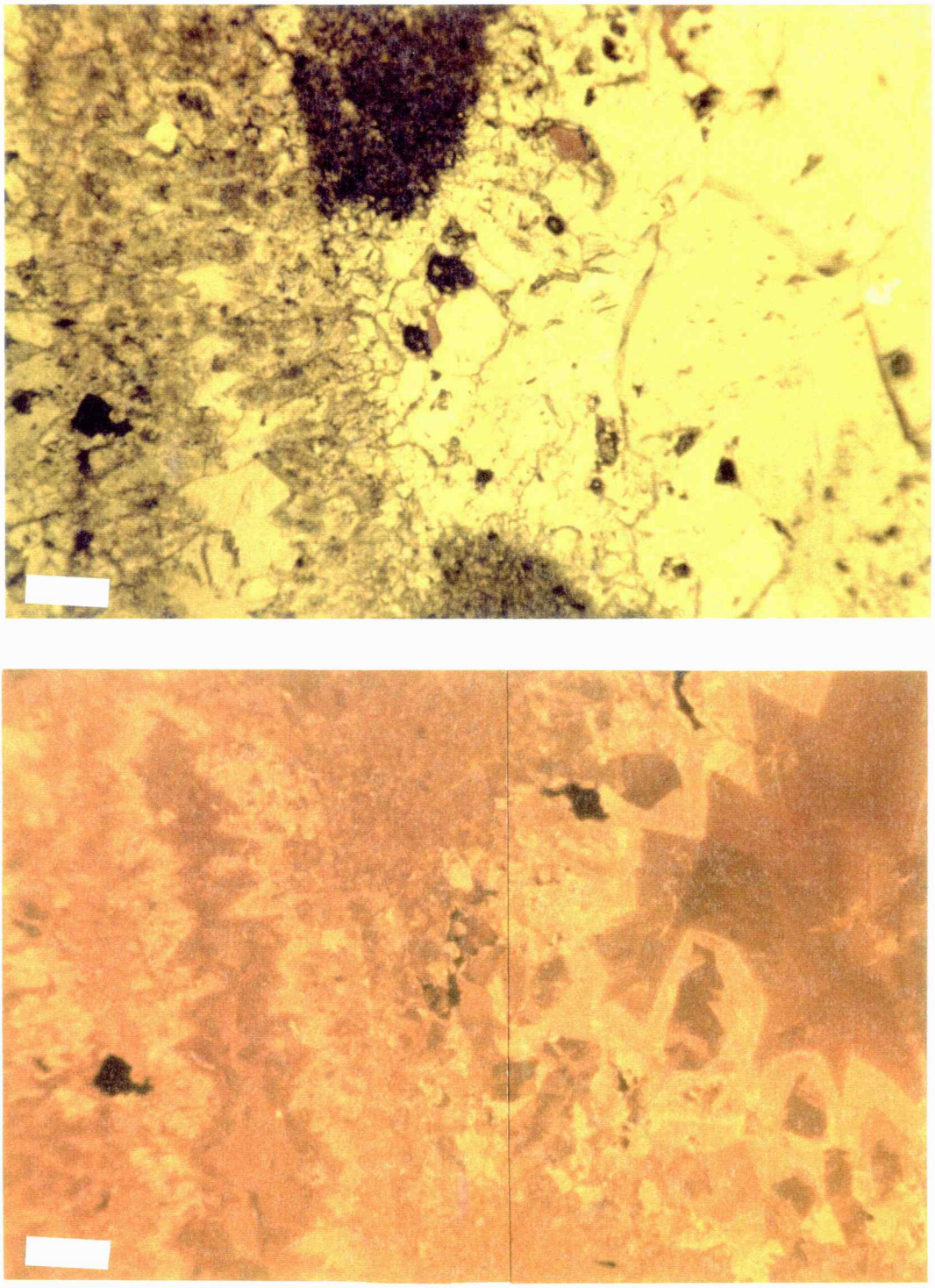

Figure 3.15. Dissolution fabrics and late-stage cementation. Scale bar 50 microns. Top of Argentine at PE8. TOP, PPL. BOTTOM, CL.

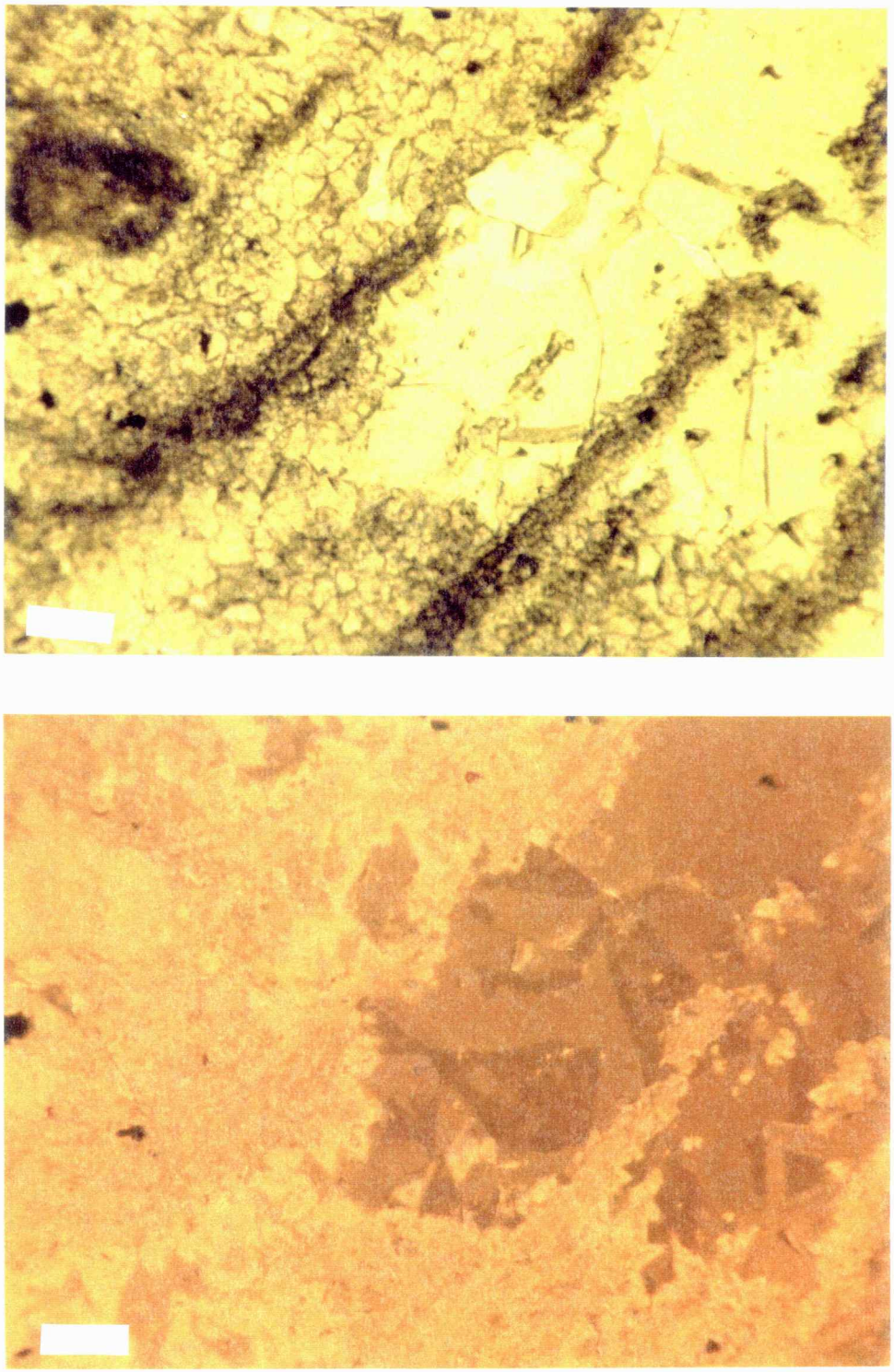

Figure 3.16. Possible crystal coarsening (Ostwald ripening) of micritic carbonate, represented by growth of sparry domains (S) surrounded by impurities. Scale bar 670 microns, PPL. TOP: Argentine Limestone, PE8. BOTTOM: Argentine Limestone, 8 feet below top, SP5.

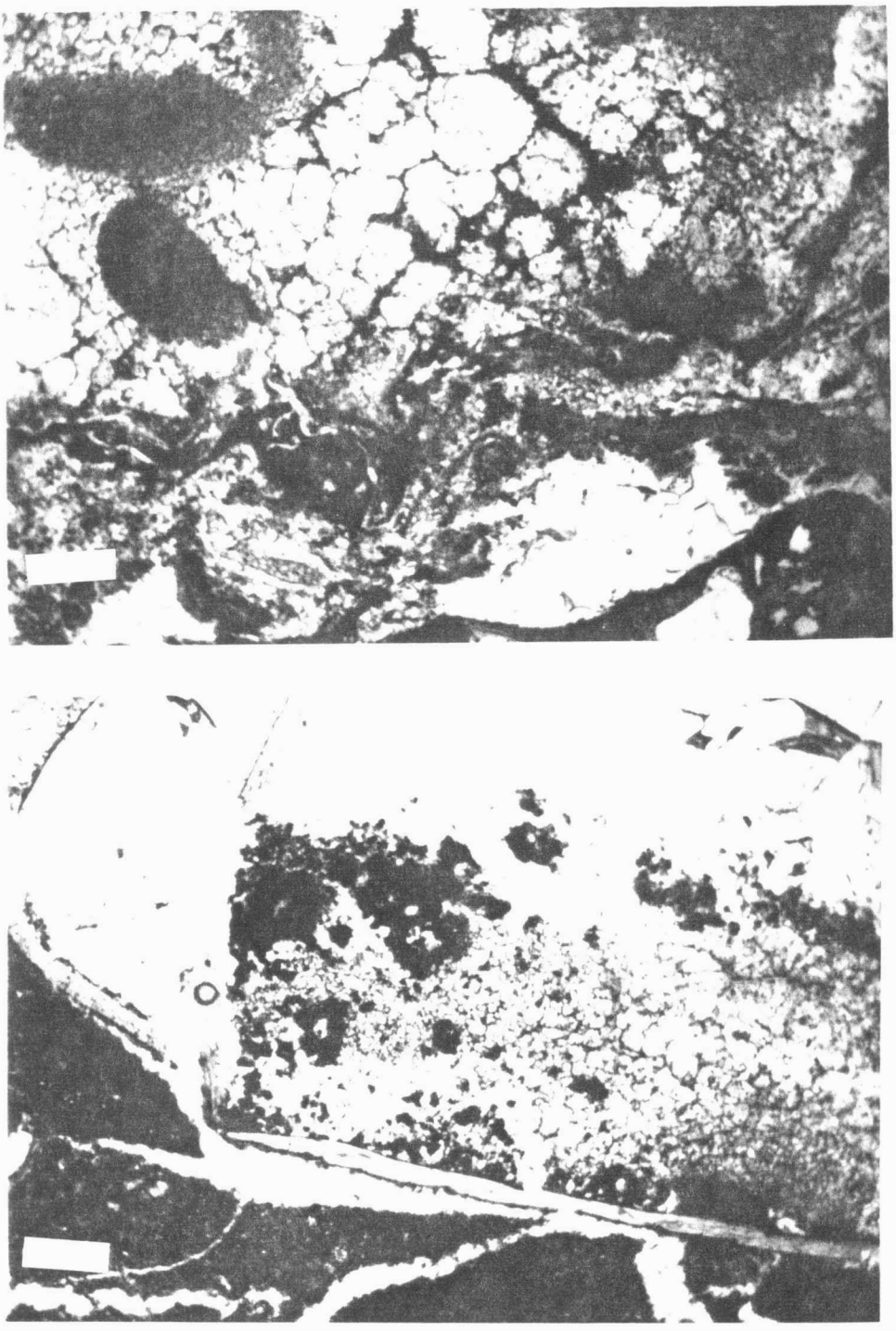

CHAPTER IV

CARBONATE GEOCHEMISTRY

Trace element distributions in calcites

Introduction

Although trace elements have enjoyed steady employment in the solution of petrologic problems, their use in diagenetic interpretations of ancient sedimentary rocks is relatively recent. Much of the published work using trace element analysis in diagenetic carbonates concerns itself with the documentation of the extent of rock interaction with meteoric water. As one example, BRAND and VEIZER (1980) used statistical trends in manganese and strontium distribution in fossil components (brachiopods, crinoids, and rugose corals) extracted from Silurian and Mississippian rocks to gauge the extent of their diagenetic equilibration with meteoric water. They argued that theoretical considerations predicted the progressive loss of strontium and acquisition of manganese by carbonates during this equilibration process.

I argue that the incorporation of trace elements in carbonate cements of the Wyandotte Limestone was governed by

their fluid/solid partition behavior (as described by the partition coefficient), and that the availability of specific trace elements in diagenetic fluids was controlled by:

1) the extent of rock interaction with meteoric water,

2) the concentration of these elements within metastable constituents of the bulk rock undergoing dissolution, and

3) the concentration of aqueous oxygen versus sulfide.

These controls will be discussed below.

Trace element partitioning

Trace amounts of Na, Mg, Mn, Fe, Cu, Zn, Sr, Ba, and Pb may be present in the $CaCO_3$ lattice, and may be accommodated in limited solid solution by direct substitution for Ca^{2+} at regular metal sites, or by interstitial residence between lattice planes. Other modes of occurrence include surface adsorption (attraction by surface ions with unsatisfied charges), or as fluid or solid impurities trapped by occlusion during host crystal growth (MCINTIRE, 1963). All work in this thesis assumes direct substitution in solid solution with $CaCO_3$ to be the mode of occurrence of trace elements studied.

Under equilibrium conditions, components present in trace quantities in an aqueous solution will partition between the fluid phase and solid mineral precipitate in a

ratio that is characteristic of the trace component, carrier component, and the host mineral (MCINTIRE, 1963). This ratio is known as the distribution coefficient D,

$$D = \frac{\left[\frac{Tr}{Cr}\right]_S}{\left[\frac{Tr}{Cr}\right]_L,}$$

where Tr/Ca is the molar ratio of the trace component to the carrier component (Ca^{2+} for calcites), and the subscripts S and L refer to solid and liquid phases, respectively. During precipitation, trace components having partition coefficients greater than unity (D > 1) are enriched in the crystalline and depleted in the aqueous phase, relative to the carrier; conversely, tracers having a D less than unity are depleted in the crystal and consequently enriched in the liquid.

A prediction of the temporal redistribution of trace elements during carbonate diagenesis can be made through a comparison of measured D values, most importantly whether D is less or greater than unity. In addition to partition behavior, important parameters controlling calcite trace element distribution in time and space are the openness of the diagenetic system, proximity to surface water recharge,

temperature, and the availability of dissolved oxygen and sulfide. These parameters interact directly or indirectly to produce unique patterns in the trace element concentrations of diagenetic calcites, permitting possible reconstructions of the physicochemical conditions under which diagenesis took place. Interpretations are greatly facilitated if the following assumptions are made:

1) aqueous and solid phases of the rock were in equilibrium, and the concentrations of the trace components in solution were dilute;

2) the temperature and pressure under which partitioning was occurring were constant;

3) the rate of precipitation was constant.

Equilibrium between aqueous and solid phases is a legitimate assumption if the ratio between the number of moles of instantaneously precipitated solid and of dissolved material in the system's fluid is small. In this case composition of the fluid, after the precipitation event, has been changed by only an infinitesimal amount, and reversibility should thus exist.

As the solution becomes progressively supersaturated, the observed D value will vary from equilibrium D according to the DOERNER and HOSKINS (1925) logarithmic (heterogeneous) distribution law. If the rate of crystallization is directly correlated with the degree of

supersaturation, high rates of crystallization should result in significant departures of D from equilibrium value. Variation of D with crystallization rate has been observed for Sr and Mn (LORENS, 1981; MUCCI, 1988). REEDER and GRAMS (1987) also found significant variations of D in calcite with respect to crystal growth sector for Mg, Mn, and Sr. Variation has been observed for D_{Sr} in calcite and aragonite during early stages of crystal growth (KITANO et al., 1971). Temperature has been found to exert a major control on $D_{Sr,aragonite}$ (KINSMAN and HOLLAND, 1968). Lastly, other coprecipitating cations, due to changes in surface free energy brought about by lattice deformation, can also alter partition coefficient values (ICHIKUNI, 1973).

Controls on strontium and magnesium distribution

As an example, assume a hypothetical marine carbonate sediment to exist with Sr^{2+} and Mg^{2+} incorporated in metastable aragonite and magnesian calcite (HMC), respectively, distributed as skeletal components and abiotic marine cements. Assume also that this carbonate is situated in the shallow subsurface relatively close to meteoric recharge, due to a post-depositional eustatic fall. During early diagenesis, these metastable phases are initially dissolved in undersaturated meteoric water. Dissolution proceeds congruently, i.e., Sr^{2+} and Mg^{2+} (and of course major cations as well) are released stoichiometrically into

solution, until calcite saturation is reached. At this point, diagenetic low-Mg calcite (dLMC) begins to precipitate, although aragonite and HMC may still be undergoing dissolution. Measured D values for both Sr and Mg in calcite are less than unity, with $D_{Mg} < 0.06$ and D_{Sr} ranging from 0.05 (for aragonite or HMC transformation to dLMC, recommended by VEIZER, 1983, p. 3-6) to 0.14 (KINSMAN, 1969). Partitioning dictates that the dLMC that precipitates in this process will acquire a lower trace metal/calcium ratio compared to that of the fluid, reflecting a transition to incongruent dissolution (LOHMANN, 1988). Conversely, this initial cycle of dissolution-reprecipitation also leaves the residual pore fluid enriched in these components (higher trace metal/Ca^{2+} ratios).

What occurs next is dependent on the openness of the hydrologic system. The velocity of the fluid through pore spaces (relative to the movement of ions to and from surfaces of precipitation and dissolution) controls whether that same parcel of water, with its now higher Mg^{2+}/Ca^{2+} and Sr^{2+}/Ca^{2+} ratios, can participate in further reactions at the same crystal site.

If the hydrologic regime is relatively open, that parcel of fluid will move downflow, and that which replaces it will once again have the identical Mg^{2+} or Sr^{2+}/Ca^{2+} ratio

of the dissolving metastable carbonate. The fluid moving downflow will precipitate more dLMC, further enriching itself in Mg^{2+} and Sr^{2+} relative to Ca^{2+}. Thus the Sr^{2+}/Ca^{2+} and Mg^{2+}/Ca^{2+} in a downflow fluid that has participated in numerous (early) cycles of dissolution and reprecipitation in transit would equal or surpass that of the original dissolving (upflow) carbonate phase.

The undersaturated meteoric water that recharges the system will dissolve not only more original metastable material, but can also remove at least some of the dLMC cements precipitated during the previous cycle. These cements were depleted in Sr and Mg, and the resulting solution will thus reflect this loss. As this fluid moves downflow and achieves calcite saturation, it will precipitate dLMC that is lower in Sr and Mg compared to earlier downflow calcites. Thus two predictions can be made concerning temporal and spatial variations of Sr and Mg in meteoric dLMC cements formed in relatively <u>open</u> diagenetic systems:

1) at a given site of precipitation, earliest formed dLMC will exhibit higher Sr/Ca and Mg/Ca ratios than its later equivalent, but

2) dLMC precipitated in downflow positions should always exhibit higher ratios than upflow precipitates formed from the same bulk solution (KINSMAN, 1969).

In addition, the composition of downflow dLMC is probably more reflective of the volumes of rock through which its parent fluid moved prior to precipitation, and less of the host rock with which it is in contact. These predictions are valid for cementation within a shallow meteoric aquifer.

Let us compare this open system model, in which a given parcel of water participates in relatively few dissolution-reprecipitation reactions at a single site, with that of a closed system, in which that parcel of water undergoes extensive reaction with a given volume of host rock. Calcite saturation will be reached in sites closer to recharge, as the boundary separating the zone of net removal from net acquisition of material is found at shallower depth. Partitioning of Sr^{2+} and Mg^{2+} in closed diagenetic systems ensures that every cycle of dissolution and reprecipitation leaves the fluid progressively enriched in these components. This process will continue until a steady state is achieved, and the tracer/calcium ratio of the dissolving phase equals that of the precipitating dLMC (KINSMAN, 1969). Such a reaction can easily be simulated numerically through iterative computation of molar ratios of trace and carrier elements in the precipitate and coexisting fluid. Figure 4.1 traces the evolution of Sr/Ca and Mg/Ca ratios of diagenetic calcites and coexisting fluids, with

precipitation in 2.5 millimole increments from a fluid saturated with a dissolving carbonate, the dissolving phase itself having between 750 and 75400 ppm Mg, and between 1000 and 9400 ppm Sr. These concentrations embrace the theoretical range of abiotic marine aragonites and magnesian calcites precipitated in equilibrium with normal seawater (the variations generated by the uncertainty in D values.) Bounding assumptions of this particular simulation are $D_{Mg,calcite}=D_{Sr,calcite}=0.05$, and a constant cation concentration of 2.5 millimoles in one liter of solution. For the sake of simplicity, the simulation treats each trace element separately, as if it were the only cation, besides Ca^{2+}, in solution. (The BASIC program generating the data for this and subsequent plots is reproduced in Appendix B). The simulation illustrates the attainment of steady state condition (zero slope), given a sufficient number of dissolution and reprecipitation cycles, under closed system diagenesis.

As stated earlier, in open diagenetic systems fluid is constantly moving downflow, and thus its participation in dissolution-reprecipitation activity <u>per site</u> is limited. Although Sr^{2+} and Mg^{2+} enrichment of a parcel of fluid should take place as downflow transit proceeds, the aqueous concentration of these elements available for cementation at a given upflow crystal site should decrease with time. This

is due to ultimate exhaustion of high-Sr and -Mg metastable phases, and progressive attack on earlier precipitated Sr- and Mg-poor dLMC.

This predicted trend of temporally decreasing Sr and Mg concentrations in pore-filling dLMC cements in open systems stands in contrast with the trend of increasing concentrations of these tracers in cements precipitated under closed system diagenesis. Under closed system diagenesis the position of the diagenetic site relative to recharge (through its relationship to fluid history) will determine the starting fluid composition, but temporal enrichment in Sr and Mg should result nonetheless.

The degree of closure or openness of the diagenetic environment also is critical in determining the P_{CO_2} of the diagenetic fluid. Atmospheric equilibration and biological respiration at or near surface environments provide the principal sources of dissolved CO_2 for diagenetic fluids (LLOYD and HEATHCOTE, 1985). Dissolution or precipitation of calcium carbonate can be effectively summarized by the reaction:

$$CaCO_3 + CO_2 + H_2O = Ca^{2+} + 2HCO_3^-$$

Because a closed system is, by definition, isolated from external inputs, the consumption of CO_2 through carbonate dissolution will deplete the fixed store of dissolved gas and raise pH (through consumption of bicarbonate HCO_3^- ion)

until calcite saturation is reached. Closed diagenetic systems thus reach calcite saturation at a higher pH and lower HCO_3^- concentration compared with open systems that are not isolated from the atmospheric CO_2 reservoir (LOHMANN, 1988).

Real diagenetic systems, in all probability, will exhibit neither ideal closed nor open behavior. The ideal models described above form two end members of a spectrum in which real behavior resides. For example, with increasing openness, the predicted closed system trend of increasing Sr^{2+} and Mg^{2+} concentration with time, should change to one of decreasing concentration (assuming that the rock and its diagenetic products form the only source of these components). This spectrum of Sr^{2+} and Mg^{2+} trends, ranging from ideal closed to progressively open, is illustrated schematically (for Sr^{2+}) in Figure 4.2.

Cements precipitated during deeper burial diagenesis would presumably differ from those emplaced in a shallow phreatic environment. Such cements would have formed under conditions of elevated temperature and pressure, and have access to more exotic, highly evolved fluids. Whether such cements have a unique and recognizable trace element signature is not well understood, and much of the discrimination between shallow phreatic and deeper burial cements is made of the basis of isotopic data, fluid

inclusion, and supporting evidence from transmitted light and cathodoluminescent petrography (LUDVIGSON, 1988; DOROBEK, 1987; GROVER and READ, 1983). Redox models (FRANK et al., 1982) focus on Eh changes, discussed below, to which Sr and Mg are insensitive, being readily available in the divalent state in both oxic and anoxic regimes. Partition theory dictates the progressive scavenging of Sr^{2+} and Mg^{2+} by fluids that ultimately reside in the burial environment. Cements characterized by significant enrichments in these elements, in tandem with textural evidence that rules out a primary marine origin, would thus be interpreted as having formed in a deeper burial setting.

Ferroan cements are often noted in burial environments, but iron content alone is not an accurate reflection of fluid-rock interaction, being controlled by local Eh conditions and sources of supply. As discussed below, the lack of sensitivity of ferric phases to early changes in Eh potential also renders iron a poor index of early diagenetic changes.

LUDVIGSON (1988) argued that fracture-filling calcites exhibiting elevated concentrations of <u>both</u> Sr^{2+} and Mn^{2+} were indicative of marine carbonates that had stabilized in a burial environment remote from recharge sites. Elevated Sr^{2+} concentrations would have resulted from previous

partition cycles, and Mn^{2+} enrichment through reduction of Mn oxide reservoirs.

In summary, the progression of Sr and Mg concentrations in void-filling diagenetic calcites provides a means to evaluate the openness or closure of the diagenetic system, i.e. the extent of rock interaction with a given volume of fluid. Conformable void-filling sequences (those that record uninterrupted cement growth), characterized by increasing concentrations of these tracers from earliest to latest cements, should identify relatively closed diagenetic systems. Conversely, cements exhibiting decreasing trends should have formed in more open diagenetic settings.

In addition, the Sr and Mg concentration of earliest-formed dLMC may or may not depart from that of original marine phases (aragonite and HMC). The magnitude and sign of that departure is an indication of the proximity of recharge. In open systems, early dLMC formed close to recharge should be poor in these tracers. This is ensured by the limited reaction time a given parcel of water spends in dissolution-reprecipitation activity at a single site, and the low values of $D_{Mg,calcite}$ and $D_{Sr,calcite}$. Early dLMC formed in more distal portions of the aquifer should show enrichment relative to proximal sites due to the previous partition history of the parent fluid. Closed systems should exhibit similar trends, with enrichment of early dLMC

occurring higher within the aquifer due to the greater number of partition cycles a given parcel of fluid will have experienced prior to final cementation. Thus proximity to recharge determines the starting point for diagenetic paths; openness or closure of the diagenetic system determines the slope of the path itself.

Controls on manganese and iron distribution

In addition to Sr^{2+} and Mg^{2+}, fluid/solid partitioning also controls the incorporation of dissolved Fe^{2+} and Mn^{2+} into diagenetic calcite. Although laboratory determinations of D have revealed its variability and sensitivity to changes in temperature and precipitation rate (LORENS, 1981), partition coefficients for both Mn^{2+} and Fe^{2+} are greater than unity ($D_{Mn,calcite}$=15, PINGITORE, 1978; $D_{Fe,calcite}$=5, VEIZER, 1983). During precipitation, dLMC will be enriched in these elements, thus leaving the fluid impoverished. However, the efficiency of partitioning here is much greater than for Sr^{2+} and Mg^{2+}. In Sr^{2+} (closed system) partitioning, each partition cycle adds an increment of Sr^{2+} to the fluid, but that increment is an ever decreasing fraction of the total store of Sr^{2+} in solution. In contrast, each (closed system) partition cycle of Mn^{2+} or Fe^{2+} draws off an ever increasing fraction of the total fluid store of these cations, and thus depletion occurs very rapidly. Therefore under closed system diagenesis, a steady

state equilibrium, in which the Mn or Fe concentration of the dissolving phases equals the reprecipitating dLMC, is approached with far fewer dissolution-reprecipitation cycles, as compared to Sr or Mg. This is graphically illustrated in Figure 4.3, which again simulates closed system behavior, and compares tracer/calcium ratios of Sr^{2+} and Mn^{2+}, using a dissolving marine aragonite source for Sr and magnesian calcite source for Mn.

Up to this point it has been assumed that the only sources of tracers available for reprecipitation in diagenetic phases are the metastable carbonates undergoing dissolution. (Recall Figure 4.1, which assumed Sr and Mg concentrations in marine aragonite and HMC of 1000-9400 and 750-75400 ppm, respectively). Normal oxic seawater is relatively poor in dissolved Mn and Fe, containing 0.2 and 2 ppb, respectively (DREVER, 1982, p. 234, table 10-1). Aragonite and HMC precipitated in equilibrium with seawater would thus contain 8 ppm Mn (D_{Mn}=15) and 25 ppm Fe (D_{Fe}=5), assuming all Mn and Fe to be in the [II] oxidation state.

Higher concentrations of Mn^{2+} could occur in marine pore waters participating in suboxic diagenesis, where upward diffusion of Mn^{2+} (reduced and mobilized in accumulating sediments) is balanced by downward oxygen diffusion. The balance of these fluxes can give rise to a layer of enriched MnO_2 in deep ocean sediments (FROELICH et

al., 1979). If this MnO_2 were later reduced in pore water supersaturated with regard to calcite, manganoan calcites could be precipitated. Such processes demand suboxic marine settings however, and it is difficult to establish whether such conditions existed during deposition of any of the Wyandotte members.

BRAND and VEIZER (1980) asserted that because meteoric water in general contains more Mn^{2+} and Fe^{2+} than seawater, increasing exposure of primary marine carbonates to meteoric water will shift their trace element composition in that direction. In addition, they argued that D values greater than unity for Mn^{2+} and Fe^{2+} also demand that diagenetic products will be enriched in these elements. As mentioned previously, they assembled statistical data using fossil components (representing original marine aragonite, HMC, and LMC), and used Sr^{2+} and Mn^{2+} concentration crossplots to show the extent of diagenetic alteration, one of which is reproduced in Figure 4.4.

Two complications exist in this approach, however. First, regardless of the source or starting concentration of Mn and Fe in solution, it is clear that these tracers are rapidly and effectively scavenged by precipitating dLMC. Also, both metals readily assume higher valence states in the presence of dissolved oxygen, and precipitate from groundwater as insoluble oxide and hydroxide phases (Fe_2O_3,

Fe_3O_4, $FeOH_3$, Mn_2O_4). These oxide precipitates may form sizeable local reservoirs that may later be liberated in solution if reducing conditions develop. LUDVIGSON (1988) invoked this mechanism to explain extreme manganese enrichments in oscillatory Mn-zoned meteoric phreatic calcites. Thus the presence of ferroan and manganoan calcites is primarily an indicator of diagenesis under anoxic conditions. Dissolved oxygen supplied in recharging groundwater is the most efficient oxidant of dissolved organic matter acquired in transit through surface soils. If excess organic matter still exists after dissolved O_2 is consumed, NO_3-, Mn_2O_4, Fe_2O_3 (or FeOOH), SO_4^{2-}, PO_4^{3-}, HCO_3^-, and N_2 will act as successive electron acceptors, the precise order and overlap determined by decreasing Gibb's free energy release for each reduction reaction, and openness or closure of the system (CHAMP, GULENS, and JACKSON, 1979). The presence of Mn or Fe in dLMC cements is thus a more accurate indicator of the anoxic environment (BERNER, 1981) than of water-rock interaction, as astutely noted by LOHMANN (1988).

Second, the approach of BRAND and VEIZER (1980) cannot reveal the <u>temporal</u> progression of trace metal concentrations from original carbonate phases to diagenetic counterparts. Fossil and rock matrix components may record information of their <u>last</u> encounter with diagenetic fluids,

but preserve little of early diagenetic history. Alternately, they may record the successive imprint of changing diagenetic regimes, but afford no easy way of resolving any temporal sequence. Void-filling calcite cements, if emplaced early in the rock's diagenetic history, potentially offer a diary of groundwater chemistry. The succession of dLMC cement zones are easily made visible through cathodoluminescence, and zones can then be analyzed for Mg, Ca, Mn, Fe, and Sr concentrations through electron microprobe analysis.

Although Mn and Fe substitution in calcites is an indication of anoxic diagenesis, the presence of one does not necessarily demand the other. BERNER (1981) characterized sedimentary and diagenetic environments based on the occurrence of certain mineral phases thermodynamically stable in the presence of dissolved O_2 versus dissolved sulfide ($H_2S + HS^-$). He divided the anoxic environment ($[O_2]<10^{-6}M$) into sulfidic ($[H_2S]>=10^{-6}M$) and nonsulfidic ($[H_2S]<10^{-6}M$), which he in turn further subdivided into post-oxic and methanic. The stability of mineral phases in the oxic and anoxic environments are determined by calculation of the standard state free energy change for the reactions listed in Table 1.

Two observations can be made concerning these reactions. First, siderite is consumed in both oxic and

anoxic environments, and is stable only in the absence of dissolved sulfide, a characteristic of the anoxic nonsulfidic environment (note that production of pyrite from siderite does not involve a change in the oxidation state of iron). Rhodochrosite on the other hand, is stable in both anoxic sulfidic and nonsulfidic (methanic and postoxic) environments. Second, there is a much greater tendency for hematite to be produced in the oxic environment, either through oxidation of pyrite or siderite ($G°_r$, -789 and -346 kJ mol^{-1}, respectively), than consumed in the anoxic sulfidic environment ($G°_r$, -106 kJ mol^{-1}). In other words, ferric iron is less unstable in an anoxic, reducing environment than ferrous iron is in an oxic regime. For iron to be available for incorporation into dLMC, it must exist in (II) valence, but the comparative insensitivity of ferric phases to dissolved oxygen makes rhodochrosite (and manganoan calcites) a far better indicator of anoxic environments (BERNER, 1981). Siderite (and therefore presumably ferroan calcite, with or without Mn^{2+}), because of its instability in the presence of dissolved sulfide, is thus a unique indicator of anoxic <u>nonsulfidic</u> environments. Ferroan void-filling calcites, if <u>intimately</u> associated with pyrite, may represent a supply of Fe^{2+} in solution in excess of dissolved S^{2-}, or a disequilibrium assemblage.

The assumption that Eh calculated or estimated from dissolved oxygen is comparable with Pt electrode-measured Eh has also been called into question (BERNER, 1981; BARNABY and RIMSTIDT, 1989). Barnaby and Rimstidt assert that Pt electrode Eh compares very well with the activities of iron and manganese redox pairs ($Fe^{2+}/Fe(OH)_3$, Mn^{2+}/MnO_2), but may be unrelated to the redox potential calculated from the $O_2(aq)/H_2O$ redox pair. Lack of agreement between redox conditions defined by independently calculated Mn^{2+} and Fe^{2+} activities also suggest that the oxide half for the Mn redox pair is more stable than pyrolusite. By using a fictive MnO_2 phase more stable than stoichiometric pyrolusite, BARNABY and RIMSTIDT (1989) were able to reconcile observed Mn^{2+} and Fe^{2+} concentrations in shallow carbonate aquifers, and thus their expected concentrations in calcite cements, with thermodynamically calculated Eh values.

Using their revised Eh-pH diagrams (Figure 4.5), it can be seen that under similar Eh conditions, Fe^{2+} should have roughly the same activity as Mn^{2+}, and therefore show a similar availability (assuming an absence of S^{2-}) to precipitating calcite. Concentrations of Mn greater than Fe in dLMC should thus be an indication both of a particular Eh regime and S^{2-} availability.

This revision of the Eh-pH stability field for Mn^{2+} has important ramifications for predictions concerning

diagenetic trends in Mn and Fe concentrations in dLMC. Previous work (HEM, 1972) predicted more Mn^{2+} in solution than Fe^{2+} for any Eh and pH likely to be encountered in natural waters. Diagenetic redox models (e.g., FRANK et al., 1982) thus typically forecasted an initial appearance of Mn in dLMC as Eh drops during burial, due to reduction and solution of tetravalent and trivalent Mn oxides. Appearance of Fe is delayed until greater reduction occurs due to the higher stability of Fe oxide phases ($G°_f$ for ferric hydroxide of -695 kJ mol^{-1} versus -466 kJ mol^{-1} for pyrolusite, BERNER, 1981). If carbonate aquifers are in equilibrium with an Mn oxide phase more stable than pyrolusite, this would also delay the appearance of Mn, and thus necessitate alternative explanations of Mn/Fe ratios that show significant departure from unity.

Diagenetic calcites that exhibit Fe concentrations in excess of Mn could be explained either by introduction of allochthonous Fe^{2+}, or an increase in Eh of a sulfidic system (presumably due to introduction of another oxidizing agent), oxidation of sulfide to sulfate, thereby making Fe previously sequestered in pyrite available for coprecipitation with dLMC.

Observed differences in Mn and Fe concentrations in dLMC may also be a function of differing partition coefficients. Because the partition coefficient for Mn in

calcite is generally recognized as greater than that for Fe, equivalent amounts of Fe and Mn in solution will not coprecipitate with calcite at the same rate. This is shown by the simulation in Figure 4.6, which assumes $D_{Mn,calcite}$=15 and $D_{Fe,calcite}$=5. Under closed system diagenesis, early cements (assuming equal Fe and Mn concentrations in the dissolving phase) would theoretically show Mn > Fe. As precipitation proceeds, relative concentrations would converge, meet, and depart again, thereafter with Fe > Mn. The concentration of both cations would ultimately approach a common value, controlled by that of the dissolving phase. Although it is more likely that concentrations of Fe and Mn in meteoric dLMC reflect redox conditions rather than such idealized partition behavior, such controls are important to consider in settings where high rock-water ratios, isolation from Eh perturbation, and closed system diagenesis may be in effect.

Summary of model for trace element variations in meteoric calcites

A model has been presented with which to interpret spatial and temporal variations in trace elements substituting for Ca in diagenetic calcite cements. This model asserts that the distribution of Sr and Mg in these calcites is strongly controlled by their similar partition behavior, and the closure or openness of the diagenetic system. Closure will produce high rock-water ratios, and

should be manifested by progressive Sr and Mg enrichment in void-filling cement sequences. Open systems, conversely, will produce low rock-water ratios and progressive depletion of these tracers. The position of the cement site relative to surface recharge should be related to the composition of the earliest cement zone precipitated. Voids closer to recharge should host earliest cements showing lower Sr and Mg concentrations compared to earliest phases precipitated in more distal sites. This matrix of possible trends for Sr and Mg, as well as Fe and Mn, is summarized schematically in Figure 4.7. (Note that this representation strives only to highlight broad differences in hydrologic regime, as reflected by relative concentrations of trace elements within growth sequences of void-filling cements, and is not intended as an actualistic model of any subsurface system).

Mn^{2+} and Fe^{2+} availability is more strictly controlled by redox reactions, the availability of other oxidants, and the concentration of dissolved sulfide, than solely by partition behavior. Partition theory alone predicts the rapid incorporation of these cations in precipitating dLMC (Fe^{2+} going first into pyrite), with temporal changes in the relative concentrations of Fe and Mn under closed system diagenesis reflecting differences in D values. The presence of ferroan and manganoan calcites can also be profitably examined from a thermodynamic perspective, using the

stability of these phases in the presence or absence of dissolved sulfide or oxygen to define equilibrium assemblages. Because they are not found in abundance in carbonates precipitated in equilibrium with normal marine water, Mn and Fe concentrations in diagenetic calcites are not reliable indicators of the degree of rock-water interaction (LOHMANN, 1988).

General application of trace element diagenetic model to Midcontinent Pennsylvanian cyclothems

There has been relatively little application of trace element techniques to meteoric cements of Midcontinent Pennsylvanian cyclothems. HECKEL (1983) predicted Fe enrichment in calcites would be restricted to reducing conditions of the deep burial connate environment, most often represented by euhedral spars developed after compaction within transgressive limestones, and presented petrographic evidence in support of this association. MEYERS (1974), in his pioneering work on cement stratigraphy within crinoidal shelf and bioherm facies of Mississippian age, used cathodoluminescence and staining techniques to reveal the compositional zonation of syntaxial meteoric calcites, and to document their persistence both laterally and vertically. His interpretation of evolving diagenetic conditions hinged on the appearance of late ferroan calcites (with or without coprecipitated Mn). GOLDSTEIN (1988)

presented a study of cement stratigraphy within Pennsylvanian (Virgilian of New Mexico) strata that focused on vertical and lateral correlation of cement zones, again identified through cathodoluminescence petrography. Cement zones were grouped as the products of phreatic lenses (15 apparently identified) developed during successive eustatic cycles. However, only minor attention was paid to the expected distribution of trace elements, and Mg and Sr data were used simply to rule out a marine origin. The temporal progression of Mn and Fe concentrations was interpreted as compatible with decreasing Eh potential during descent from near to subsurface regimes.

Abundant petrographic evidence collected throughout the Midcontinent outcrop belt has indeed borne out the predicted association (HECKEL, 1983) of particular diagenetic fabrics and textures to genetic members of the Kansas-type cyclothem. Integrating a trace element model with this successful textural framework should yield a means to interpret diagenetic environments on an even finer scale, and to address enigmatic diagenetic textures and associations that have eluded satisfactory explanation thus far.

For example, the discrimination between meteoric diagenetic environments characterized by relatively open versus restricted pore fluid circulation is not easily made

on the basis of textural evidence. Blocky calcite euhedra should be the characteristic precipitate in either case. The temporal distribution of Sr and Mg could provide a reliable and consistent means of distinguishing e.g., the active-saturated and the stagnant-saturated zone of the meteoric phreatic environment. The products of neomorphism (e.g., exquisite preservation of skeletal microfabrics, crystal coarsening, etc.), a process HECKEL (1983) ascribed to the stagnant-saturated zone, could be analyzed in terms of their trace element geochemistry, and further insight gained as to the physicochemical environment in which this process occurred.

HECKEL (1983) also explained the typical lack of textural evidence of extensive meteoric diagenesis in transgressive limestones by their confinement in the marine phreatic environment (prior to ultimate descent into the deeper burial connate regime), with the overlying offshore core shale member providing protection as an aquiclude. Void fills in the underlying transgressive member should theoretically host a trace element history typical of closed system diagenesis, and bear little evidence of early equilibration with meteoric fluids.

Cathodoluminescence petrography has revealed a complex history of meteoric cementation for the Wyandotte Limestone. The purpose of trace element analysis of void-filling

cements within the Wyandotte Limestone is to better characterize the physicochemical conditions under which (early meteoric) diagenesis of stratigraphic members took place. Temporal variations in Sr and Mg concentrations are examined as indicators of the path and extent of equilibration of rock components with meteoric fluids. Relative and absolute concentrations of Mn and Fe in this case will probably reflect the proximity of local sources (both from marine and prodeltaic shales), but should nevertheless differentiate between residence in oxic versus anoxic, sulfidic versus nonsulfidic environments. Lastly, comparison between the inferred succession of diagenetic environments expressed by trace element variation within void fills from different Wyandotte stratigraphic members at the same locality, and from the same member in adjacent but different inferred depositional environments, could reveal associations between depositional and early diagenetic environments that are largely transparent to standard petrographic examination.

Application of cathodoluminescence (CL)

Since its introduction as a petrographic technique, CL has seen increasing application as a qualitative and even semi-quantitative tool, as it offers a relatively inexpensive, nondestructive, but highly sensitive means of

resolving microscale variations in mineral composition. Among the principal uses in sedimentary petrology are

1. the graphic delineation of crystal growth zones and interpretation of equilibrium Fe and Mn concentrations, and thus the redox potential, of the coexisting solution (DOROBEK, 1987; FRANK, CARPENTER, and OGLESBY, 1982; GROVER and READ, 1983);
2. resolution of crystal fabrics and textural relationships that are transparent to transmitted light microscopy;
3. correlation of growth zones (cement stratigraphy) having equivalent luminescent intensity and sequence, permitting interpretation and reconstruction of diagenetic events on a regional scale (MEYERS, 1974, GOLDSTEIN, 1989).

Much recent work has focused on defining with greater precision and accuracy how the relative and absolute concentrations of the activator-quencher pair,[3] Mn^{2+} and

---

[3]An activator ion, in the case of CL, emits visible light subsequent to absorption of energy from the incident electron beam. Mn^{2+}, in octahedral coordination in silicates, oxides, carbonates, and phosphates, is one of the most common activators, with energy transitions occurring in the unfilled 3d orbitals. Because these outer electrons are involved in coordination, Mn^{2+} activation is thus quite sensitive to site geometry and coordination environment, short-range cation ordering, lattice defects, etc., i.e., any contribution to crystal field strength.

A quencher ion is one having an absorption band that overlaps the emission peak of the activator ion. Fe^{3+}, Fe^{2+}, Ni^{2+}, and Co^{2+} are common examples, with Fe^{2+} the most common quencher in sedimentary calcite. Sensitizer ions are activators that exhibit no or reduced emission of their own in the proximity of a second activator, but instead transfer

Fe^{2+}, control the intensity of the luminescent response in calcite. In the most recent published effort to date, HEMMING, MEYERS, and GRAMS (1989) used microprobe analysis coordinated with spectrophotometric measurement of luminescent intensity (taken at a peak emission wavelength of 6400 Å) of Mn-, Fe-zoned calcites to document this control. Although minor discrepancies exist in their data, their conclusions are in general agreement with previous work: CL intensity was best correlated with absolute Mn concentration at a constant Fe/Mn ratio. At low intensities however, quite a range in Fe/Mn values produced identical measured intensity. Thus CL intensity is a function both of Fe/Mn ratio and absolute Mn and Fe concentrations.[4]

---

energy to the latter, which then responds with an intense emission. Pb^{2+}/Mn^{2+} is a common sensitizer/activator pair in calcite. Self-quenching occurs when high concentrations of activators interact, and results in energy transfer and nonradiative decay. WAYCHUNAS (1988) asserts that $MnCO_3$ is exempt from self-quenching behavior, which seemingly contradicts MASON's (1987) prediction that calcites with sufficient Mn substitution should be extinct. Given that solid solution between $CaCO_3$ and $MnCO_3$ is incomplete, it is as yet unclear whether self-quenching is observed for manganoan carbonates.

[4]They also noted that the maximum CL intensity of calcite may be solely controlled the Fe/Mn ratio, and that given sufficient Mn (>~150 ppm), even high Fe concentrations (10,000 ppm) will not extinguish luminescence. Above 100 ppm Mn, luminescence was generally observed, and because this concentration coincided with the approximate electron microprobe detection limit for Mn, they also concluded that CL in calcite may be activated by less than 100 ppm Mn. At low Fe concentrations (<0.1% by weight), intensity appeared to respond primarily to Mn concentration.

The primary use of CL in this thesis was twofold. First, as has already been discussed, CL petrography was used as a way of revealing the temporal relationship of various diagenetic features, such as compaction, neomorphism, and precipitation of early meteoric versus later burial cements. Second, CL was used to select void fills that preserved both some relics of metastable marine mineralogy, either as cement or skeletal grains, as well as an early meteoric cement sequence, and thus the stabilization history of the rock. Many voids contain cement that most likely formed in a burial setting, particularly those at the tops of algal mounds, whose residence in the undersaturated meteoric environment would have removed any early cement that had managed to precipitate. CL thus permitted the mapping of growth zones, and selection of appropriate microprobe transects. These data are discussed below.

Presentation of microprobe data

Discussion of individual microprobe transects

Trace element data (Mg, Mn, Fe, and Sr) were collected from seven cement transects: four from the Wyandotte algal mound complex at the SP5 Wagstaff quarry algal mound (Frisbie, Argentine, and Farley), two from PE8 (Argentine and Farley), one from BU6 (Farley), and one from LE2

(Farley). The four transects from SP5 will be discussed in detail, as they capture early cementation history, and illustrate the distinction between open and closed systems as discussed in the previous sections. A broad comparison of the path and extent of early diagenesis using data from other transects is made as well. The dataset itself appears in Appendix A.

Transect SP5-tFb

Figure 4.8 is a map of the calcite void fill collected 3.5 feet from the top of Frisbie Limestone at SP5, showing 20 microprobe sites along transect A-B, and the general CL petrography of the void fill area. The companion Figure 4.9 shows the inset area under CL at higher magnification. Sites 4 through 16 clearly define an oldest to youngest cement sequence, beginning with earliest, brightly luminescent cement (site 4), followed by subzoned cement of decreasing CL intensity (sites 5-8), poorly luminescent cement (sites 9-14), and final infilling with brightly luminescent cement (sites 15-16).

The division of this cement sequence into zones based on CL intensity is also reflected in the pattern of trace element distribution within each zone. Figure 4.10 plots the trace element concentration at each probe site, expressed as the log of the carbonate in weight percent. Following a minor initial drop in Sr concentration from

earliest, brightly luminescent cement at site 4, the pattern through sites 5 to 14 (moderately to poorly luminescent cement) is one of overall increase in Sr, suggesting precipitation in a closed system. Mg shows more variable behavior, paralleling Sr enrichment through certain zones, but also exhibiting local changes in concentration that are poorly or even negatively reflected by Sr. These local inconsistencies suggest either that physico-chemical changes that affected partitioning of one trace element may not have had an identical effect on other species, or that solid phase reservoirs for Mg may have existed that have not been accounted for in the overall model.

The earliest cement (site 4) contains roughly 1900 ppm Fe and 2100 ppm Mn, indicating anoxic conditions. Subsequent simultaneous depletion of Mn and enrichment in Fe (reflected by the monotonic decrease in CL intensity over sites 5-9) suggests that while Mn was rapidly scavenged by cement, Fe was being added to the system. Assuming a closed system, Fe previously locally sequestered in sulfides may have become available given a slight rise in Eh, as explained previously. Sites 9 through 14 exhibit slight overall increases in Fe and Mn but maintain a Fe/Mn ratio of about 20.

The appearance of a late luminescent cement at sites 15 and 16 is marked by a large increase in Mn concentration,

and contrasting, large decreases in Fe, Sr, and Mg (over an order of magnitude in the case of Sr). Large Sr and Mg decreases indicate a fundamental change in overall pore water chemistry, possibly reflecting a late stage transition to open circulation. The simultaneous decrease in Fe and increase in Mn may have been a response to increased availability of dissolved sulfide, and the precipitation of Fe^{2+} in sulfide minerals rather than calcite (although no sulfides are visible within the cements themselves). MnS is stable only at very high concentrations of dissolved sulfide (BERNER, 1981), and thus available Mn^{2+} would have coprecipitated immediately with calcite. This transition may thus have marked a return to the anoxic sulfidic regime, possibly concurrent with a later eustatic high stand.

Transect SP5-bAg

Luminescent calcites collected from the base of the Argentine at SP5 display a cement stratigraphy similar to but less extensive than that of the underlying Frisbie, and lacking late stage luminescent spars. Figure 4.11 describes the general petrography and position of the microprobe transect. Figures 4.12 and 4.13 show in detail the CL petrography and compositional data, respectively, from a portion of the transect having a continuous growth sequence (sites 28, earliest, to 11, latest). Similarities between these data and the Frisbie transect include the initial

trend of Mn>Fe (sites 28 through 26), followed thereafter by Fe>Mn (sites 25 through 11, Fe/Mn approximately 5), and a general increase in Sr concentration. In contrast to the Frisbie, fluctuations in Mg concentrations are modest, and average concentration of Mg is higher. The presence of an early sulfide rim (Figure 4.11) predating calcite cementation is evidence of residence in the anoxic sulfidic environment, brought about most likely by the bacterial reduction of marine sulfate during anaerobic oxidation of algal organic matter.

Transect SP5-8bIC

Early calcite cement sequences within the upper Argentine are not commonly preserved, as most voids are algal in origin and retain only late cements that are exceedingly clear and free of inclusions and zonation, and display an even, moderate luminescence. The brachiopod cavity of transect SP5-8bIC (Figure 4.14) does host luminescent, relict early marine cement, followed by poorly luminescent, subzoned cement, and lastly by late cement just described. Figures 4.15 and 4.16 show CL petrography of the transect and elemental data, respectively. Compositional data for the first cement generation is unavailable. Poorly luminescent, subzoned cement (sites 2 through 4) shows decreasing concentrations of Mg, Sr, and Fe, and an increasing Mn concentration. Note that site 3 is a brightly

luminescent subzone within a dark field, and this is reflected by greater Mn concentration relative to sites on either side. The similar partition behavior of Sr and Mg is also reflected by their rough parallelism over this interval. The temporal relationship of the late cement data is not known with certainty due to the absence of CL zonation. Assuming the cements at sites 8 through 15 followed each other in time, they show generally increasing Fe and Mn, and decreasing Sr. No consistent Mg trend is present.

Transect SP5-bFa

A brachiopod void fill of the Farley Limestone is also used in transect SP5-bFa, whose general petrography is shown in Figure 4.17. Figures 4.18 and 4.19 show CL petrography and compositional data, respectively. Micrite is represented at site 1, and sites 2 through 8 represent early meteoric cement. Early cement shows a progressive depletion in Sr and Mg, with both elements again exhibiting roughly parallel behavior. Mn is relatively constant through this interval. Fe shows an overall increase from below detection limit at site 2 (Fe/Mn equal to or less than 0.1) to approximately 600 ppm at site 8 (Fe/Mn approximately 1.75). The remaining sites represent later, homogeneous cement with depleted Sr and Mg relative to earlier zones, Fe/Mn close to unity (sites 9-13), and early cement zones (encountered in

reverse order) towards the opposite margin of the void fill (sites 14-20).

In summary, the four transects show unique patterns in enrichment or depletion of Sr, Mg, Fe, and Mn. Early cements of the upper Frisbie and basal Argentine show Sr enrichment. Simultaneous Fe enrichment and Mn depletion is also characteristic, resulting in Fe/Mn ratios between 5 and 20, with Fe enrichment possibly controlled by sulfide dissolution. In contrast, early cements of the upper Argentine and basal Farley show temporally decreasing Sr. The behavior of Mn and Fe is more variable, with Fe decreasing in the Argentine and increasing in the Farley over early cement intervals, although both trend toward Fe/Mn ratios not far from unity. Mg appears to mimic Sr in systems during depletion, but shows local departures from Sr in systems undergoing Sr enrichment.

Comparisons of the path of early cementation in the Wyandotte Limestone

BRAND and VEIZER (1980) have argued that Mn is imported to and Sr lost from metastable marine components during progressive contact with meteoric water, and that equilibration of the bulk components thus follows the paths described in Figure 4.4, determined by the solubility of the carbonate mineral. These paths are not necessarily those recorded by a particular cement sequence. As has been

stressed previously, it is the relative openness or closure of the hydrologic system that determines whether Sr increases or decreases during continued precipitation. In addition, although Mn (and Fe) are more essentially dependent on Eh, once anoxic conditions in a closed system have been established and are maintained, the path of Mn change in a cement sequence should also behave according to partition theory. Cements precipitated by rock-dominated pore waters of closed systems will thus follow the L-shaped path of Figure 4.4, but in the opposite direction.

In contrast, cement precipitated in an open system will record declining Sr (as Sr is progressively depleted from upflow source areas of the aquifer). If anoxic conditions are present, Mn will increase as updip reserves of Mn oxide are mobilized. Thus the path for open system cement will mimic that of the bulk rock itself, as described in Figure 4.4.

These contrasting paths of Sr and Mn enrichment and depletion during early cementation are illustrated in Figure 4.20 (top), which plots Sr/Ca versus Mn in semilog format. Although the progress of a given cement sequence appears somewhat chaotic or random on a fine scale, in the case of the Frisbie (SP5-tFb) and basal Argentine (SP5-bAg) there is a general, overall change from high Mn/low Sr to low Mn/high Sr, thus describing diagenesis in a relatively closed

system. Note that the Sr concentration of early cement in both these rocks ultimately closes on a value near the equilibrium concentration of Sr in marine aragonite cement, in agreement with the simulations of Figure 4.1. Conversely, both the upper Argentine (SP5-8bIC) and Farley (SP5-bFa) early cement trends of decreasing Sr and increasing Mn mimic those predicted by BRAND and VEIZER (1980) for the bulk rock (compare Figure 4.4), and describe early meteoric diagenesis in an open system.

Figure 4.20 (bottom) also compares the open and closed system paths of the early cements just described at SP5 to those of cements at PE6/8 (Farley and Argentine) and BU6 (Farley). The progressive Sr depletion and Mn enrichment recorded by these cements indicate precipitation in an open but anoxic hydrologic system in which Mn oxides were reduced and incorporated into cement. Note that despite the differences in lithology of the Farley (geopetal brachiopod-algal calcilutite) and Argentine Limestone (onkoid-sponge) at PE6 and PE8, the Sr and Mn distributions within early cements of both rocks are remarkably similar. This suggests that precipitation occurred under similar conditions, possibly (although not necessarily) during the same diagenetic episode. The sequence recorded at BU6 (measured in two separate, slightly overlapping transects) exhibits initial depletion in Sr without corresponding enrichment in

Mn, which is similar to the trend observed for the Farley and upper Argentine at SP5 (SP5-bFa and SP5-8bIC, respectively, Figure 4.20 top).

The Mn concentration of virtually all early Wyandotte cements indicates an Eh potential sufficient to reduce Mn oxides. Whether Mn was continually enriched during Sr depletion, however, would have depended on both the overall maintenance of anoxic conditions and whether anoxic water had access to Mn oxide reservoirs. As Eh potential in groundwater systems is controlled primarily by organic matter oxidation, it is possible that the early enrichment in Mn at PE6/8 reflects proximity to the supply of fresh water, organic matter, and Mn oxides of the Lane Shale. The remains of terrestrial flora in the Lane Shale, which increase in abundance towards the type area, indicate that organic matter content was probably high. Groundwater flow through this clastic section could have had access both to the underlying Argentine as well as the overlying Farley Limestone at PE6/8. This is depicted in Figure 4.21, which also maps a possible boundary between open and closed diagenetic systems, controlled by proximity to recharge, permeability, etc. In contrast, cements of the upper Argentine and basal Farley at SP5 and BU6 underwent initial Sr loss without great Mn enrichment, and thus may have precipitated in water of somewhat higher Eh compared to that at PE6/8.

Table 1. Redox reaction energies.
(from BERNER, 1981)

mineral undergoing oxidation/reduction		Gibb's free energy change (δG_r, kJ mol^{-1})
oxidation reactions		
PYRITE	$3O_{2\ aq} + 4FeS_{2\ pyr} > 2Fe_2O_{3\ hem} + 8S$	-789
SIDERITE	$O_{2\ aq} + 4FeCO_{3\ sid} > Fe_2O_{3\ hem} + 4CO_2$	-346
RHODOCHROSITE	$O_{2\ aq} + 2MnCO_{3\ rhod} > 2MnO_{2\ birn} + 2CO_2$	-53
ALABANDITE	$O_{2\ aq} + MnS_{alab} > MnO_{2\ birn} + S$	-227
reduction reactions		
HEMATITE	$3H_2S_{aq} + S + Fe_2O_{3\ hem} > 2FeS_{2\ pyr} + 3H_2O$	-106
SIDERITE	$H_2S_{aq} + S + FeCO_{3\ sid} > FeS_{2\ pyr} + CO_2 + H_2O$	-79
BIRNESSITE	$2H_2S_{aq} + MnO_{2\ birn} > MnS_{alab} + S + 2H_2O$	-107
BIRNESSITE	$H_2S_{aq} + CO_2 + MnO_{2\ birn} > MnCO_{3\ rhod} + S + H_2O$	-118

Note: All reactions are at 298°K. All H_2O is in liquid phase, all CO_2 in gas phase, and all S as standard state, rhombic form. Note that Fe does not change oxidation state in the production of pyrite from siderite.

Figure 4.1. Calculated equilibrium Mg/Ca, Sr/Ca ratios of liquid and coexisting diagenetic calcite precipitate (dLMC) formed during closed system, incongruent dissolution of marine carbonate. Simulation used a 10^{-5} mole precipitation increment, constant 2.5×10^{-3} molar cation concentration in solution, and constant dissolution rate. Concentrations in ppm refer to the dissolving (source) phase.

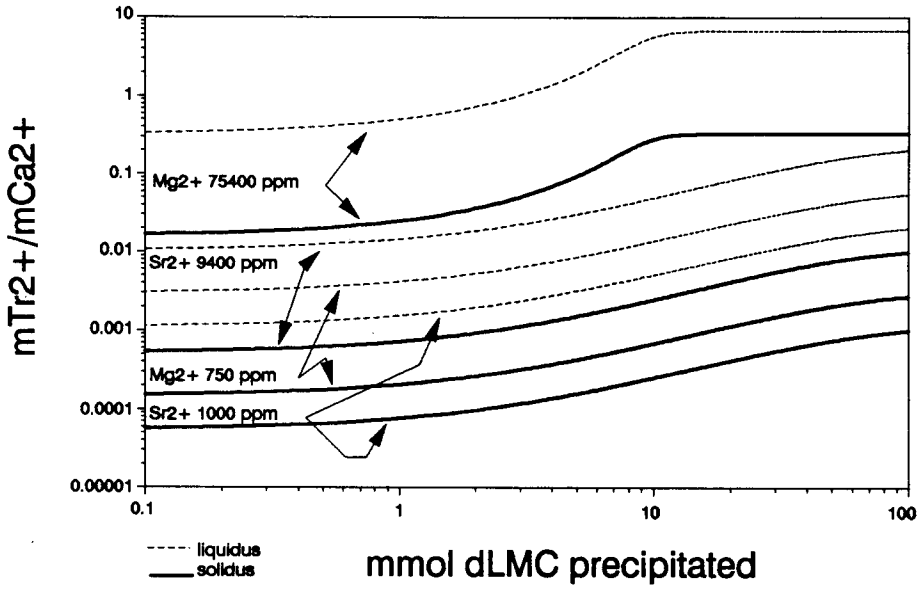

Figure 4.2. Calculated effect of increasing openness of a diagenetic system on evolving Sr concentration in calcite. As openness increases, a given fluid parcel spends less time reacting at the diagenetic site before replacement by more fluid, whose trace element ratio reflects previous dissolution-reprecipitation cycles. Parameters similar to Figure 4.1.

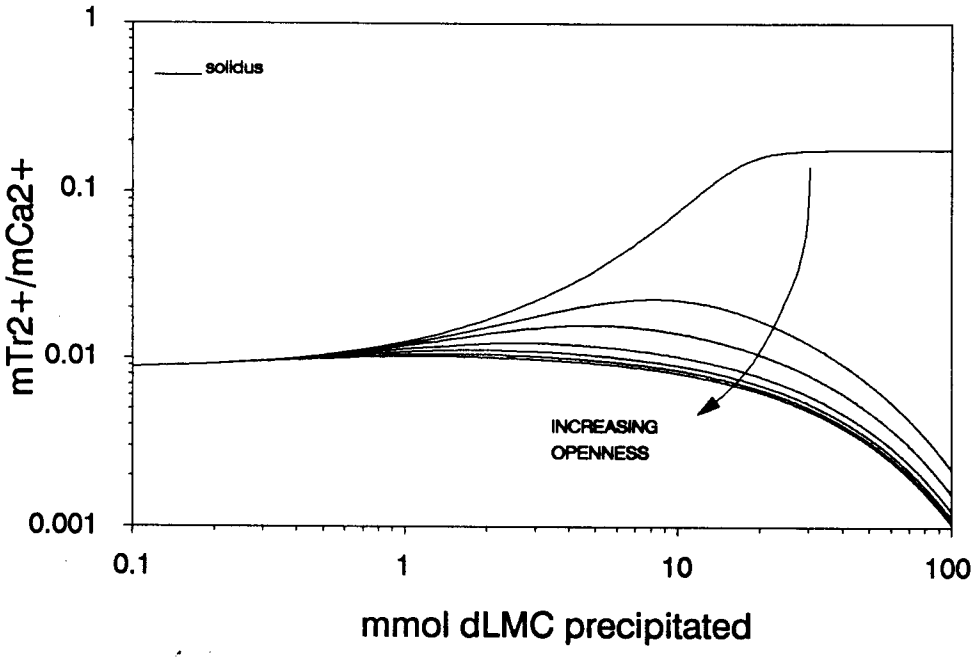

Figure 4.3. Comparison of calculated Sr/Ca and Mn/Ca ratios in newly precipitating dLMC during closed system diagenesis. Precipitation increment 10^{-4} mole, with constant 2.5×10^{-3} molar cation concentration in solution. Note that steady state condition has not been achieved for Sr.

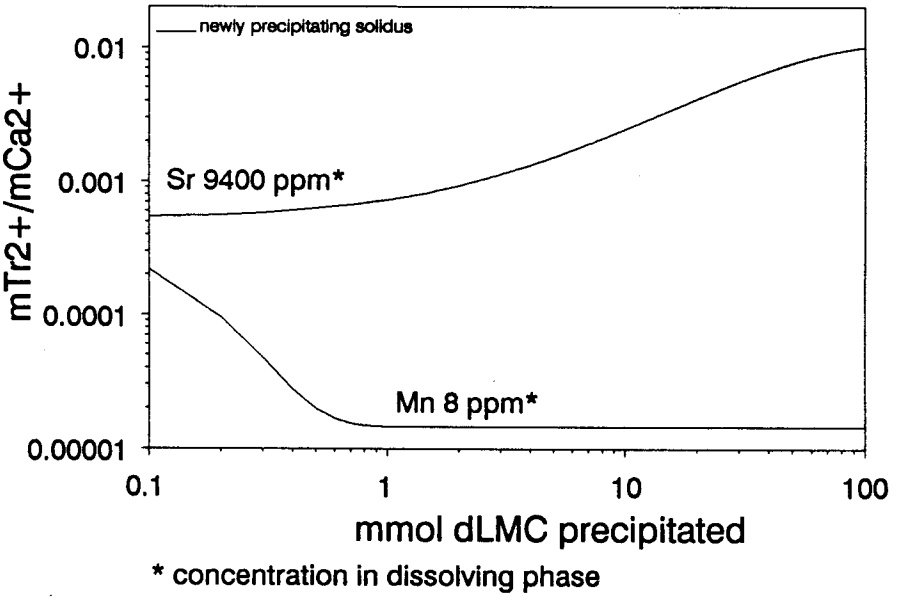

Figure 4.4. Sr versus Mn for alteration of marine skeletal components. Fields A, HMC, LMC are aragonite, magnesian calcite, and low magnesian calcite, respectively, in equilibrium with sea water, calculated from partition coefficients (from VEIZER, 1983).

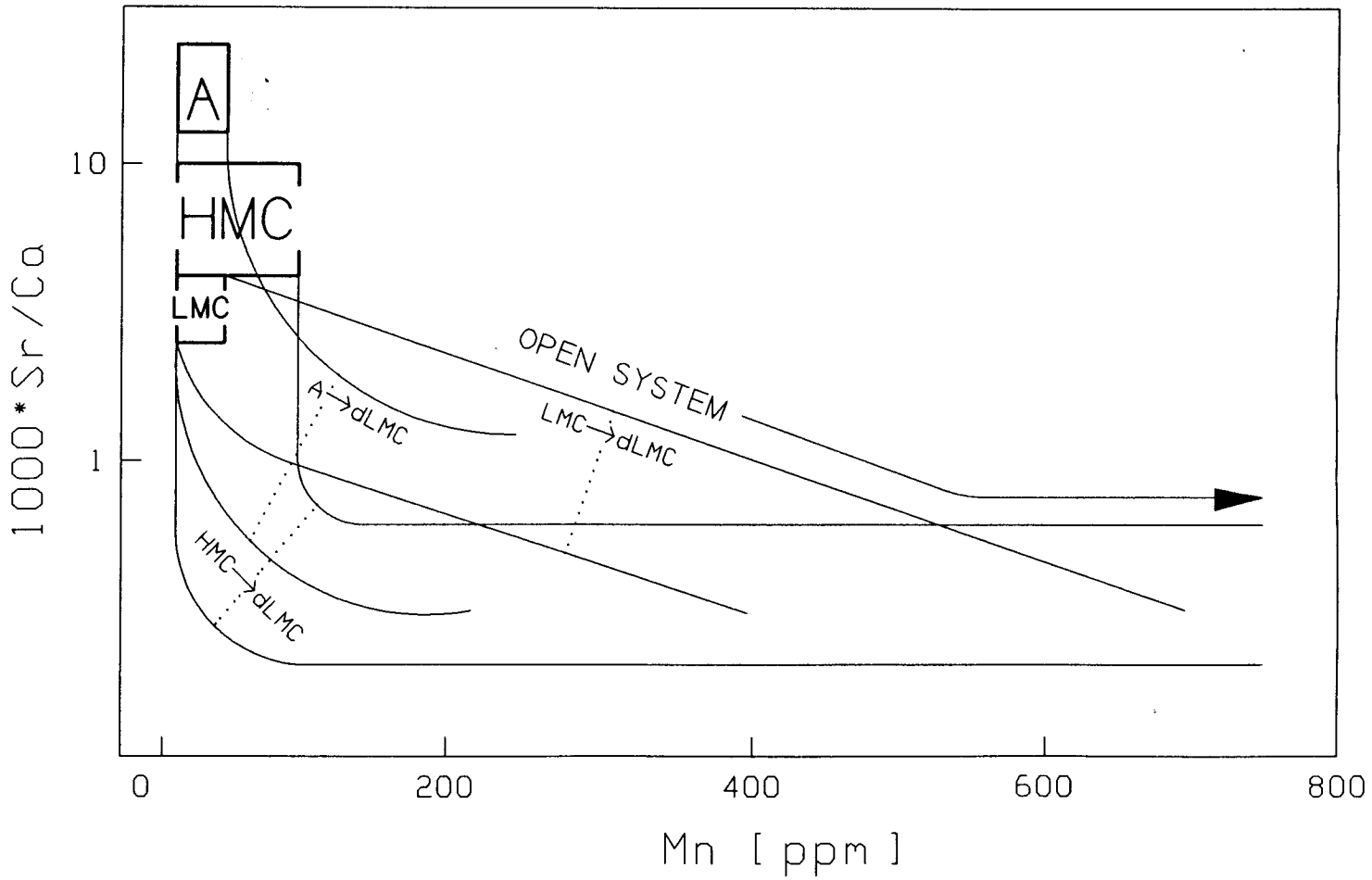

Figure 4.5. Eh-pH diagram for system Fe-CO_2-S-H_2O. Activity contours calculated for MnO_2 in equilibrium with Mn^{2+} are for a nonstoichiometric Mn oxide (more stable under reducing conditions than pyrolusite), using apparent free energies of formation of complex Mn oxides. Note that these activities are roughly similar to those of Fe^{2+} in equilibrium with $Fe(OH)_3$. Adapted from BARNABY and RIMSTIDT (1989).

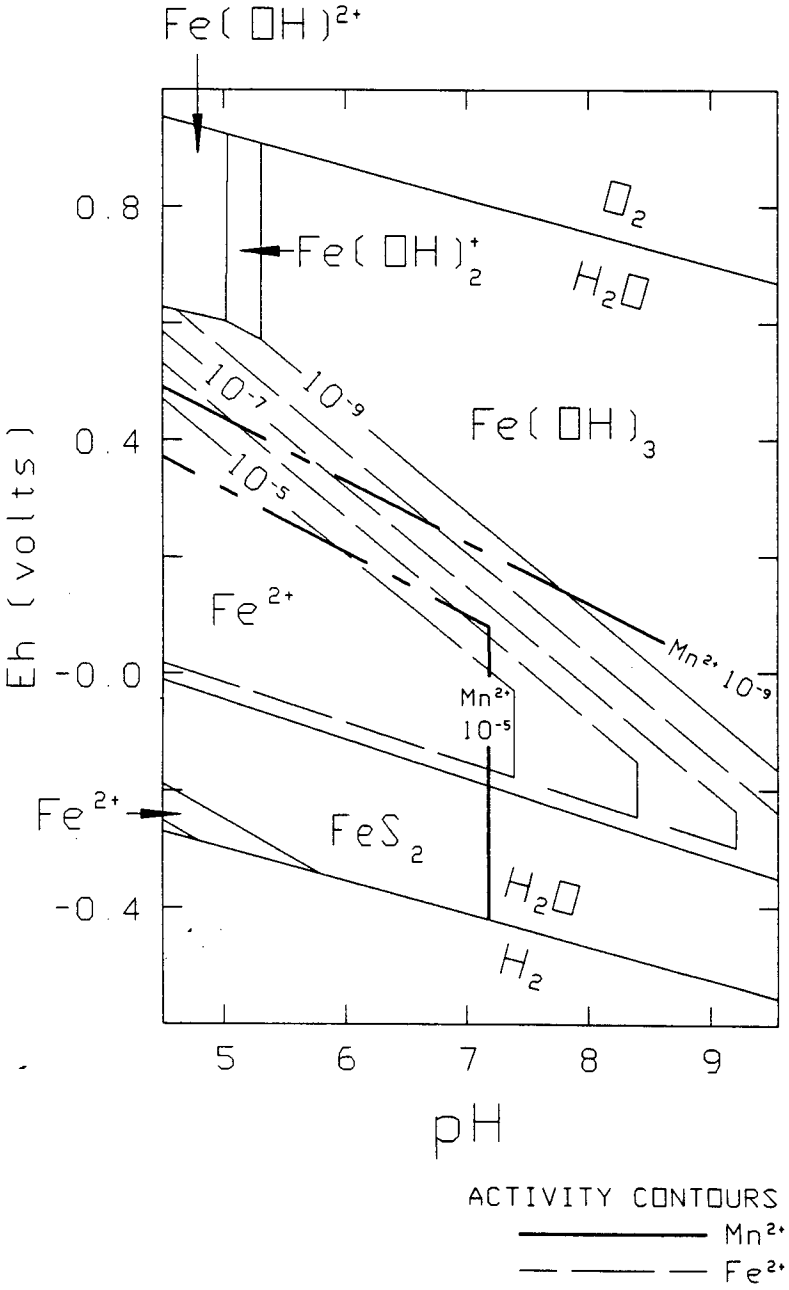

Figure 4.6. Comparison of Mn and Fe uptake in dLMC under closed system diagenesis. Concentration in dissolving phase 0.1 mole percent, other parameters as for Figure 4.1.

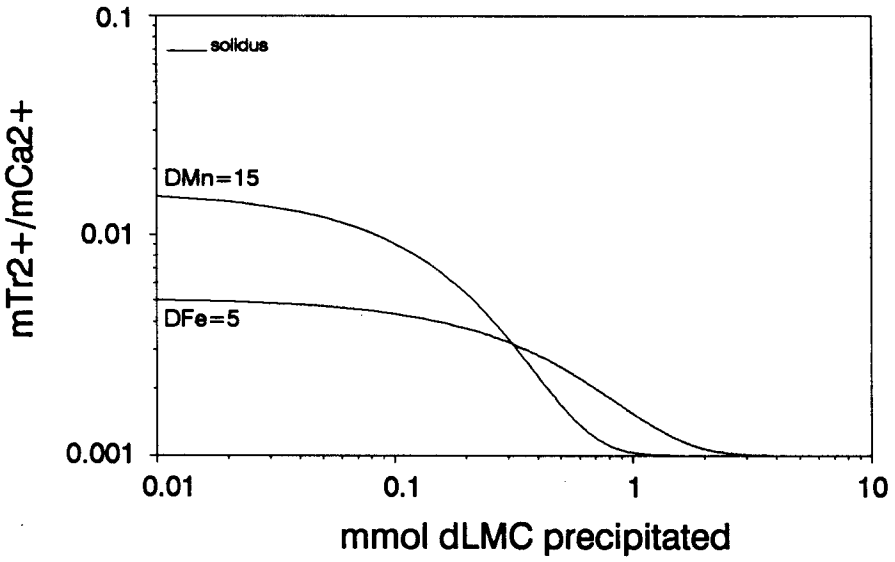

Figure 4.7. Summary of possible trends in Sr, Mg, Fe, and Mn concentrations.

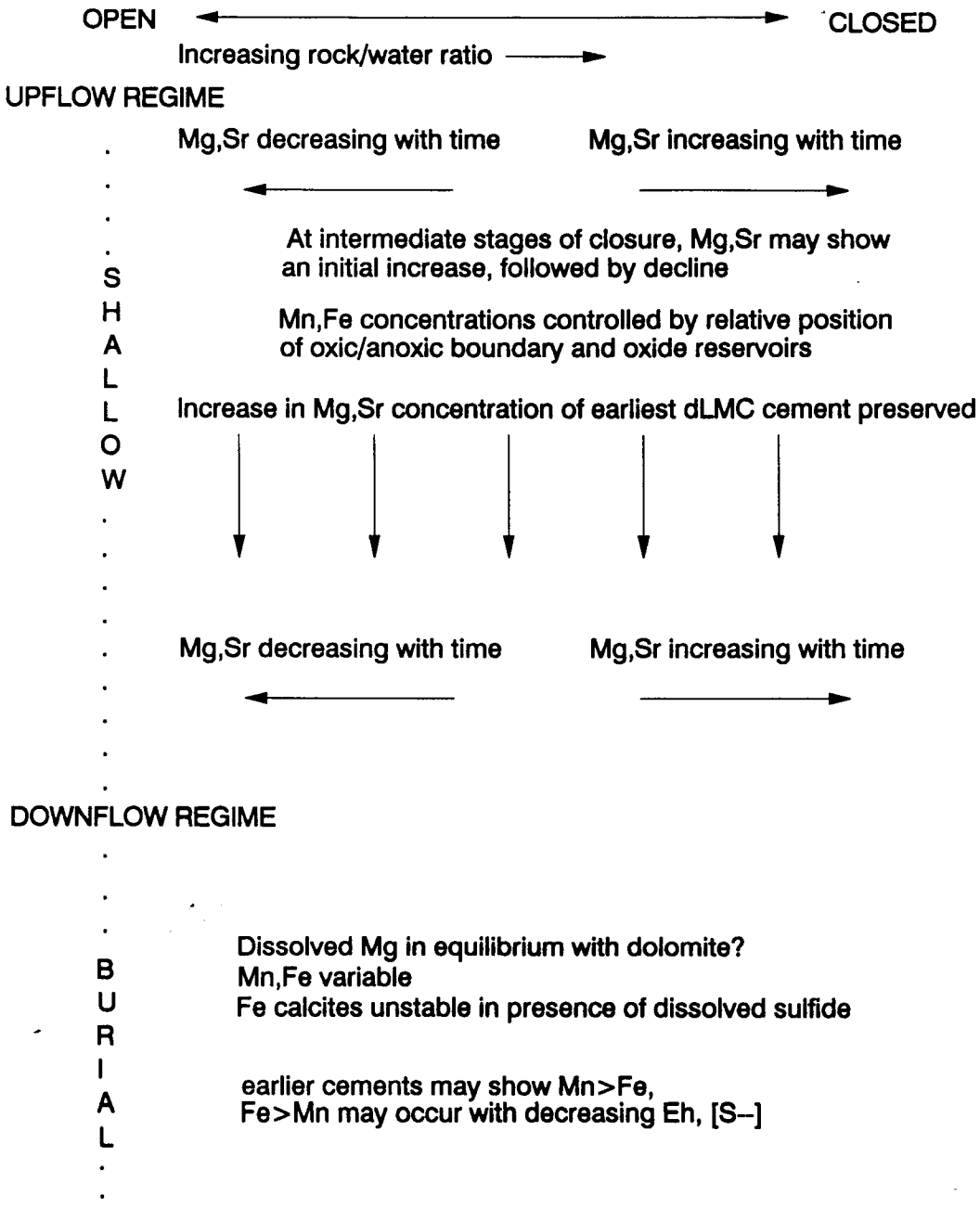

Figure 4.8. Map of void fill for microprobe transect SP5-tFb (top of Frisbie Limestone). Boundaries are zones marked by distinct changes in CL intensity. Inset area shown in Figure 4.9.

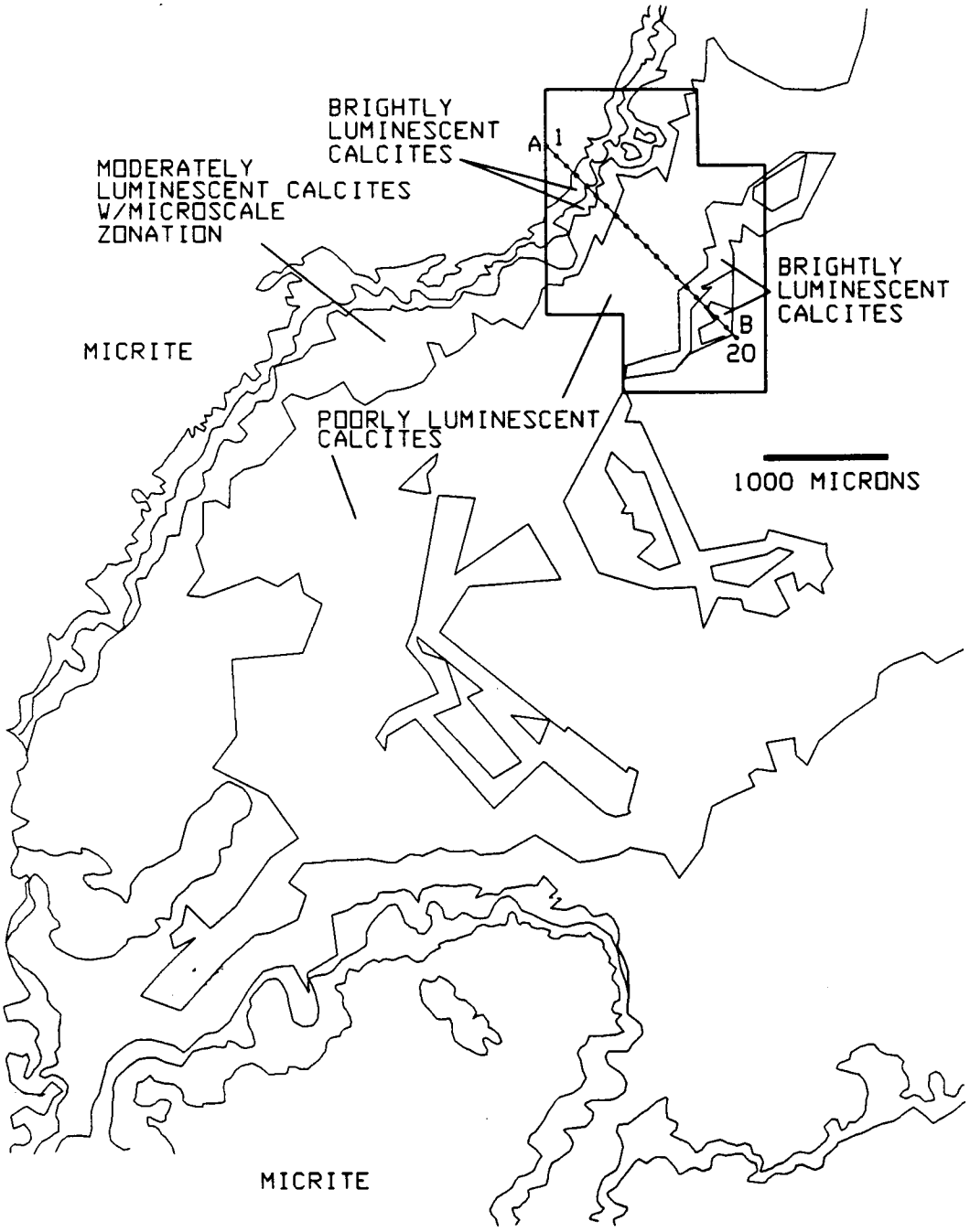

Figure 4.9. CL photomicrograph of SP5-tFb microprobe transect. Extinct area is plucked material. Scale bar 500 microns.

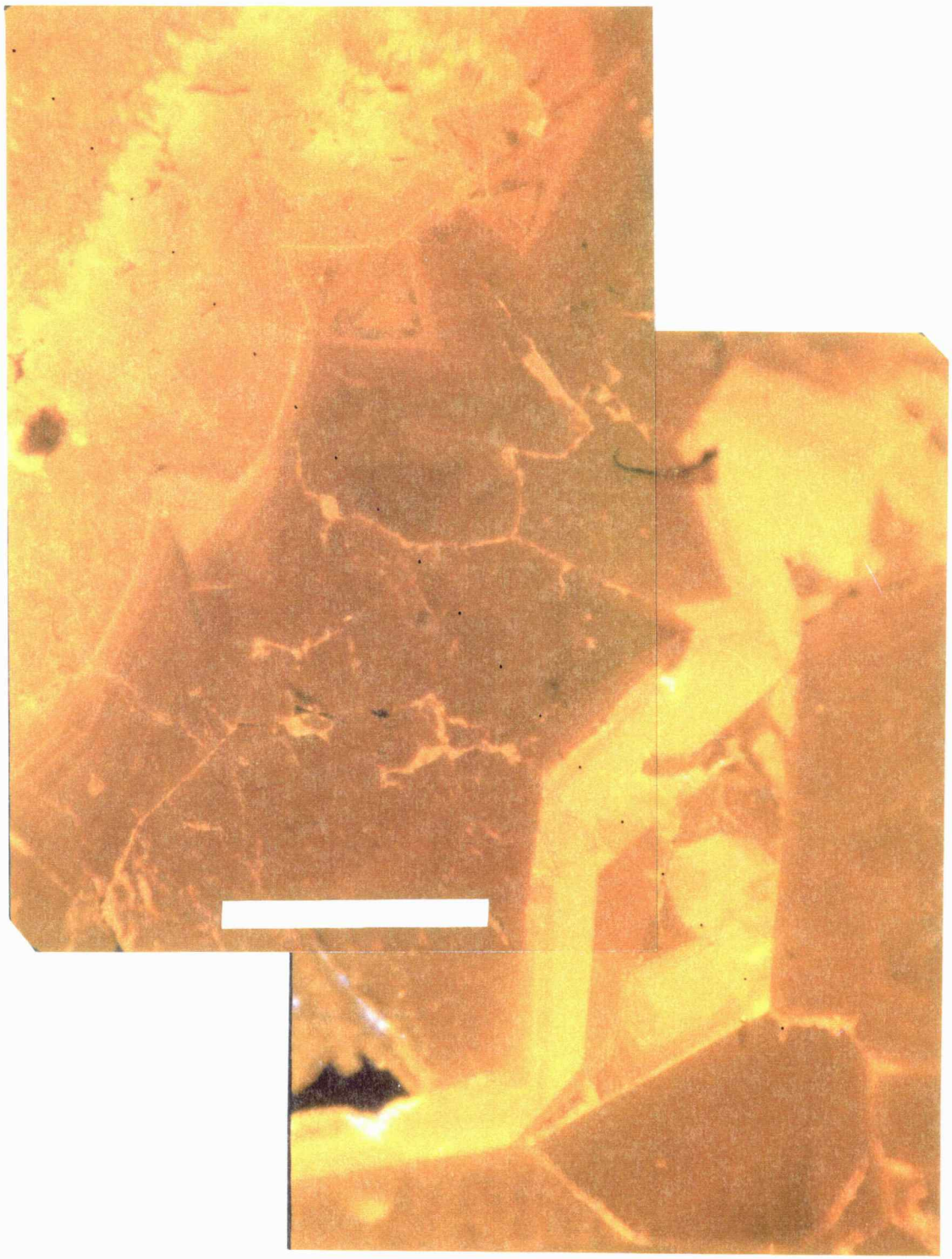

Figure 4.10. Trace element composition of early calcite cement of SP5-tFb transect.

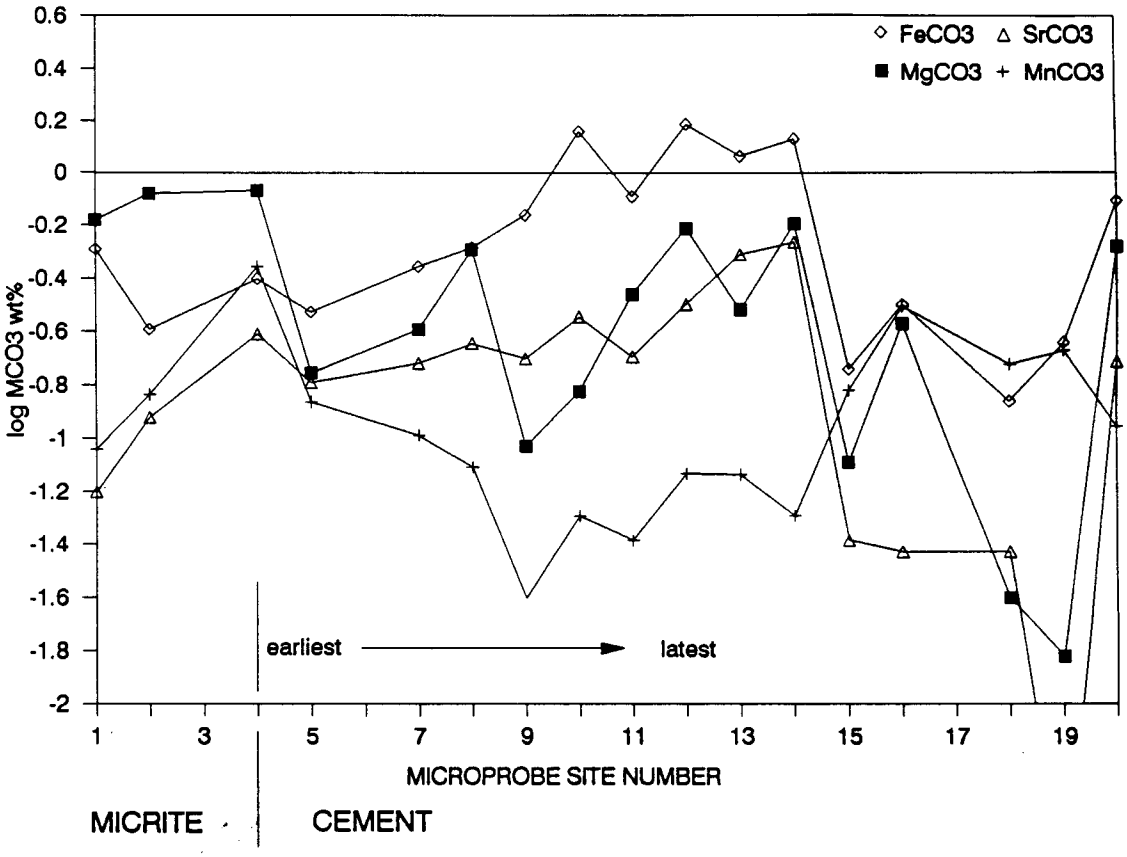

Figure 4.11. Map of void fill for microprobe transect SP5-bAg (base of Argentine Limestone). Inset area shown in Figure 4.12.

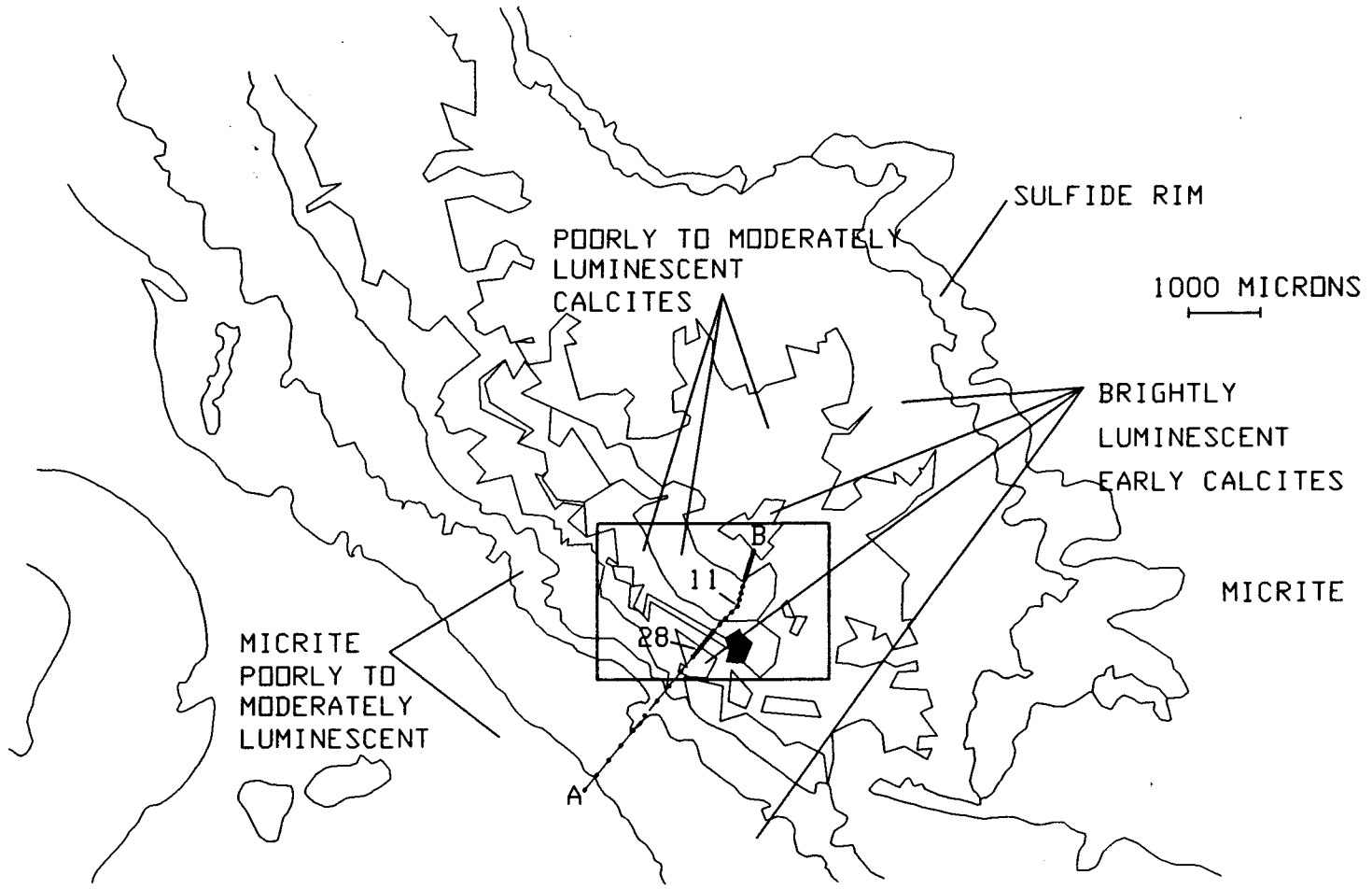

Figure 4.12. CL photomicrograph of SP5-bAg microprobe transect. Filled circles are sites discussed in text.

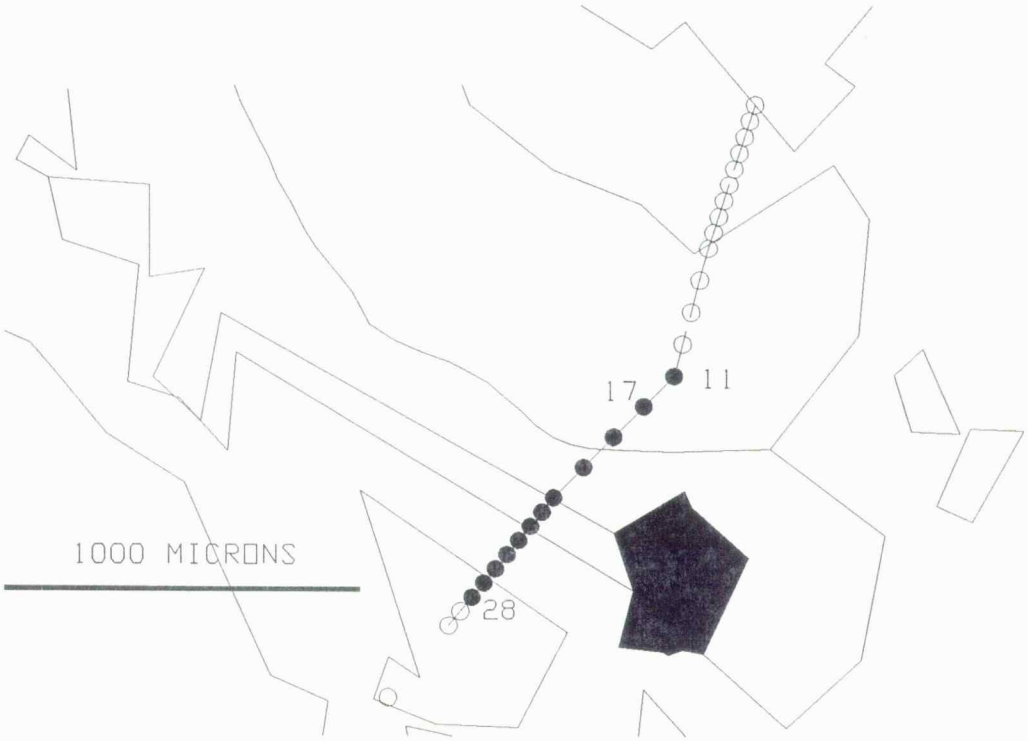

Figure 4.13. Trace element composition of early calcite cement of SP5-bAg transect.

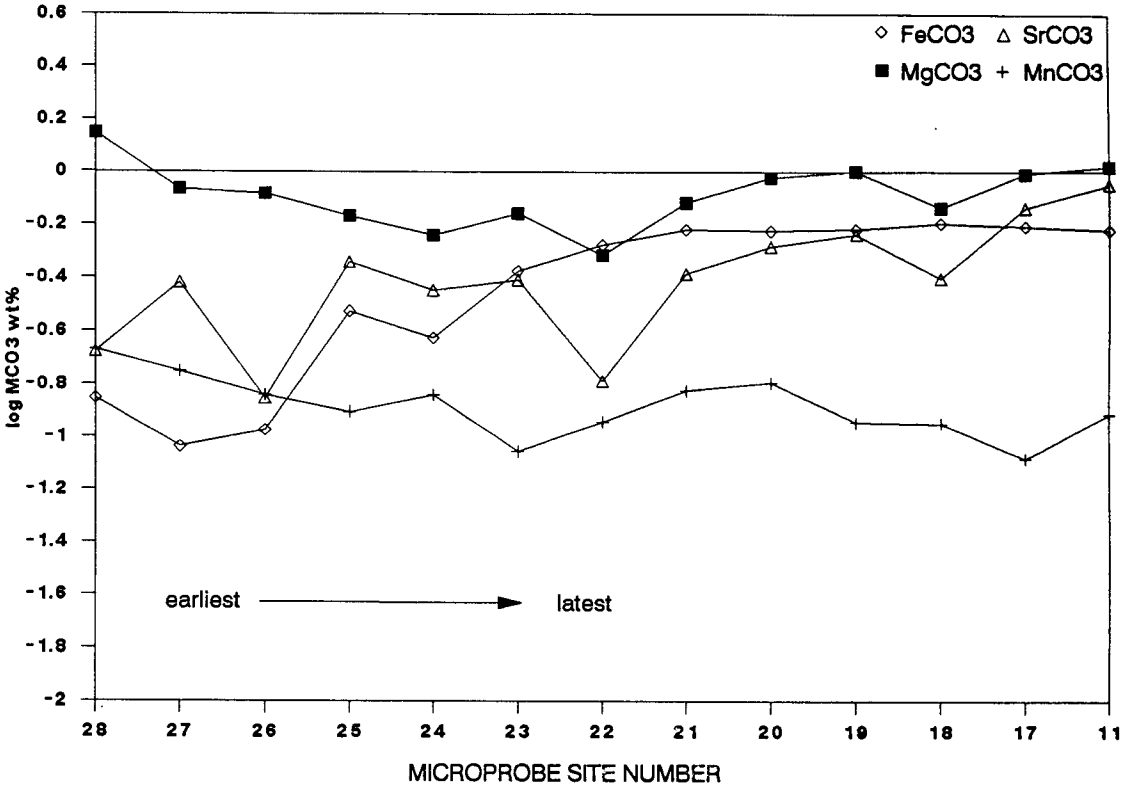

Figure 4.14. Map of void fill for microprobe transect SP5-8bIC (near top of Argentine Limestone). Inset area shown in Figure 4.15. Filled circles are sites discussed in text.

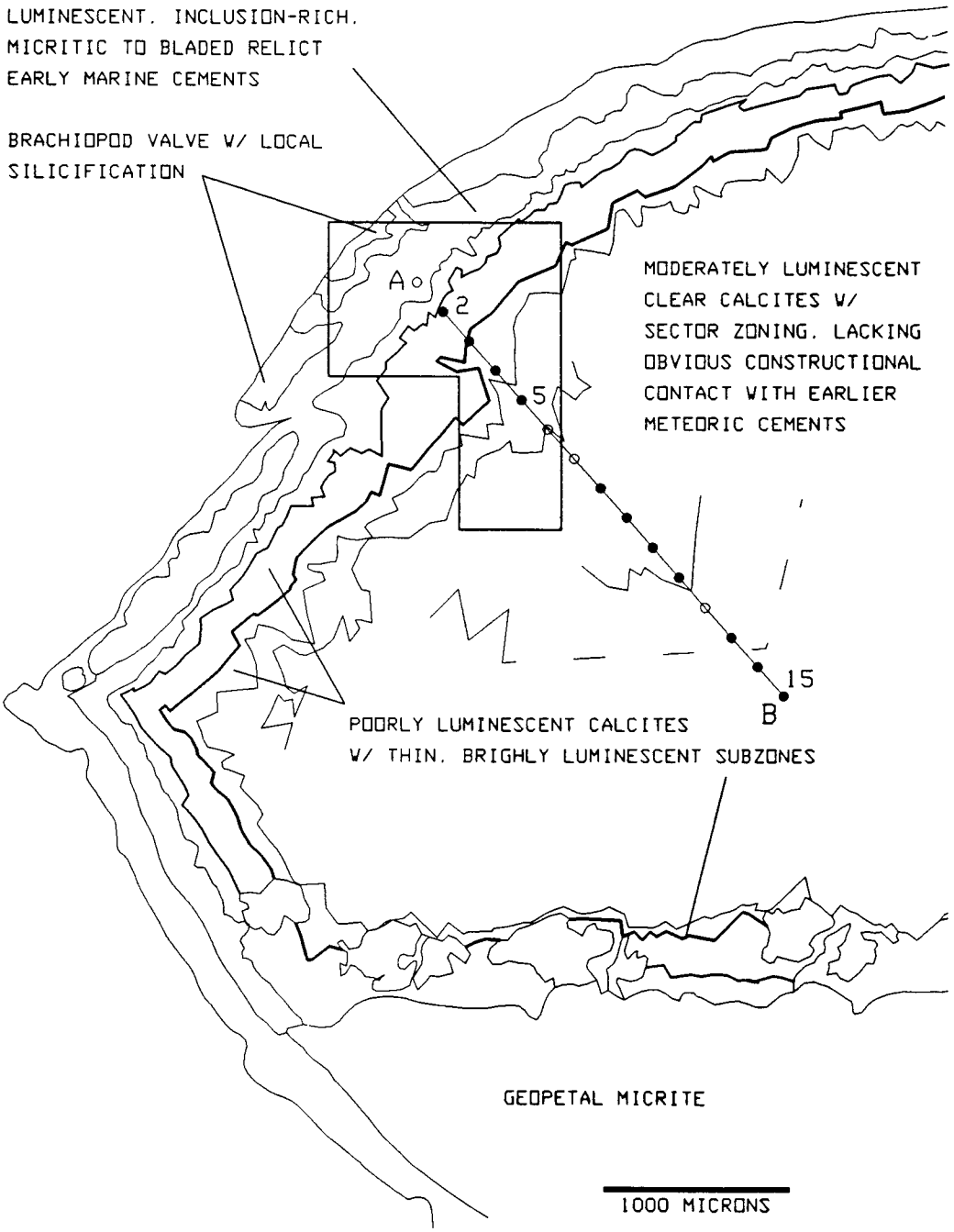

Figure 4.15. CL photomicrograph of SP5-8bIC microprobe transect. Scale bar 500 microns.

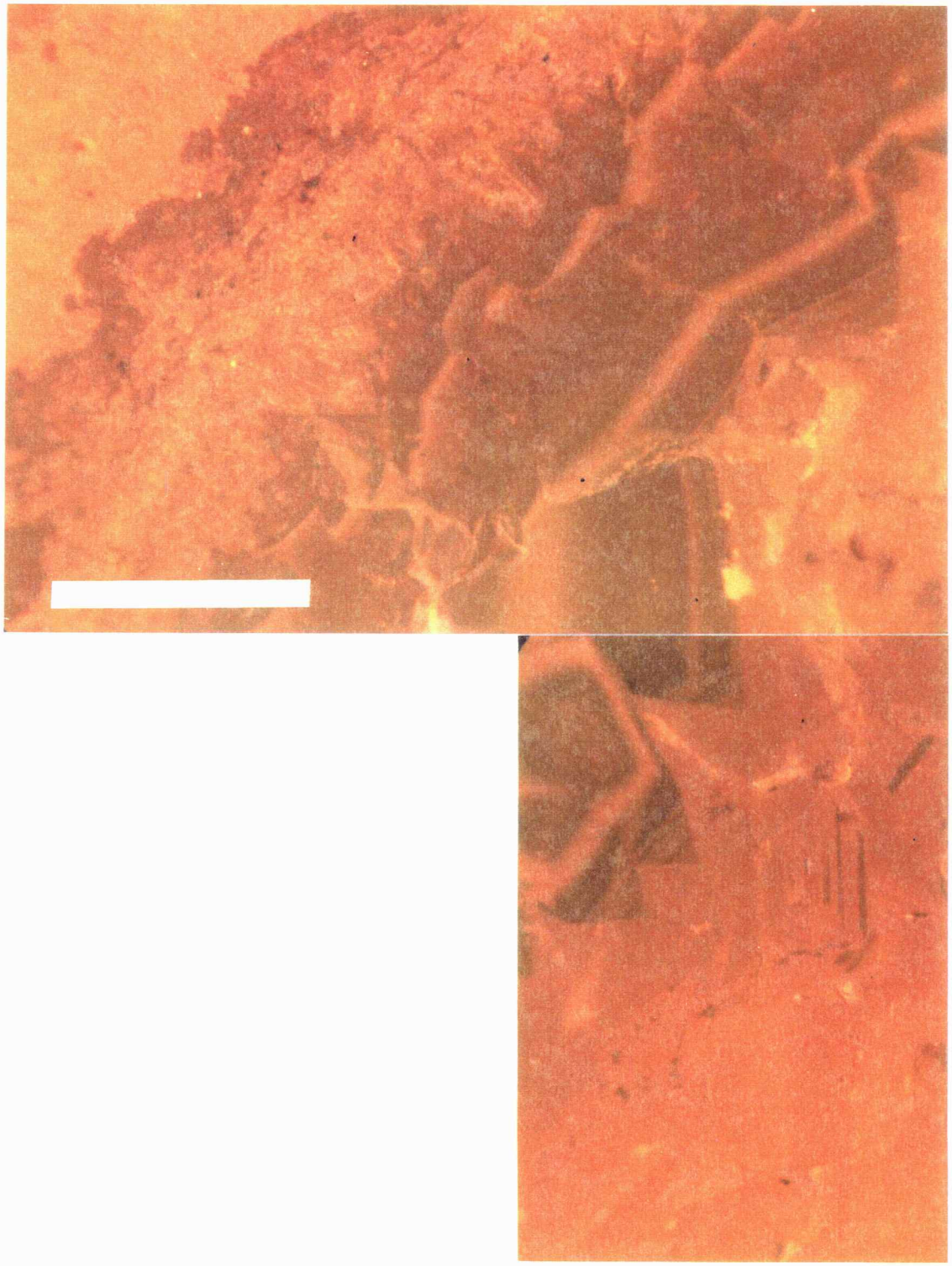

Figure 4.16. Trace element composition of early calcite cement of SP5-8bIC transect.

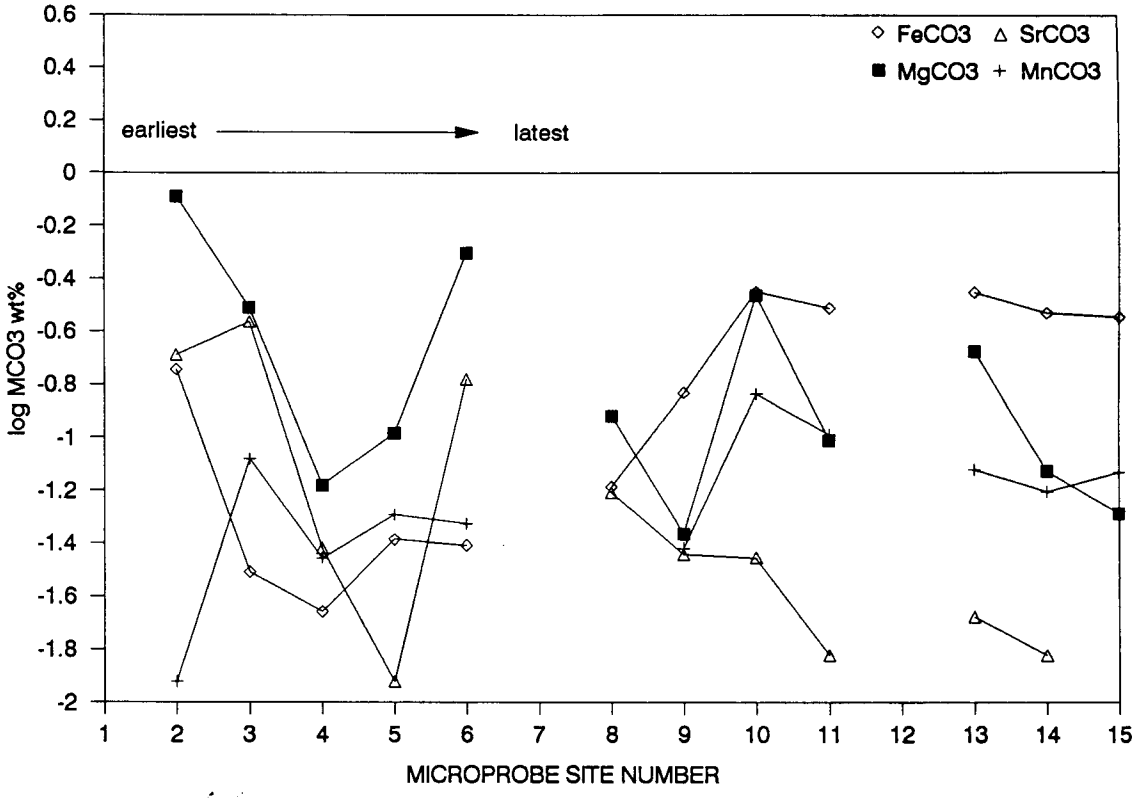

Figure 4.17. Map of void fill for microprobe transect SP5-bFa (base of Farley Limestone). Inset area shown in Figure 4.18. Filled circles are sites discussed in text.

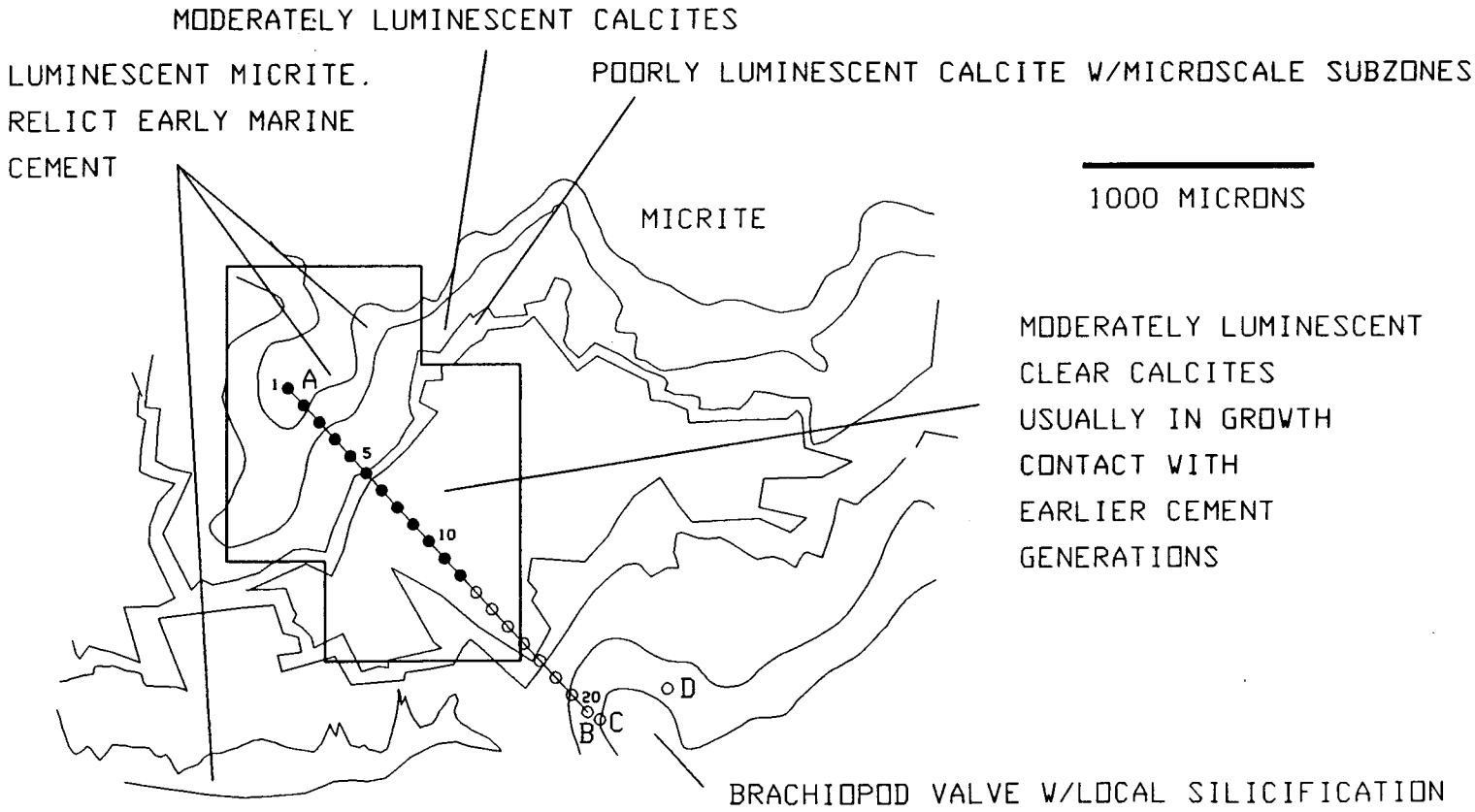

Figure 4.18. CL photomicrograph of SP5-bFa microprobe transect. Scale bar 500 microns. Site 1 is at upper left.

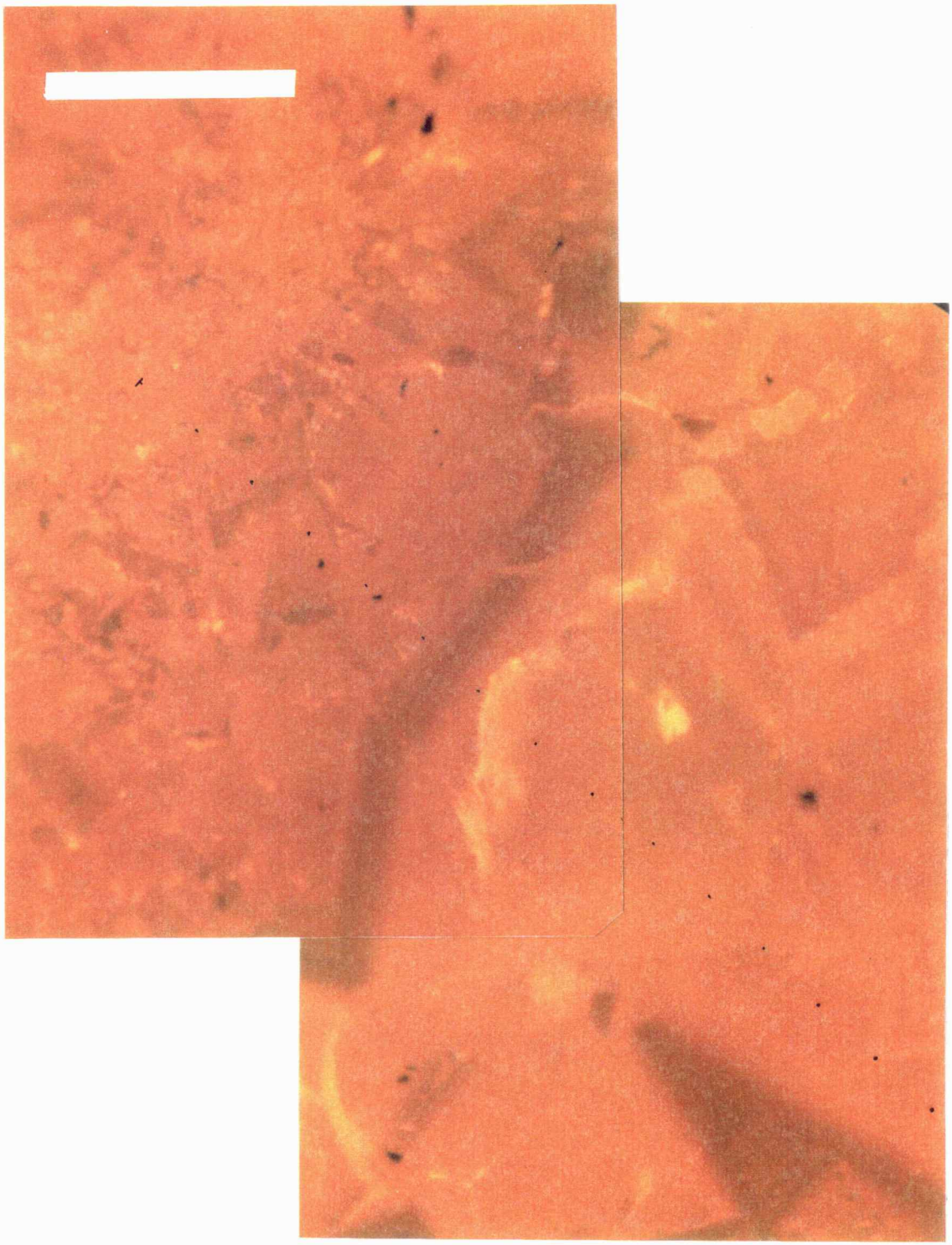

Figure 4.19. Trace element composition of early calcite cement of SP5-bFa transect.

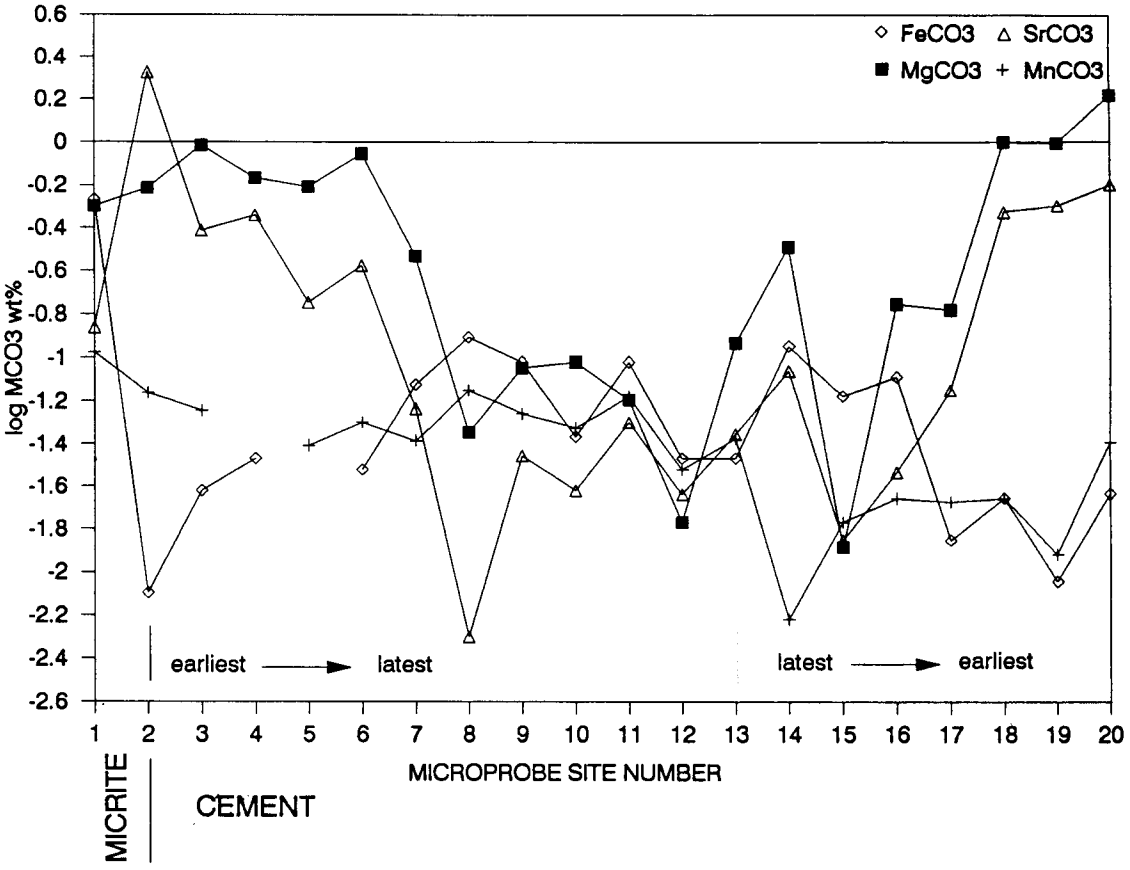

Figure 4.20. Early cement paths as a function of Sr versus Mn. A: Closed and open system cements at SP5 algal mound. Note endpoint of cements relative to calculated equilibrium field for marine calcite and aragonite. B: Open system paths at PE8 and BU6.

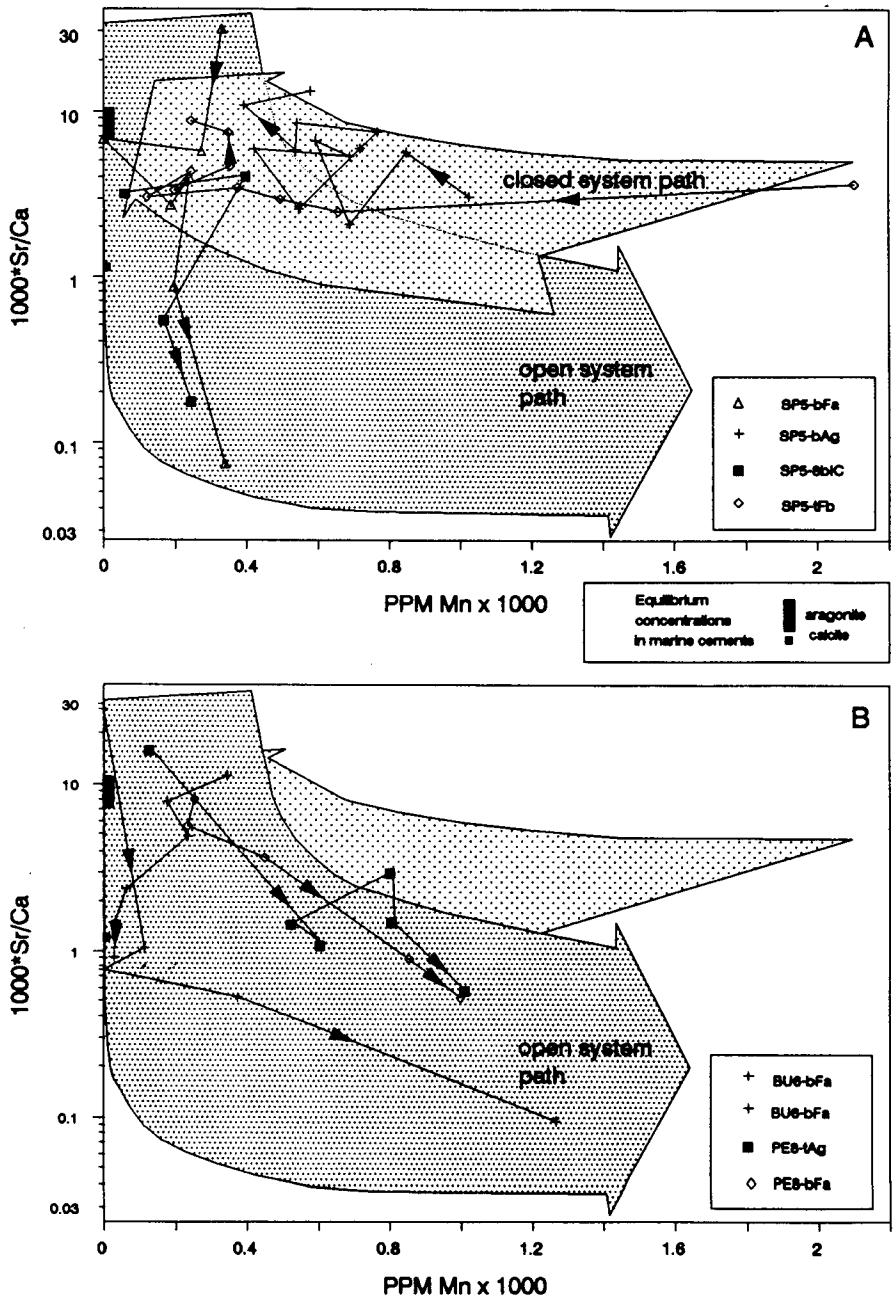

Figure 4.21. Possible distribution of closed versus open diagenetic systems suggested by cement geochemical trends. Symbols as in Figure 2.24.

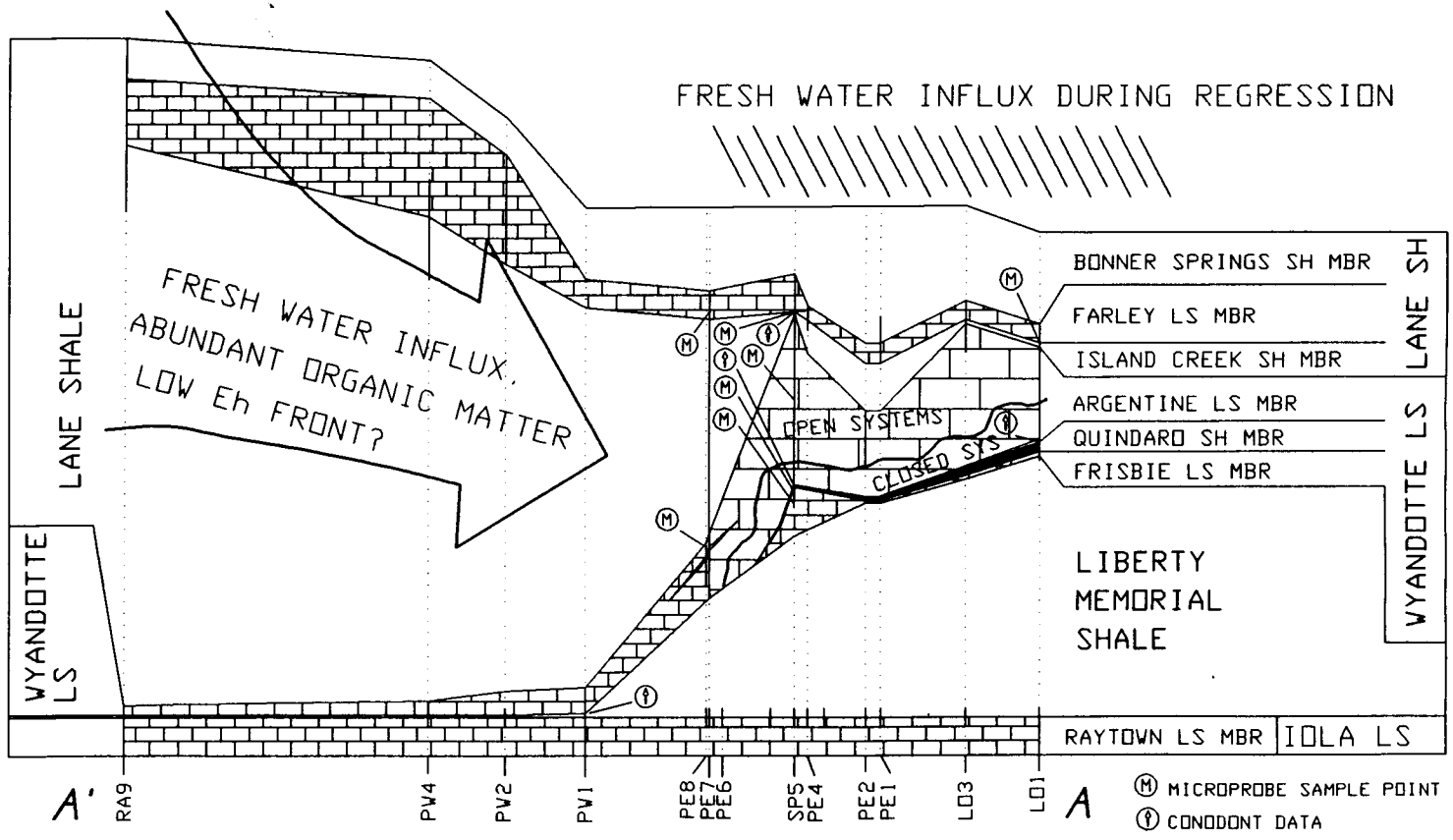

CHAPTER V

CONCLUSIONS AND SUGGESTIONS FOR FURTHER STUDY

Thesis conclusions can be summarized as follows:

1. Traditional correlation of the Wyandotte Limestone in Miami County failed to recognize importance of the laterally persistent Quindaro Shale as a marine marker horizon, which thus establishes the identity of the over- and underlying carbonate intervals. This in turn allows recognition of depositional feedback control of carbonate and clastic systems of the Wyandotte Limestone. This control was recognized in Johnson County by CROWLEY (1969), and is most clearly evident in Miami County in the relationship of Wyandotte members Frisbie Limestone, Quindaro Shale, and Argentine Limestone with the underlying Liberty Memorial Shale. Prior to Wyandotte deposition, progradation of the Liberty Memorial delta from the northeast formed a thick prodelta lobe in eastern Miami County. During the subsequent marine cycle, the elevated sea floor over the lobe formed a suitable habitat for small algal mounds of the Frisbie Limestone to develop in well-lit but deepening water. During deepest water deposition of the Quindaro Shale, high faunal abundance and diversity were

also associated with this prodelta platform. In western Miami County where the Liberty Memorial was essentially absent, the Frisbie was also absent, possibly due to lack of clear water conditions during initial transgression, and water depths in excess of the limit for benthic phylloid algae thereafter. The Quindaro Shale formed a diastemic horizon in this area.

Subsequent sea level fall once again exposed the elevated portions of the sea floor in eastern Miami County to warm, well-lit, shallow water, allowing substantial algal mounds of the Argentine Limestone to form. Deeper water conditions in western Miami County instead saw a condensed, carbonate mud-poor section in which an open marine fauna flourished, and phylloid algae were much reduced in importance.

Regression climaxed with progradation of the Lane and Island Creek deltas, although influence of the latter in Miami County was probably minor. The greatest thickness of clastics was received in areas floored by thin Argentine, and thus the Lane isopach shares complementary thickness relationships with the underlying section. Development of algal mounds and ooid shoals in the Farley Limestone during the second, albeit less extensive, marine invasion was again controlled by sea floor topography inherited both from the Lane Shale platform (e.g., the mound centered around the

town of Lane in extreme SW Miami and NW Linn Counties) and the Liberty Memorial-Argentine platform as well (Stilwell Bank in southeast Johnson County).

2. Textural and geochemical patterns within the Wyandotte show variable but predictable effects of meteoric diagenesis. Preservation of metastable biogenic and abiogenic carbonate mineralogies is most likely in closed diagenetic systems with high rock-water ratios. These can be identified by an early cement stratigraphy that shows overall temporal trends of increasing Sr and decreasing Mn. In contrast, early meteoric cements (in contact with relict marine cement) that show an overall depletion in Sr and enrichment in Mn indicate cementation in an open system in which rock-water ratios were low. Open meteoric systems tend to cannibalize early-formed cements at upflow sites and reprecipitate them at downflow sites, and thus much of the pore space in rocks that hosted open meteoric diagenesis contain only late cements that probably formed during deeper burial.

3. Closed system diagenesis is observed in the Frisbie and basal Argentine within the lower reaches of the algal mound complex south of Wagstaff in central Miami County (SP5). Open systems are more typical of the upper section of the bank (upper Argentine and Farley), whose pore spaces are typically filled with lucid calcites. These calcites

lack the CL zonation that is seen locally only in contact with early marine cement. Open system diagenesis is also observed in both the Argentine and the Farley in the transitional area just west of the algal bank at SP5. Low rock-water ratios and fresh-water access may have been controlled by the thickened sequence of Lane Shale, which as a delta, could have established a freshwater lens.

4. Fe and Mg appear to be less reliable diagenetic indicators than Sr and Mn. The availability of Fe for coprecipitation in calcite is complicated by competition from sulfides and the metastability of Fe oxides in the absence of dissolved oxygen. Mg exhibits changes in concentration during closed system diagenesis that are not reflected in Sr. The understanding of this relationship demands a more complete understanding of controls on Mg availability and coprecipitation in calcite during meteoric diagenesis.

5. CL petrography provides an excellent means of revealing the temporal and spatial relationships of diagenetic features. The distinction between early meteoric and later burial calcites is made with the assumption that the former precipitated at shallow depths, and (at least for open systems) subject to perturbation from the surface environment. Cements formed in the relative isolation of a burial setting should thus be texturally and chemically more

homogeneous. This assumption has been substantiated by the observation that lucid, inclusion-free calcites either completely fill voids that preserve no early cement, or follow (with or without a dissolution surface) zoned cements that are in contact with at least relict marine cements. These lucid calcites also display an even luminescence that suggest relatively invariant Fe and Mn concentrations.

The distinction between meteoric and deeper burial cements does beg for more quantification. This could be best achieved by more extensive, high resolution isotopic, trace element, and fluid inclusion sampling of late cements.

This thesis also provides only limited replication of early trace element data (through transects that run from the margin to the center of a void fill and back to the opposite margin). Any subsequent microprobe sampling should thus be designed to provide a statistical measure of reproducibility and variance for a given cement zone.

6. Lastly, the availability of possibly intact marine cements within the Frisbie Limestone south of Louisburg (LO6) offers the opportunity to extract the original isotopic composition of seawater (e.g., GIVEN and LOHMANN, 1985). Fine scale analysis of isotopic and trace metal composition of aragonite or magnesian calcite fibrous cements here and comparison with data collected from other transgressive sparite facies (HECKEL, 1983) could yield both

an isotopic seawater value for the Late Pennsylvanian as well as reveal distinctions and relationships between meteoric and burial diagenesis.

APPENDIX A.

MICROPROBE DATASET

SITE#	TRSCT#	$MgCO_3$	$CaCO_3$	$MnCO_3$	$FeCO_3$	$SrCO_3$	TOTAL[5]
BU6bFaA01	1	0.631	108.267	0.083	0.32	0.368	109.669
BU6bFaBD1	2	0.885	103.475	0.052	0.336	0.13	104.878
BU6bFaBD2	3	0.836	103.726	0.059	1.061	0.155	105.837
BU6bFaBD3	4	1.086	100.276	0.024	0.383	0.193	101.962
BU6bFaBD4	5	1.05	103.554	0.046	0.054	0.075	104.779
BU6bFaBD5	6	1.303	104.371	0.072	0.028	0.806	106.58
BU6bFaBD6	7	2.296	97.36	0.037	0.000	0.528	100.221
BU6bFaBD7	8	1.546	102.92	0.049	0.025	0.351	104.891
BU6bFaBD8	9	0.461	103.179	0.013	0.000	0.168	103.821
BU6bFaBD9	10	0.338	102.154	0.007	0.04	0.108	102.647
BU6bFaBD10	11	0.349	103.044	0.006	0.306	0.066	103.771
BU6bFaEF1	12	0.384	104.548	0.203	0.242	0.064	105.441
BU6bFaEF2	13	0.15	103.95	0.05	0.165	0.037	104.352
BU6bFaEF3	14	0.128	101.305	0.113	0.317	0.03	101.893
BU6bFaEF4	15	0.251	104.358	0.149	0.27	0.074	105.102
BU6bFaEF5	16	0.201	104.123	0.204	0.804	0.01	105.342
BU6bFaEF6	17	0.181	103.391	0.295	0.901	0.049	104.817
BU6bFaFG1	18	0.227	103.694	0.265	0.946	0.007	105.139
BU6bFaFG2	19	0.267	106.053	0.078	0.18	0.039	106.617
BU6bFaFG3	20	0.202	104.579	0.000	0.127	0.056	104.964
BU6bFaFG4	21	0.305	104.146	0.024	0.08	0.075	104.63
BU6bFaFG5	22	0.446	101.53	0.000	0.000	1.923	103.899
BU6bFaFG6	23	0.974	101.762	0.064	0.27	0.379	103.449
SP5s17AB1	24	0.772	0.089	0.044	0.54	0.047	1.492
SP5s17AB2	25	0.816	95.579	0.012	0.18	0.204	96.791
SP5s17AB3	26	0.309	99.663	0.083	0.031	0.273	100.359
SP5s17AB4	27	0.066	106.313	0.035	0.022	0.038	106.474
SP5s17AB5	28	0.104	102.699	0.051	0.041	0.012	102.907
SP5s17AB6	29	0.499	109.25	0.047	0.039	0.166	110.001
SP5s17AB7	30	0.489	0.039	0.043	0.113	0.052	0.736
SP5s17AB8	31	0.121	103.011	0.000	0.065	0.062	103.259
SP5s17AB9	32	0.043	104.034	0.038	0.147	0.036	104.298
SP5s17AB10	33	0.345	102.338	0.146	0.356	0.035	103.22
SP5s17AB11	34	0.097	104.059	0.102	0.307	0.015	104.58
SP5s17AB12	35	0.032	0.004	0.000	0.128	0.008	0.172
SP5s17AB13	36	0.211	104.682	0.075	0.354	0.021	105.343

[5]Sites having totals greater than 110% and less than 90% were ignored.

SP5s17AB14	37	0.074	105.822	0.062	0.294	0.015	106.267
SP5s17AB15	38	0.051	102.501	0.073	0.283	0.000	102.908
PE8bFaAB1	1	1.441	109.574	0.035	0.002	0.122	111.174
PE8bFaAB2	2	1.939	101.536	0.034	0.007	0.157	103.673
PE8bFaAB3	3	1.319	102.392	0.058	0.016	0.186	103.971
PE8bFaAB4	4	1.755	94.753	0.156	0.709	0.709	98.082
PE8bFaAB5	5	0.802	97.93	0.271	0.991	0.275	100.269
PE8bFaAB6	6	0.288	101.234	0.131	0.322	1.475	103.45
PE8bFaAB7	7	1.383	97.256	0.143	0.455	0.385	99.622
PE8bFaAB8	8	1.206	102.319	0.149	0.585	0.279	104.538
PE8bFaAB9	9	0.301	94.923	0.195	0.609	0.059	96.087
PE8bFaAB10	10	0.533	102.403	0.091	0.535	0.351	103.913
PE8bFaAB11	11	0.236	103.239	0.161	0.768	0.092	104.496
PE8bFaAB12	12	0.324	104.197	0.187	0.507	0.135	105.35
PE8bFaAB13	13	0.494	101.845	0.097	0.553	0.108	103.097
PE8bFaAB14	14	1.441	105.614	0.174	1.18	0.538	108.947
PE8bFaAB15	15	2.327	105.104	0.053	0.077	0.585	108.146
PE8bFaAB16	16	1.522	104.205	0.000	0.009	0.481	106.217
PE8bFaAB17	17	1.391	101.253	0.049	0.000	0.393	103.086
PE8bFaAB18	18	1.152	108.667	0.094	0.232	0.276	110.421
PE8bFaAB19	19	0.363	102.236	0.179	0.713	0.064	103.555
PE8bFaAB20	20	0.203	101.825	0.209	0.408	0.037	102.682
PE8tAgAB1	21	1.589	106.278	0.134	0.145	0.268	108.414
PE8tAgAB2	22	0.046	105.505	0.075	0.000	0.865	106.491
PE8tAgAB3	23	0.296	106.179	0.064	0.133	1.35	108.022
PE8tAgAB4	24	0.392	105.046	0.028	0.2	1.163	106.829
PE8tAgAB5	25	0.249	108.509	0.128	0.526	0.084	109.496
PE8tAgAB6	26	0.302	102.056	0.111	0.643	0.106	103.218
PE8tAgAB7	27	0.38	106.182	0.169	0.975	0.225	107.931
PE8tAgAB8	28	0.412	102.915	0.17	0.702	0.109	104.308
PE8tAgAB9	29	0.188	105.714	0.184	0.685	0.0002	106.771
PE8tAgAB10	30	0.116	111.23	0.135	0.558	0.000	112.039
PE8tAgBC1	31	0.177	105.286	0.257	0.65	0.0002	106.37
PE8tAgBC2	32	0.045	104.277	0.213	0.302	0.043	104.88
PE8tAgBC3	33	0.177	106.62	0.402	0.717	0.029	107.945
PE8tAgBC4	34	0.203	105.836	0.474	0.786	0.04	107.339
PE8tAgBC5	35	0.283	104.327	0.373	1.055	0.057	106.095
PE8tAgBC6	36	0.303	106.9	0.439	1.304	0.074	109.02
PE8tAgDE1	37	0.865	101.274	0.304	1.559	0.262	104.264
PE8tAgDE2	38	0.847	101.351	0.299	1.703	0.297	104.497
PE8tAgDE3	39	0.647	105.782	0.173	1.358	0.578	108.538
PE8tAgDE4	40	0.971	99.103	0.257	1.248	0.151	101.73
PE8tAgDE5	41	0.765	102.685	0.273	1.784	0.45	105.957
PE8tAgDE6	42	0.866	102.565	0.264	1.413	0.303	105.411
PE8tAgDE7	43	0.922	98.934	0.218	1.341	0.45	101.865
PE8tAgDE8	44	0.762	100.564	0.221	1.311	0.5	103.358
PE8tAgDE9	45	1.097	88.211	0.162	1.42	0.2	91.09
PE8tAgDE10	46	0.959	99.002	0.262	1.468	0.408	102.099
SP5bAgAB1	1	0.932	102.142	0.082	0.101	0.531	103.788
SP5bAgAB2	2	1.163	100.163	0.125	0.259	0.863	102.573
SP5bAgAB3	3	1.068	104.076	0.126	0.373	0.753	106.396

SP5bAgAB4	4	0.961	102.469	0.17	0.334	0.829	104.763
SP5bAgAB5	5	0.783	103.367	0.167	0.18	0.839	105.336
SP5bAgAB6	6	0.959	99.641	0.091	0.201	0.526	101.418
SP5bAgAB7	7	0.888	103.316	0.155	0.193	0.5	105.052
SP5bAgAB8	8	0.879	102.354	0.136	0.24	0.507	104.116
SP5bAgAB9	9	0.849	100.614	0.106	0.226	0.223	102.018
SP5bAgAB10	10	0.948	104.463	0.189	0.334	0.288	106.222
SP5bAgBC1	15	0.906	103.189	0.138	0.406	0.502	105.141
SP5bAgBC2	14	0.998	100.437	0.059	0.459	0.821	102.774
SP5bAgBC3	13	0.418	96.692	0.093	0.416	0.448	98.067
SP5bAgBC4	12	0.901	101.708	0.081	0.482	0.719	103.891
SP5bAgBC5	11	1.045	101.764	0.121	0.6	0.891	104.421
SP5bAgCD1	16	1.084	110.031	0.108	0.658	0.949	112.83
SP5bAgCD2	17	0.978	101.465	0.082	0.618	0.729	103.872
SP5bAgCD3	18	0.728	103.002	0.112	0.637	0.395	104.874
SP5bAgCD4	19	1.004	103.817	0.113	0.605	0.58	106.119
SP5bAgCD5	20	0.951	105.56	0.16	0.598	0.522	107.791
SP5bAgDE1	21	0.763	104.063	0.15	0.606	0.413	105.995
SP5bAgDE2	22	0.485	95.569	0.114	0.53	0.163	96.861
SP5bAgDE3	23	0.698	99.823	0.088	0.421	0.391	101.421
SP5bAgDE4	24	0.576	100.602	0.144	0.236	0.357	101.915
SP5bAgDE5	25	0.68	104.155	0.124	0.298	0.456	105.713
SP5bAgDE6	26	0.829	101.937	0.144	0.106	0.14	103.156
SP5bAgDE7	27	0.858	101.705	0.177	0.092	0.381	103.213
SP5bAgDE8	28	1.402	102.956	0.214	0.14	0.21	104.922
SP5bAgDE9	29	1.119	101.694	0.252	0.148	0.193	103.406
SP5bAgDE10	30	0.898	104.981	0.171	0.139	0.478	106.667
SP5bAgEF1	31	1.289	102.455	0.239	0.171	0.22	104.374
SP5bAgEF2	32	0.797	103.494	0.175	0.136	0.807	105.409
SP5bAgEF3	33	0.661	96.332	0.033	0.182	0.117	97.325
SP5bAgEF4	34	1.192	102.743	0.146	0.067	0.416	104.564
SP5bAgEF5	35	0.027	1.338	0.000	96.849	0.003	98.217
SP5bAgEF6	36	0.859	98.991	0.076	0.267	0.227	100.42
SP5bAgEF7	37	0.537	104.81	0.156	0.283	0.38	106.166
SP5bAgEF8	38	0.914	90.709	0.032	0.214	0.182	92.051
SP5bAgEF9	39	0.143	6.411	0.05	0.036	0.000	6.64
SP5bAgEF10	40	0.525	104.672	0.123	0.6	0.098	106.018
SP5bQuAB1	41	0.662	102.493	0.091	0.514	0.063	103.823
SP5bQuAB2	42	0.831	98.783	0.146	0.255	0.12	100.135
SP5bQuAB3	43	0.536	21.54	0.01	0.109	0.000	22.195
SP5bQuAB4	44	0.852	100.277	0.44	0.398	0.246	102.213
SP5bQuAB5	45	0.176	98.534	0.137	0.297	0.162	99.306
SP5bQuAB6	46	23.018	62.475	0.231	4.706	0.577	91.007
SP5bQuAB7	47	0.255	98.263	0.103	0.44	0.191	99.252
SP5bQuAB8	48	0.512	99.612	0.078	0.521	0.227	100.95
SP5bQuAB9	49	0.094	100.086	0.025	0.69	0.199	101.094
SP5bQuAB10	50	0.15	99.698	0.051	1.441	0.285	101.625
SP5bQuAB11	51	0.348	92.128	0.041	0.812	0.202	93.531
SP5bQuAB12	52	0.615	102.793	0.074	1.536	0.318	105.336
SP5bQuAB13	53	0.303	99.971	0.073	1.16	0.49	101.997
SP5bQuAB14	54	0.642	95.352	0.051	1.353	0.546	97.944

SP5bQuAB15	55	0.081	104.143	0.151	0.181	0.041	104.597
SP5bQuAB16	56	0.267	100.37	0.311	0.315	0.037	101.3
SP5bQuAB17	57	0.934	86.951	0.239	1.163	0.018	89.305
SP5bQuAB18	58	0.025	103.563	0.188	0.137	0.037	103.95
SP5bQuAB19	59	0.015	98.706	0.211	0.227	0.002	99.161
SP5bQuAB20	60	0.522	99.212	0.11	0.78	0.193	100.817
SP5EF4AB1	1	0.5	100.536	0.106	0.542	0.138	101.822
SP5EF4AB2	2	0.613	103.087	0.069	0.008	2.118	105.895
SP5EF4AB3	3	0.968	102.07	0.057	0.024	0.387	103.506
SP5EF4AB4	4	0.684	102.722	0.000	0.034	0.457	103.897
SP5EF4AB5	5	0.621	99.266	0.039	0.000	0.179	100.105
SP5EF4AB6	6	0.887	101.892	0.05	0.03	0.265	103.124
SP5EF4AB7	7	0.293	102.849	0.041	0.075	0.058	103.316
SP5EF4AB8	8	0.045	104.041	0.071	0.125	0.005	104.287
SP5EF4AB9	9	0.09	100.789	0.055	0.096	0.035	101.065
SP5EF4AB10	10	0.096	102.681	0.047	0.043	0.024	102.891
SP5EF4AB11	11	0.064	104.884	0.066	0.096	0.05	105.16
SP5EF4AB12	12	0.017	100.092	0.03	0.034	0.023	100.196
SP5EF4AB13	13	0.117	101.931	0.042	0.034	0.044	102.168
SP5EF4AB14	14	0.323	102.508	0.006	0.113	0.087	103.037
SP5EF4AB15	15	0.013	100.401	0.017	0.066	0.014	100.511
SP5EF4AB16	16	0.176	102.346	0.022	0.081	0.029	102.654
SP5EF4AB17	17	0.165	95.898	0.021	0.014	0.07	96.168
SP5EF4AB18	18	1.003	101.47	0.022	0.022	0.471	102.988
SP5EF4AB19	19	0.985	100.334	0.012	0.009	0.501	101.841
SP5EF4AB20	20	1.651	102.902	0.04	0.023	0.629	105.245
SP5EF4C01	21	0.671	100.701	0.039	0.000	1.769	103.18
SP5EF4D01	22	0.529	100.478	0.102	0.665	0.219	101.993
SP5EF4EF1	23	0.702	100.242	0.085	0.184	0.281	101.494
SP5EF4EF2	24	0.289	98.612	0.031	0.000	2.428	101.36
SP5EF4EF3	25	1.059	103.975	0.018	0.000	0.626	105.678
SP5EF4EF4	26	1.104	99.684	0.000	0.000	0.711	101.499
SP5EF4EF5	27	0.255	102.785	0.06	0.077	0.083	103.26
SP5EF4EF6	28	0.537	100.323	0.000	0.01	0.723	101.593
LE2bFaA01	29	0.488	102.069	0.339	0.556	0.176	103.628
LE2bFaBC1	30	2.405	100.561	1.176	0.000	0.049	104.191
LE2bFaBC2	31	2.899	98.613	0.041	0.012	0.048	101.613
LE2bFaBC3	32	0.966	99.442	0.027	0.000	0.073	100.508
LE2bFaBC4	33	2.866	97.243	0.059	0.031	0.064	100.263
LE2bFaBC5	34	1.114	102.082	0.037	0.000	0.000	103.233
LE2bFaBC6	35	3.012	76.381	1.029	0.000	0.000	80.422
LE2bFaBC7	36	0.996	98.468	0.068	0.026	0.018	99.576
LE2bFaBC8	37	1.151	92.098	0.027	0.119	0.027	93.422
LE2bFaBC9	38	1.416	94.061	0.833	0.000	0.02	96.33
LE2bFaBC10	39	2.659	94.359	0.626	0.000	0.052	97.696
LE2bFaD01	40	0.651	101.576	0.232	1.289	0.392	104.14
LE2bFaE01	41	0.441	106.006	0.508	1.307	0.044	108.306
LE2bFaFG1	42	0.324	105.164	0.22	1.062	0.316	107.086
LE2bFaFG2	43	0.957	104.116	0.501	0.152	0.084	105.81
LE2bFaFG3	44	1.531	94.079	0.374	0.000	0.03	96.014
LE2bFaFG4	45	0.707	101.721	0.071	0.03	0.025	102.554

LE2bFaFG5	46	0.534	105.63	0.087	0.000	0.013	106.264

APPENDIX B

BASIC PROGRAM (TRACE.BAS)

```
TRACE.BAS: simulation of trace element partitioning during
     closed system diagenesis through iteration of
     mol-for-mol dissolution and reprecipitation


DIM D AS DOUBLE           'Partition coefficient of TRACER
DIM TCATCON AS DOUBLE     'initial cation concentration
DIM CL AS DOUBLE          'CARRIER concentration in solution
DIM TL AS DOUBLE          'TRACER concentration in solution
DIM TS AS DOUBLE          'moles of TRACER added to solid each
                           iteration
DIM ITERMOL AS DOUBLE     'precipitation interval in moles
DIM SOURCE AS DOUBLE      'weight concentration of dissolving
                           phase
DIM TCLIQ AS DOUBLE       'ratio of TRACER to CARRIER in
                           liquid
DIM TRAPPM AS DOUBLE      'weight percent of TRACER in last
                           dLMC precipitated
DIM TCCEM AS DOUBLE       'ratio of TRACER to CARRIER in dLMC
                           precipitate
DIM TRMOL AS DOUBLE       'temporary variable in mol to weight
                           conversion
DIM CAMOL AS DOUBLE
DIM NMOL AS DOUBLE
DIM MMOLS AS DOUBLE
DIM XPOS AS DOUBLE
DIM YPOS AS DOUBLE
DIM DECAY AS SINGLE


DIM FILENO AS INTEGER     'file counter
DIM I AS SINGLE           'iteration step:
                           dissolution-reprecipitation events
DIM IMAX AS SINGLE        'maximum number:
                           dissolution-reprecipitation events
DIM DISPINC AS INTEGER

'define atomic weights
DEF FNAWT (ELEM$)
DIM AWMg AS DOUBLE: AWMg = 24.305
DIM AWCa AS DOUBLE: AWCa = 40.08
DIM AWMn AS DOUBLE: AWMn = 54.938
```

```
DIM AWFe AS DOUBLE: AWFe = 55.847
DIM AWSr AS DOUBLE: AWSr = 87.62
DIM AWCO3 AS DOUBLE: AWCO3 = 60.009

DIM AWMgCO3 AS DOUBLE: AWMgCO3 = 84.314
DIM AWMnCO3 AS DOUBLE: AWMnCO3 = 114.947
DIM AWFeCO3 AS DOUBLE: AWFeCO3 = 115.856
DIM AWSrCO3 AS DOUBLE: AWSrCO3 = 147.629
DIM AWCaCO3 AS DOUBLE: AWCaCO3 = 100.089

EL$ = UCASE$(ELEM$)
IF EL$ = "MG" THEN
    FNAWT = AWMg
ELSEIF EL$ = "MN" THEN
    FNAWT = AWMn
ELSEIF EL$ = "FE" THEN
    FNAWT = AWFe
ELSEIF EL$ = "SR" THEN
    FNAWT = AWSr
ELSEIF EL$ = "MGCO3" THEN
    FNAWT = AWMgCO3
ELSEIF EL$ = "MNCO3" THEN
    FNAWT = AWMnCO3
ELSEIF EL$ = "FECO3" THEN
    FNAWT = AWFeCO3
ELSEIF EL$ = "SRCO3" THEN
    FNAWT = AWSrCO3
ELSEIF EL$ = "CACO3" THEN
    FNAWT = AWCaCO3
ELSEIF EL$ = "" THEN
    PRINT "Furnish elemental symbol"
    BEEP: FNAWT = 0
ELSE
    PRINT "NO atomic weight in LIBRARY for "; ELEM$: BEEP:
FNAWT = 0
    PRINT "REFURNISH solution parameters:"
END IF
END DEF

'mol to weight percent conversion
DEF fnMOLPPM (IMOL, NMOL, ELEM$)
fnMOLPPM = 1000000! * IMOL * FNAWT(ELEM$) / ((IMOL *
FNAWT(ELEM$)) + ((NMOL - IMOL) * FNAWT("CaCO3")))
END DEF

'weight percent to mol conversion
DEF fnPPMMOL (NMOL, SOURCE, ELEM$)
'assume 1 gram
TRMOL = SOURCE / FNAWT(ELEM$)
CAMOL = (1000000 - SOURCE) / FNAWT("CaCO3")
'TRMOL/CAMOL=molar ratio of trace to carrier
```

```
fnPPMMOL = (NMOL * TRMOL) / (CAMOL + TRMOL)
END DEF

DEF fnXPLTPOS (XPOS)
fnXPLTPOS = (7600 * XPOS / XMAX) + 1500
END DEF

DEF fnYPLTPOS (YPOS)
fnYPLTPOS = (5700 * YPOS / YMAX) + 1800
END DEF

'
'
'
'
'
'                                  [Tr]
'                                  [--]
'                                  [Cr]s
'                          D =  ---------
'                                  [Tr]
'                                  [--]
'                                  [Cr]aq
'
'
'
'
'MAIN PROGRAM start
'open output files
    LBINC = 0
10  CLOSE : CLS :  I = 0: ICOUNT = 0
SCREEN 0: SCREEN 12: COLOR 3
WIDTH 80
PRINT USING "EDIT this date if not correct [\        \]";
DATE$;
INPUT " ", NEWDATE$
    IF LEN(NEWDATE$) > 0 THEN DATE$ = NEWDATE$
IF DRV$ = "" THEN
    INPUT "ENTER DRIVE for output files [D:]", DRV$
    IF DRV$ = "" THEN
        DRV$ = "D:"
    ELSEIF INSTR(DRV$, "\") > 0 THEN
        DRV$ = DRV$
    ELSE
        DRV$ = MID$(DRV$, 1, 1) + LTRIM$(":")
    END IF
END IF
FILENO = FILENO + 1
PRINT USING "ENTER filenumber [##] "; FILENO;
INPUT "", NEWFILENO$
IF NEWFILENO$ <> "" THEN FILENO = VAL(NEWFILENO$)
INFIL$ = DRV$ + MID$(DATE$, 1, 5) + "(" +
LTRIM$(STR$(FILENO)) + ".OUT"
OPEN INFIL$ FOR OUTPUT AS 1

KEY(10) ON
```

```
ON KEY(10) GOSUB 40
'ENTER initial solution parameters
20  PRINT "INITIAL SOLUTION PARAMETERS"
    INPUT "ENTER total (mol/l) cation concentration in
liquid phase [.0025] ", TCATCON
    IF TCATCON = 0 THEN TCATCON = .0025#
30  PRINT USING "ENTER tracer element [\\]"; ELEM$; : INPUT
" ", NEWELEM$
    IF LEN(NEWELEM$) > 0 THEN ELEM$ = NEWELEM$
    IF FNAWT(ELEM$) = 0 THEN GOTO 30

35 LOCATE CSRLIN - 1, 30
PRINT USING "PARTITION COEFFICIENT [##.###]"; D;
INPUT " ", NEWD
IF NEWD > 0 THEN
    D = NEWD
ELSEIF NEWD = 0 AND D = 0 THEN
    SOUND 2000, 5
    PRINT "D must be > zero"
    GOTO 35
END IF
PRINT USING "ENTER tracer concentration in dissolving phase
[\    \] (if mol% add M)"; LTRIM$(STR$(SOURCE));
INPUT " ", NEWSOURCE$
'start insert
IF UCASE$(RIGHT$(NEWSOURCE$, 1)) = "M" THEN
    NEWSOURCE$ = STR$(fnMOLPPM(VAL(NEWSOURCE$), 100, ELEM$))
    PRINT USING "##.##^^^^ PPM"; VAL(NEWSOURCE$)
END IF
IF VAL(NEWSOURCE$) > 0 THEN SOURCE = VAL(NEWSOURCE$)
'end insert

IF ITERMOL = 0 THEN ITERMOL = .0001
PRINT "ENTER precipitation interval ";
PRINT USING "[##.##^^^^]"; ITERMOL;
INPUT " ", NEWITERMOL
IF NEWITERMOL > 0 THEN
    ITERMOL = NEWITERMOL
END IF
IF ITERMOL = 0 THEN ITERMOL = .0001

IF TCATCON <= ITERMOL THEN
       BEEP: PRINT "ITERMOL<=TCATCON: furnish new
parameters": GOTO 20
END IF
IF MMOLS = 0 THEN MMOLS = 100
PRINT USING "ENTER MAXIMUM MMOL OF PRECIPITATE TO FORM [###]
"; MMOLS;
INPUT "", REVMOLS
IF REVMOLS > 0 THEN
    MMOLS = REVMOLS
```

```
ELSEIF OLDMOLS > 0 AND REVMOLS = 0 THEN
    MMOLS = OLDMOLS
ELSE
    MMOLS = 100
END IF
OLDMOLS = MMOLS
'calculate maximum iterations necessary
'to achieve desired MMOLS
IMAX = MMOLS / (1000 * ITERMOL)
45 PRINT "DISPLAY INCREMENT ["; IMAX / 100; "]";
INPUT " ", DISPINC
IF DISPINC = 0 THEN DISPINC = IMAX / 100
IF DISPLINC < 1 AND DISPLINC > 0 THEN
    BEEP
    PRINT "DISPLAY INCREMENT MUST BE >=1: EDIT . ."
    GOTO 45
    END IF
IF DECAY = 0 THEN DECAY = 1
PRINT USING "ENTER DECAY/ENRICHMENT FACTOR IF DESIRED
[##.####]"; DECAY;
INPUT " ", NDECAY
IF NDECAY > 0 THEN DECAY = NDECAY

LINE INPUT "ENTER A PLOT TITLE ", TITLE$

'DISPLAY parameters
'get trace moles in liquid
TL = fnPPMMOL(TCATCON, SOURCE, ELEM$)
CL = TCATCON - TL
TCAQINIT = TL / CL
CLS
GOSUB 2500
GOSUB 5000
PRINT ""
PRINT "                    PLOT TITLE = "; LTRIM$(TITLE$)
PRINT "   TOTAL CATION CONCENTRATION ="; : PRINT USING
"##.##^^^^"; TCATCON
PRINT " INITIAL TRACER CONCENTRATION ="; : PRINT USING
"##.##^^^^"; TL
PRINT "INITIAL CARRIER CONCENTRATION ="; : PRINT USING
"##.##^^^^"; CL
PRINT "   INITIAL TRACE/CARRIER (aq) ="; : PRINT USING
"##.##^^^^"; TCAQINIT
PRINT USING "                          \\ "; UCASE$(MID$(ELEM$, 1,
1)) + LTRIM$(LCASE$(MID$(ELEM$, 2, 1)));
PRINT "PCoeff ="; : PRINT USING "###.##"; D
PRINT "         MMOLS TO PRECIPITATE ="; : PRINT USING
"##.##^^^^"; MMOLS
PRINT "     PRECIP BY MOLE ITERATION ="; : PRINT USING
"##.##^^^^"; ITERMOL
```

```
PRINT "   MAXIMUM NUMBER OF SOL-REPS ="; : PRINT USING
"##.##^^^^"; IMAX
INPUT "<ENTER> to continue, any other key to RESTART ",
PROC$
IF PROC$ <> "" THEN CLOSE : FILENO = FILENO - 1: GOTO 10

IF OLDYMAX = 0 THEN OLDYMAX = YMAX
47 PRINT USING "EDIT Y AXIS MAXIMUM [##.##^^^^] <CR> to
accept"; OLDYMAX;
INPUT " ", CHOICE$
REVYMAX = VAL(CHOICE$)
IF REVYMAX > 0 THEN 'if there was an entry then use it
    YMAX = REVYMAX
ELSE 'if no entry, assume default or loop for suggestion
    PRINT USING "USE [##.##^^^^]? OR SUGGEST (<CR> FOR
DEFAULT)"; OLDYMAX;
    INPUT " ", CHOICE$
    IF NOT CHOICE$ = "" THEN
        BEEP
        GOSUB 2500
        OLDYMAX = YMAX
        GOTO 47
    ELSE
        YMAX = OLDYMAX
        END IF
END IF
OLDYMAX = YMAX
LOCATE 25, 1: PRINT "OUTPUT FILE: "; INFIL$; " -- <F10> TO
ABORT"
'clear bottom half of screen
FOR J = 1 TO 80
    FOR K = 16 TO 24
        LOCATE K, J: PRINT CHR$(0);
    NEXT K
NEXT J
'clear left half of screen
FOR J = 1 TO 80
    FOR K = 1 TO 7
        LOCATE K, J: PRINT CHR$(0);
    NEXT K
NEXT J
GOSUB 5000

'LOCATE 24, 1: FOR J = 1 TO 79: PRINT CHR$(45); : NEXT J
'LOCATE 16, 1: FOR J = 1 TO 79: PRINT CHR$(45); : NEXT J

VIEW PRINT 16 TO 25

'set title line for output file
PRINT #1, USING "\\MMOL "; ELEM$;
PRINT #1, USING "\\Caaq "; ELEM$;
```

```
PRINT #1, USING "\\Caso "; ELEM$;
PRINT #1, USING "\\PPM"; ELEM$

ROW = CSRLIN + 1
LOOPSTART = TIMER
'loop until equilibrium or IMAX reached
WHILE I * ITERMOL * 1000 < MMOLS
    TS = ITERMOL * D * TL / (CL + (D * TL))
    CS = ITERMOL - TS
    I = I + 1 'I=iterations
    TCLIQ = TL / CL
    TCCEM = TS / CS
    TL = TL - TS
    CL = CL - CS
    TRAPPM = fnMOLPPM(TS, ITERMOL, ELEM$)
'determine if DISplay INCrement reached
    IF I = 1 OR DISPINC < 1 THEN
        GOSUB 1000
        GOSUB 2000
    ELSEIF I / DISPINC - INT(I / DISPINC) = 0 THEN
        GOSUB 1000
        GOSUB 2000
    END IF
GOSUB 1500 'write to file
'restore fluid saturation
'determine mols TRACER delivered by next batch dissolution
    REPTL = fnPPMMOL(ITERMOL, SOURCE, ELEM$)
    SOURCE = (SOURCE + (SOURCE * DECAY)) / 2

'determine mols CARRIER
    REPCL = ITERMOL - REPTL
'add to existing fluid
    TL = TL + REPTL
    CL = CL + REPCL
    IF TL < 0 THEN
        SOUND 1000, 5
        CLS 2
        PRINT "TL<0 "
        INPUT "REDEFINE parameters, <ENTER> when ready",
RETURN$
        GOTO 10
    ELSEIF CL < 0 THEN
        SOUND 1000, 5
        CLS 2
        PRINT "CL<0 "
        INPUT "REDEFINE parameters, <ENTER> when ready",
RETURN$
        GOTO 10
    END IF
    WEND
```

```
40 KEY(10) OFF
GOSUB 1000 'last screen updates
GOSUB 2000
CLOSE
LOCATE 23, 1
SOUND 2000, 5
INPUT " PLOTTER HARDCOPY [N] "; GOPLOT$
IF GOPLOT$ <> "" THEN GOSUB 4000

LOCATE 24, 1
PRINT " SAVE "; INFIL$; " FOR SIGMAPLOT [N]";
INPUT " ", SIGMA$
IF SIGMA$ = "" THEN
    GOTO 50
ELSE
    OPEN INFIL$ FOR INPUT AS 1
    SIGFIL$ = MID$(INFIL$, 1, LEN(INFIL$) - 3) + "SPT"
    OPEN SIGFIL$ FOR OUTPUT AS 3
    LINE INPUT #1, header$
    PRINT #3, header$
    Dataline = 0
    WHILE NOT EOF(1)
        INPUT #1, I, TCLIQ, TCCEM, TRAPPM
        PRINT #3, USING "#######.#########"; I, TCLIQ,
TCCEM, TRAPPM
        Dataline = Dataline + 1
        LOCATE 24, 43
        PRINT USING "#####"; Dataline
        WEND
    CLOSE
END IF
LOCATE 24, 50
SOUND 2000, 5
PRINT " SAVED"
KILL INFIL$
50 LOCATE 23, 1
PRINT " CONTINUE [Y]                ": LOCATE 23, 14: INPUT
" ", REP$
IF REP$ = "" THEN
    LOCATE CSRLIN - 1, 1
    PRINT " REUSE "; INFIL$; " [Y]";
    INPUT REUSE$
    IF REUSE$ = "" THEN FILENO = FILENO - 1
    GOTO 10
END IF

SCREEN 12: WIDTH 80, 50
PRINT "*** END RUN TRACER1"
PRINT ""
FILES MID$(INFIL$, 1, LEN(INFIL$) - 6) + "*.*"
```

```
END

'SUBROUTINES-----------------------------------------------
1000 'write PRINT statments to screen
LOCATE ROW, 1
PRINT USING "###### TOTAL SOLREPS"; I;
PRINT USING "###.## minutes elapsed "; (TIMER - LOOPSTART) /
60;
PRINT USING "  ####.#  MMOL PRECIPITATED"; I * ITERMOL *
1000
COLOR 15: PRINT " [TCLIQ] mol[TRACER]/mol[CARRIER] of liquid
";
PRINT USING "##.###^^^^"; TCLIQ
COLOR 12: PRINT " [TCCEM] mol[TRACER]/mol[CARRIER] of cement
";
COLOR 3
PRINT USING "##.###^^^^"; TCCEM
PRINT USING " [TRAPPM] [\\] last dLMC precipitate"; ELEM$;
PRINT USING "####### PPM"; fnMOLPPM(TS, ITERMOL, ELEM$)
PRINT USING " TOTAL CONCENTRATION OF FLUID: ##.#^^^^"; TL +
CL
PRINT " "; CHR$(127); " SOURCE - DIAGENETIC dLMC PHASES";
PRINT USING "####### PPM"; SOURCE - TRAPPM;
PRINT USING "  SOURCE: ####### PPM"; SOURCE

RETURN

1500 'write to output file
PRINT #1, USING "###.######^^^^ "; I * ITERMOL * 1000;
PRINT #1, USING "###.######^^^^ "; TCLIQ, TCCEM;
PRINT #1, USING "###.######^^^^ "; TRAPPM
RETURN

2000 'video plot display loop
IF ICOUNT = 0 THEN
    GOSUB 3000
    oldcpx = 0
    oldcpy = TCCEM
    oldlpx = 0
    oldlpy = TCAQINIT
    ICOUNT = -1
END IF

LINE (oldcpx, oldcpy)-(I * ITERMOL * 1000, TCCEM), 12
LINE (oldlpx, oldlpy)-(I * ITERMOL * 1000, TCLIQ), 15
oldcpx = I * ITERMOL * 1000: oldcpy = TCCEM
oldlpx = I * ITERMOL * 1000: oldlpy = TCLIQ

RETURN

2500 'return graphics viewport logical dimensions
```

```
XMIN = 0
XMAX = MMOLS
YMIN = 0
Factor = 1
CFactor = 0
IF D >= 1# THEN
    YMAX = (TCAQINIT * D) + (.2 * (TCAQINIT * D))
ELSEIF D = 0 THEN
    BEEP
    GOTO 10
ELSE
    YMAX = (TCAQINIT / D) + (.2 * (TCAQINIT / D))
END IF
RETURN

3000 'initialize graphics viewport
INPUT "FULL (0) or HALF (1) SCREEN DISPLAY [0] ", NUL
IF NUL = 0 THEN
    VIEW (1, 20)-(630, 250), 1, 3
ELSE
    VIEW (340, 20)-(630, 250), 1, 3
END IF
WINDOW (XMIN, YMIN)-(XMAX, YMAX)
LOCATE CSRLIN - 1, 1
PRINT SPACE$(50)
RETURN

4000 'HP7475 hardcopy
COUNT = 0: NOTITLE = 0
LOCATE 23, 1
PRINT "LOAD PLOTTER, hit <CR>"
INPUT "", PLOT$
KEY(10) ON: ON KEY(10) GOSUB 4020
LOCATE 23, 1
OPEN "COM1:4800,S,7,1,RS,CS65535,CD,DS" FOR RANDOM AS 2
PRINT #2, CHR$(27) + ".Y";
PRINT #2, "IN;PS4;SP1;"
PRINT #2, "IP 1500,1800,9100,7500;VS;SP1;"
INPUT "PLOT TITLES AND AXES [N] ", PLOT$
IF PLOT$ = "" THEN
    NOTITLE = -1
    GOTO 4015
ELSE
'26 chr input str
    NOTITLE = 0
    GOTO 4011
END IF
'initialize plotter and set scaling of P1 and P2

4011 'frame plot
PRINT #2, "PA"; fnXPLTPOS(XMIN); fnYPLTPOS(YMAX); ";PD,";
```

```
PRINT #2, USING "###### ,"; fnXPLTPOS(XMIN),
fnYPLTPOS(YMIN); fnXPLTPOS(XMAX), fnYPLTPOS(YMIN);
fnXPLTPOS(XMAX), fnYPLTPOS(YMAX); fnXPLTPOS(XMIN),
fnYPLTPOS(YMAX);
PRINT #2, ";PU;"
'axis ticks and labels
XTICK = (XMAX - XMIN) / 5
YTICK = (YMAX - YMIN) / 5
FOR L = 0 TO 5
    PRINT #2, "PA"; fnXPLTPOS(XMIN + L * (XTICK));
fnYPLTPOS(YMIN); ";XT;"
    PRINT #2, "PA"; fnXPLTPOS(XMIN + L * (XTICK));
fnYPLTPOS(YMIN);
    PRINT #2, ";CP-4,-2;LB";
    PRINT #2, USING "##.#^^^^"; XMIN + L * (XTICK);
    PRINT #2, CHR$(3);
    NEXT L
FOR L = 0 TO 5
    PRINT #2, "PA"; fnXPLTPOS(XMIN); fnYPLTPOS(YMIN + L *
(YTICK)); ";YT;"
    PRINT #2, "PA"; fnXPLTPOS(XMIN); fnYPLTPOS(YMIN + L *
(YTICK));
    PRINT #2, ";CP-11,-.25;LB";
    PRINT #2, USING "##.##^^^^"; YMIN + (L * (YTICK));
    PRINT #2, CHR$(3);
    NEXT L
'axis titles
XMID = (XMAX - XMIN) / 2
YMID = (YMAX - YMIN) / 2
PRINT #2, "PA"; fnXPLTPOS(XMID), fnYPLTPOS(YMIN);
";CP-10,-5;LBMMOLS dLMC PRECIPITATED"; CHR$(3);
PRINT #2, "PA"; fnXPLTPOS(XMID), fnYPLTPOS(YMIN); ";CP";
-LEN(TITLE$) / 2; ",-7;LB" + TITLE$ + CHR$(3)
PRINT #2, "LT3;PA"; fnXPLTPOS(XMIN), fnYPLTPOS(YMIN);
"CP0,-5;LBliquid"; CHR$(3); "PD;PR500,0;PU;"
PRINT #2, "LT;PA"; fnXPLTPOS(XMIN), fnYPLTPOS(YMIN);
"CP0,-6;LBsolid"; CHR$(3); "PD;PR500,0;PU;SP1;"
PRINT #2, "PA"; fnXPLTPOS(XMIN), fnYPLTPOS(YMID);
";CP-3,-1;DI0,1;LBM/Ca"; CHR$(3);

4015 'file input
PRINT #2, ";PU;DI;IW1500,1800,9100,7500;PA"
OPEN INFIL$ FOR INPUT AS 1
LINE INPUT #1, header$
'plot liquid composition
PRINT #2, "LT3;SP"; LBINC + 2; ";PA"
WHILE NOT EOF(1)
    INPUT #1, I, TCLIQ, TCCEM, TRAPPM
    COUNT = COUNT + 1
    LOCATE 23, 40: PRINT USING "#######"; fnXPLTPOS(I),
fnYPLTPOS(TCLIQ)
```

```
    PRINT #2, USING "#######.,"; fnXPLTPOS(I),
fnYPLTPOS(TCLIQ);
    PRINT #2, ";OE;PA"
    MOD$ = INPUT$(LOC(2), #2)
    IF VAL(MOD$) = 3 THEN
        SOUND 2000, 1
        LOCATE 23, 60: PRINT USING "ERROR=\\"; MOD$
        PRINT #2, ";PU"
        COUNT = 0
        'count of 1 or greater
        'indicates an point w/i bounds, no ERR
    ELSEIF VAL(MOD$) = 0 THEN
        PRINT #2, ";PD";
    ELSE
        PRINT #2, ";PA";
    END IF
    IF TCLIQ > YMAX THEN
       YLASTOUT = fnYPLTPOS(TCLIQ)
       XLASTOUT = fnXPLTPOS(I)
    ELSE
       YLASTOUT = 0
    END IF
    IF COUNT = 1 THEN PRINT #2, ";PD"
WEND
PRINT #2, ";PU;LT;IW;"
GOSUB 4030: PRINT #2, ";PU;"
CLOSE 1
COUNT = 0
OPEN INFIL$ FOR INPUT AS 1
LINE INPUT #1, header$
PRINT #2, "PU;LT;IW 1500,1800,9100,7500;PA"
'plot cement
WHILE NOT EOF(1)
    INPUT #1, I, TCLIQ, TCCEM, TRAPPM
    COUNT = COUNT + 1
    LOCATE 23, 40: PRINT USING "#######"; fnXPLTPOS(I),
fnYPLTPOS(TCLIQ)
    PRINT #2, USING "#######.,"; fnXPLTPOS(I),
fnYPLTPOS(TCCEM);
    PRINT #2, ";OE;PA"
    MOD$ = INPUT$(LOC(2), #2)
    IF VAL(MOD$) > 0 THEN
        SOUND 2000, 1
        LOCATE 23, 60: PRINT USING "RANGE ERROR=\\"; MOD$
        PRINT #2, ";PU"
        COUNT = 0
    ELSEIF VAL(MOD$) = 0 THEN
        PRINT #2, ";PD";
    ELSE
        PRINT #2, ";PA";
    END IF
```

```
    IF TCCEM > YMAX THEN
       YLASTOUT = fnYPLTPOS(TCCEM)
       XLASTOUT = fnXPLTPOS(I)
    ELSE
       YLASTOUT = 0
    END IF
    IF COUNT = 1 THEN PRINT #2, ";PD"
WEND
'title script
'plot information box option
PRINT #2, ";PU;IW;"
GOSUB 4030

'upper line label
PRINT #2, ";PU;PA9200,"; 7500 - (400 * LBINC);
";SI.1051875,.1513125;"
PRINT #2, USING "LBD ##.##"; D;
PRINT #2, CHR$(3); "CP;"
PRINT #2, USING "LB\\"; ELEM$;
PRINT #2, USING "##.###^^^^ PPM"; SOURCE;
PRINT #2, CHR$(3); "CP;"
PRINT #2, USING "LB##.#^^^^ MMOL"; ITERMOL
PRINT #2, CHR$(3); "SI;PA10365,7600;SP0;"
LBINC = LBINC + 1

CLOSE
LOCATE 23, 1
INPUT "PLOT DATA BOX [N]          ", PLOT$
IF PLOT$ = "" THEN RETURN
OPEN "COM1:4800,S,7,1,RS,CS65535,CD,DS" FOR RANDOM AS 2
PRINT #2, ";PU;IP;SP1;PA110,100;DI0,1;SI.1051875,.1513125;"
PRINT #2, "LB";
PRINT #2, USING "SOURCE OF \\ "; ELEM$;
PRINT #2, USING "##.#^^^^ PPM"; SOURCE;
PRINT #2, CHR$(3); "PA210,100;LB"
PRINT #2, USING "PARTITION COEFFICENT D ##.##"; D;
PRINT #2, CHR$(3); "PA310,100;LB"
PRINT #2, USING "TOTAL CATIONS ##.##^^^^"; TCATCON;
PRINT #2, CHR$(3); "PA410,100;LB"
PRINT #2, USING "PRECIPITATE ##.####^^^^ MMOL@"; MMOLS;
PRINT #2, USING " ##.#^^^^ STEPS "; ITERMOL;
PRINT #2, CHR$(3); "PA510,100;LB"
PRINT #2, USING "\          \"; DATE$;
PRINT #2, CHR$(3); "PA610,100;LB"
PRINT #2, USING "\          \"; TIME$;
PRINT #2, CHR$(3);
'reset plotter
PRINT #2, "PU;SP0;PA10365,7600;"
4010 CLOSE
RETURN
'event for plot interrupt
```

```
4020 PRINT #2, "IN;PU;SP0;PA10365,7600;"
CLOSE
GOTO 50

4030 'handle curve termination labels
LOCATE 23, 1
INPUT "PLOT line label [N]       ", PLOT$
IF PLOT$ = "" THEN RETURN

IF YLASTOUT >= YMAX THEN
    PRINT #2, ";PU;IW;PA"; XLASTOUT, YMAX
ELSE
    YLASTOUT = 0
END IF

PRINT #2, ";PU;PR100,0;"
PRINT #2, ";PU;SI.1051875,.1513125;LB"
PRINT #2, USING "D ##.##"; D;
PRINT #2, CHR$(3); "CP 0,-1;LB"
PRINT #2, USING "\\"; ELEM$;
PRINT #2, USING "##.#^^^^"; SOURCE;
PRINT #2, CHR$(3); "SI;"
RETURN

5000 'display plot axial limits data
LOCATE 1, 48
PRINT "PLOT "; ELEM$; " * MMOL PRECIPITATE"
LOCATE 3, 1
PRINT "  AXIAL DIMENSIONS OF PLOT:"
PRINT "  XMIN = "; : PRINT USING " ###.#^^^^"; XMIN
PRINT "  XMAX = "; : PRINT USING " ###.#^^^^ MMOL"; XMAX
PRINT "  YMIN = "; : PRINT USING " ###.#^^^^"; YMIN
PRINT "  YMAX = "; : PRINT USING " ###.#^^^^"; YMAX
RETURN
```

APPENDIX C.

STRATIGRAPHIC DATA[6]

	Physical Description	Legal Description SECTION	TWP,RGE	COUNTY
AN1	M#3	SE SE 26	T15S R22E	Miami
AN6	Qy M#12, Cr#16	SE 7, SW 8	T16S R23E	Miami
AN7	N#84	0.8ms/NEcor 22	T15S R22E	Miami
BE1		NW SE NE 26	T46N R33W	Cass (MO)
BE2	N#37	SEcor 10	T14S R25E	Johnson
BU1		NW NE 4	T16S R25E	Miami
BU2	RC s/Bucyrus	C SW SW 1	T16S R24E	Miami
BU6	RC K69 n/K68	app NW NW 30	T16S R25E	Miami
DS1	Cr#2A	SW NE 25	T12S R22E	Johnson
DS2	Cr#2	NW NW NW 1	T13S R22E	Johnson
DS3	RC and Qy, K10	SE 6	T13S R23E	Johnson
ED1	Holliday Drive	C NE NW 6	T12S R24E	Johnson
GTNW1		C SL SW SW 31	T18S R21E	Franklin
LA1	M#40	SW NW 17	T18S R22E	Miami
LA4	abnd Qy	C SL W/2 20	T18S R22E	Franklin
LA5	A#13	NE SE 9	T19S R21E	Franklin

[6]**M#1** refers to locality 1 of MILLER (1966); similarly, **N#** refers to NEWELL (1935), **Cr#** to CROWLEY (1969), **A#** to BALL, BALL, and LAUGHLIN (1963). Other abbreviations used in physical descriptions: **Qy**=Quarry, **RC**=roadcut, **RD**=road ditch, **K**=Kansas State Highway, **surf** indicates erosional surface at top of section, **nd**=no data, **abnd**=abandoned, **mm**=mile marker, **cov**=covered, **abs**=absent, **m**=mile, **ba cov**=base of unit covered, **sx**=section, **app**=approximately. Compass abbreviations; **s/**, **nw/**, etc., indicates south of, northwest of, etc., **cor**=corner of.

Stratigraphic nomenclature abbreviations: **MrmLs**=Merriam Limestone, **BSpgSh**=Bonner Springs Shale, **Wyandtt**=Wyandotte Limestone, **FaLs**=Farley Limestone, **Ick-LSh**=Island Creek-Lane Shale, **AgLs**=Argentine Limestone, **baAgsh**=unnamed shale near base of Argentine Limestone, **baAgls**=basal bed of Argentine Limestone, **QuSh**=Quindaro Shale, **FbLs**=Frisbie Limestone, **LMemSh**=Liberty Memorial Shale, **RtnLs**=Raytown Limestone, **MnCkSh**=Muncie Creek Shale. All isopach measurements are in feet.

LA8	4 Corners Qy	C NW NW	23	T19S	R21E	Linn
LA9	RC 1.4w/RRX	C WL	7	T18S	R22E	Miami
LA10	Qy SW Osawatomie	C NW SE	20	T18S	R22E	Miami
LA11	RC sw/LA10	C SL W/2	20	T18S	R22E	Miami
LA12	N#110	SWcor	20	T18S	R22E	Miami
LA13	N#119	s/NWcor	13	T19S	R21E	Miami
LE1	Cr#17	SW SW SW	10	T13S	R24E	Johnson
LE2	RC K150 @K69	C NL NW NE	31	T13S	R25E	Johnson
LE3	Cr#31	SE	7	T13S	R25E	Johnson
LE4	Cr#18	NE NE NE	13	T13S	R24E	Johnson
LE5		app C WL SW	29	T13S	R25E	Johnson
LO1	RC K68 @K69	SEcor	30	T16S	R25E	Miami
LO3	K68 @1.7wK69	C NL NW	35	T16S	R24E	Miami
LO6	RC s/Louisburg	C WL SW SW	5	T17S	R25E	Miami
OL1	Craig Qy	SL SE SE SW	25	T12S	R23E	Johnson
OL2	Cr#9	NE NE	32	T13S	R23E	Johnson
PE1	RC K68 @3.6wK69	C NL NE NW	33	T16S	R24E	Miami
PE2	RC K68	C NL NW NW	33	T16S	R24E	Miami
PE3	RC K68 @2.6eK7	C NL NW NW	32	T16S	R24E	Miami
PE4	RC K68 @2.2eK7	C NL NE	31	T16S	R24E	Miami
PE5	RC K68 @1.5eK7	C SW SW SW	30	T16S	R24E	Miami
PE6	RC K68 @0.4eK7	SL SE SE SE	26	T16S	R23E	Miami
PE7	RC K68 @K7	NL NW NE	35	T16S	R23E	Miami
PE8	RC K7 @0.1sK68	W/2 NW NE	35	T16S	R23E	Miami
PE9	RC K7 @0.5sK68	C	35	T16S	R23E	Miami
PE15	K7 @LkMiola	C	11	T16S	R23E	Miami
PE16	N#141	W/2 NE	14	T17S	R23E	Miami
PE17	RC K68	W/2 SL SE SE	31	T16S	R24E	Miami
PE23	N#139	E/2 NW	25	T17S	R23E	Miami
PE24	N#138	E/2 NE	25	T17S	R23E	Miami
PE25	N#137	W/2 NE	36	T17S	R23E	Miami
PE26	N#148	NW NW NW	31	T17S	R24E	Miami
PE27	M#34, N#147	SW SW SW	29	T17S	R24E	Miami
PE28	N#151	E/2 SE	6	T18S	R24E	Miami
PO1		SW SE SW	12	T17S	R20E	Franklin
PO2		C N/2	24	T17S	R20E	Franklin
PW1	RC K68 w/BullCk	C SL SE	29	T17S	R22E	Miami
PW2	RC K68 @4.5wK7	C SL SE SE	25	T16S	R22E	MIAMI
PW4	RC K68 @6.4wK7	C SL SW SW	26	T16S	R22E	Miami
PW5	M#24	SEcor	6	T17S	R23E	Miami
PW6	RD w/PlumCk Ch	C SL SW SE	21	T17S	R22E	Miami
PW10	abnd Qy M#25	SE SE SE	7	T17S	R23E	Miami
PW11	Qy w/Paola	C SW SE SE	18	T17S	R23E	Miami
PW12	RC K7 @mm124	C N/2 NW	6	T18S	R23E	Miami
PW14	N#104	0.2mw/NEcor	13	T17S	R22E	Miami
PW15	N#112	SEcor	15	T17S	R22E	Miami
RA6	A#2	SE/4	8	T17S	R21E	Franklin
RA7	A#3	EL	7	T17S	R21E	Franklin
RA8	RC e/Stanton	C EL NE	25	T17S	R21E	Miami
RA9	RC TurkeyCk	WL NW NW	10	T17S	R21E	Franklin
SH1	RC and Qy Cr#5		29	T11S	R25E	Wyandotte

SH2	RC Cr#4	NE NE NW	4	T12S R25E	Johnson
SP1	RC e/Hillsdale	W/2 SW SE	11	T16S R23E	Miami
SP5	Qy s/Wagstaff	W/2 NW NE	30	T16S R24E	Miami
SP6	RRX sw/Wagstaff	C SE SE SE	13	T16S-R23E	Miami
ST5	RC K69 N#33	W/2 NE	30	T14S R25E	Johnson
ST6	Qy Cr#11	SW SE	31	T14S R25E	Johnson

	°W LONG	°N LAT	GL DATUM	ISOPACHS MrmLs	BSpgSh	Total Wyandtt	FaLs
AN1	94.9297	38.7093			17.4	92.1	10.2
AN6	94.8980	38.6690		2.1	11.3	124.4	15.8
AN7	94.9457	38.7271				12.0	12
BE1	94.5353	38.7809	965			46.0	5.7
BE2	94.6116	38.8318				nd	
BU1	94.6450	38.6939	1060			0.4	g
BU2	94.7090	38.6793	1010		surf	46.6	8.0
BU6	94.6920	38.6339	1075		surf	7.5	2.0
DS1	94.9150	38.9790			27	28.0	27
DS2	94.9259	38.9554			12	26.0	c
DS3	94.8936	38.9473				47.3	28.8
ED1	94.7916	39.0417	910	surf	8.0	104.0	45.0
GTNW1	95.1368	38.4338	930		surf	6.0	6.0
LA1	95.0110	38.4879				nd	
LA4	95.1014	38.4452	970		surf	27.0	27.0
LA5	95.0901	38.4095		1.5	0.3	43.5	43.5
LA8	95.0643	38.3874	1040	surf	3.0	34.0	34.0
LA9	95.0272	38.4992	980			8.0	8.0
LA10	95.0004	38.4675	920			5.5	
LA11	95.0060	38.4624	1020			100.0	5.0
LA12	95.0099	38.4624				nd	
LA13	95.0727	38.3952				nd	>20
LE1	94.7414	38.9280			27	34.6	6
LE2	94.6741	38.8835	936		cov	14.2	6.2
LE3	94.6719	38.9318			45	82.1	14.1
LE4	94.6885	38.9266			>43	85.1	13.1
LE5	94.6675	38.8880					
LO1	94.6943	38.6211	1080			22.9	
LO3	94.7258	38.6213	1040		surf	11.0	4.0
LO6	94.6753	38.5949	1060			10.5	
OL1	94.8078	38.9706			16	57.1	26.6
OL2	94.8709	38.8830			37	68.7	25.7
PE1	94.7615	38.6212	1015	surf	5.7	4.3	4.3
PE2	94.7676	38.6213	975			12.0	
PE3	94.7853	38.6212	920			nd	
PE4	94.7922	38.6211	980		surf	3.0	3.0
PE5	94.8080	38.6211	1065	10.0	cov	nd	
PE6	94.8287	38.6213	1020			7.0	7.0
PE7	94.8343	38.6208	1010		surf	58.3	6.0
PE8	94.8354	38.6184	970			7.0	

PE9	94.8354	38.6136	975			7.0	
PE15	94.8348	38.5846	950			9.5	
PE16	94.8312	38.5781				nd	
PE17	94.7911	38.6065	930			nd	
PE23	94.8254	38.5485				nd	
PE24	94.8090	38.5484				nd	
PE25	94.8124	38.5343				nd	
PE26	94.8080	38.5343				nd	
PE27	94.7882	38.5348				nd	
PE28	94.7884	38.5074				nd	
PO1	95.1499	38.5800				nd	
PO2	95.1467	38.5616				15.0	15
PW1	94.8872	38.6217	910			5.5	
PW2	94.9209	38.6211	1045			23.0	23.0
PW4	94.9535	38.6219	1040			8.0	8.0
PW5	94.9180	38.5925				52.8	12.9
PW6	94.9846	38.5499	995			10.0	10.0
PW10	94.9018	38.5803				111.7	
PW11	94.9023	38.5664	900			6.7	
PW12	94.9146	38.5184	940			2.5	
PW14	94.9219	38.5779				14.0	14
PW15	94.9556	38.5639				nd	>10
RA6	95.1024	38.5814		2.8	26	23.1	23.1
RA7	95.1207	38.5861		6	24	5.0	5
RA8	95.0280	38.5434	970			40.0	40.0
RA9	95.0833	38.5929	915	7.5	37.5	14.0	14.0
SH1	94.6576	39.0703			33	65.0	24
SH2	94.6443	39.0438			25	42.0	5
SP1	94.8346	38.6674	990		surf	14.0	14.0
SP5	94.7979	38.6334	1010		surf	49.4	8.0
SP6	94.8087	38.6511	1070			nd	
ST5	94.6746	38.8071				nd	>27
ST6	94.6749	38.7836			28	87.0	33

	ICk-LSh	AgLs	baAgsh	baAgls	QuSh	FbLs	LMemSh
AN1	81.9						
AN6	108.6						
AN7	>18						
BE1	0.5	35.2			3.2	1.5	44.0
BE2							22
BU1	0.4	cov					
BU2	1.6	37.0	abs	abs	cov		
BU6	0.5	5.0			cov		
DS1	COV	COV			COV	1	38
DS2	1	25			cov	cov	45
DS3	1.5	17					
ED1	11.0	44.0	0.0	0.0	1.0	3.0	47.5
GTNW1	cov						
LA1							

LA4	cov						
LA5	>33						
LA8	cov						
LA9							
LA10	cov	1.0	0.5	4.0	abs	abs	0.5
LA11	95.0						
LA12	>100						
LA13	>15						
LE1	16	11			0.1	1.5	38
LE2	8.0	cov					
LE3	68	cov					
LE4	72	cov					
LE5		>2.7					
LO1	surf	20.0	abs	abs	2.0	0.9	>1.2
LO3	1.0	6.0			cov		
LO6		5.0	abs	abs	3.5	2.0	65.7
OL1	7	15			3.5	5	45
OL2	0.5	35			5.5	2	40
PE1	cov						
PE2		12.0			cov		
PE3							
PE4	cov						
PE5							
PE6							
PE7	45.3	2.8	0.8	3.5	abs?	abs?	
PE8	surf	2.8	0.8	3.5	abs?	abs?	
PE9	surf	2.8	0.8	3.5	abs?	abs?	
PE15	surf	9.5	abs	abs	abs	abs	38.0
PE16							
PE17							
PE23							20
PE24							20
PE25							20
PE26							22
PE27							24.1
PE28							19
PO1							
PO2							
PW1		5.5			abs	abs	0.8
PW2	cov						
PW4	>13.3	cov					
PW5	39.9	<5					
PW6	ba cov	cov					
PW10	108	3.7					3.8
PW11		1.5	0.5	4.7	abs?	abs?	11.9
PW12		2.5	abs?	abs?	abs?	abs?	0.2
PW14							
PW15	~106						
RA6	>24						
RA7	>40						
RA8	ba cov						

RA9	>4	cov					
SH1	7	33			0	1	38
SH2	4	32			0.5	0.5	21
SP1	>31.2	cov					
SP5	0.6	36.1	abs	abs	0.6	4.2	cov
SP6							
ST5	2	<36				3	27.5
ST6	2	50			0	2	22

	RtnLs	MnCkSh	Remarks
AN6			Wy submerged
AN7			from NEWELL (1932), locality N#84
BE1	6.8	0.5	from GENTILE (1983), strat section #3
BE2	4.5		from NEWELL (1932), locality N#37
BU2			described in MILLER (1966), p.17
DS3			described by HARRIS (1985)
ED1	7.5	3.8	
LA1			basal AgLs, top RtnLs not exposed
LA5			from BALL, BALL, and LAUGHLIN (1963)
LA10	15.0		Muncie Creek Shale litters quarry floor
LA12			from NEWELL (1932), N#110
LA13			from NEWELL (1932), locality N#119
LE1			from CROWLEY (1969) Cr#17
LE3			from CROWLEY (1969) Cr#31
LE4			from CROWLEY (1969) Cr#18
LO1	cov		top Raytown Ls not exposed
LO6	cov		LM thickness from MILLER (1966); 7' currently exposed
OL1			from CROWLEY (1969), Cr#1
OL2			from CROWLEY (1969), locality Cr#9
PE15	6.5	0.2	LM thickness from composite with PE16
PE23			IslCkSh and LMSh poorly distinguished
PE24			" "
PE25			" "
PE26			" "
PE27	5.1	0.2	from MILLER (1966), NEWELL (1932)
PE28	5.5	0.2	
PO2			HECKEL (pers. comm.)
PW1	8.0	ba cov	
PW10	16.6		MILLER (1966) M#25; CROWLEY (1969) Cr#12
PW11	16.6	0.5	
PW12	6.0	cov	
PW14			from NEWELL (1932), locality N#104
RA6			from BALL, BALL, and LAUGHLIN (1963)
RA7			from BALL, BALL, and LAUGHLIN (1963)
SH1			from CROWLEY (1969) Cr#5
SH2			from CROWLEY (1969) Cr#4
SP1			AgLs not exposed

REFERENCES

BALL, S. M., BALL, M. M., and LAUGHLIN, D. J., 1963. Geology of Franklin County, Kansas: Kansas Geol. Survey. Bull. 163, p. 1-57.

BARNABY, R. J., and RIMSTIDT, J. D., 1989. Redox conditions of calcite cementation interpreted from Mn and Fe contents of authigenic calcites: Bull. Geol. Soc. Amer. Bull., v. 198, n. 6, p. 795-804.

BERNER, R. A., 1981. A new geochemical classification of sedimentary environments: J. Sed. Pet., v. 51, n. 2, p. 359-365.

BRAND, U., and VEIZER, J., 1980. Chemical diagenesis of a multicomponent carbonate system, 1. Trace elements: J. Sed. Pet., v. 50, p. 1219-1236.

CHAMP, D. R., GULENS, J., and JACKSON, R. E., 1979. Oxidation-reduction sequences in ground water flow systems: Can. J. Earth Sci. v. 16, p. 12-23.

CROWLEY, D. J., 1969. Algal Bank complex in Wyandotte Limestone (Late Pennsylvanian) in eastern Kansas: Kansas Geol. Survey Bull. 198, p. 1-52.

DOERNER, H. A., and HOSKINS, W. M., 1925. Coprecipitation of radium and barium sulfates: J. Amer. Chem Soc., v. 47, p. 662-675.

DOROBEK, S. L., 1987. Petrography, geochemistry, and origin of burial diagenetic facies, Siluro-Devonian Helderberg Group (carbonate rocks), Central Appalachians: Amer. Assoc. Pet. Geol. Bull., v. 71, n. 5, p. 492-514.

DREVÉR, J. I., 1982. The Geochemistry of Natural Waters (2d ed.): New Jersey, Prentice Hall, 437 pp.

FRANK, J. R., CARPENTER, A. B., and OGLESBY, T. W., 1982. Cathodoluminescence and composition of calcite cement in the Taum Sauk Limestone (Upper Cambrian), southeast Missouri: J. Sed. Pet., v. 52, no. 2, p. 631-638.

FROELICH, P. N., KLINKHAMMER, G. P., BENDER, M. L., LUEDTKE, N. A., HEATH, G. R., CULLEN, D., and DAUPHIN, P., 1979. Early oxidation of organic matter in pelagic sediments of the eastern equatorial Atlantic: suboxic diagenesis: Geochim. Cosmsochim. Acta, v. 43, 1075-1090.

GIVEN, R. K., and LOHMANN, K. C., 1985. Derivation of the original isotopic composition of Permian marine cements: J. Sed. Pet., v. 55, p. 430-439.

GOLDSTEIN, R. H., 1988. Cement stratigraphy of Pennsylvanian Holder Formation, Sacramento Mountains, New Mexico: Amer. Assoc. Pet. Geol. Bull., v. 72, n. 4, p. 425-438.

GROVER, G., and READ, J. F., 1983: Paleoaquifer and deep burial related cements defined by regional cathodoluminescent patterns, Middle Ordovician carbonates, Virginia: Amer. Assoc. Pet. Geol., v. 67, no. 8, p. 1275-1303.

HAMBLIN, W. K., 1969. Marine paleocurrent directions in limestones of the Kansas City Group (Upper Pennsylvanian) in eastern Kansas: Kansas Geol. Survey Bull. 194, pt. 2, p. 1-25.

HARRIS, J. W., 1985. Description of field trip stops: Stop 4, in Watney, W. L., Kaesler, R. L., and Newell, K. D., (eds.), S.E.P.M., Midcontinent Section, Proc. 3rd Ann. Mtg. & Field Conf., p. 40-44.

HECKEL, P. H., 1977. Origin of phosphatic black shale facies in Pennsylvanian cyclothems of Mid-continent North America: Amer. Assoc. Petrol. Geol. Bull., v. 61, no. 7, p. 1045-1068.

----------, 1980. Paleogeography of eustatic model for deposition of Midcontinent Upper Pennsylvanian cyclothems, in Fouch, T.D., Magathan, E. R., (eds.), Rocky Mtn Sec. S.E.P.M., W-C. U.S. Paleogeog. Symp. 1: Paleozoic Paleogeography of West-Central United States, p. 197-215.

----------, 1983. Diagenetic model for carbonate rocks in Midcontinent Pennsylvanian eustatic cyclothems: Jour. Sed. Petrology, v. 53, p. 733-759.

----------, 1985. Description of field trip stops: Stop 1, in Watney, W. L., Kaesler, R. L., and Newell, K. D., (eds.), S.E.P.M., Midcontinent Section, Proc. 3rd Ann. Mtg. & Field Conf., p. 29.

----------, 1986. Sea-level curve for Pennsylvanian eustatic marine transgressive-regressive depositional cycles along midcontinent outcrop belt, North America: Geology, v. 14, p. 330-334.

----------, 1987. Topics of correlation and nomenclature: Newsletter of the Midcontinent Pennsylvanian Stratigraphic Working Group, p. 1-28.

HEM, J. D., 1972. Chemical factors that influence the availability of iron and manganese in aqueous systems: Geol. Soc. Amer. Bull., v. 83, p. 443-450.

HEMMING, N. G., MEYERS, W. J., and GRAMS, J. C., 1989. Cathodoluminescence in diagenetic calcites: The role of Fe and Mn as deduced from electron probe and spectrophotometric measurements: J. Sed. Pet., v. 59, no. 3, p. 404-411.

ICHIKUNI, M., 1973. Partition of strontium between calcite and solution: Effect of substitution by manganese: Chem. Geol., v. 11, p. 315-319.

KINSMAN D. J., and HOLLAND, H. D., 1968. The co-precipitation of cations with $CaCO_3$-IV. The co-precipitation of Sr^{2+} with aragonite between 16° and 96°C: Geochim. Cosmochim. Acta, v. 33, p. 1-17.

KINSMAN, D. J., 1969. Interpretation of Sr^{+2} concentrations in carbonate minerals and rocks: J. Sed. Pet., v. 39, n. 2, p. 486-508.

KITANO, Y., HOBUKO, K., and TAMOTSU, O., 1971. Measurements of distribution coefficients of strontium and barium between carbonate precipitation and solution-Abnormally high values of distribution coefficients measured at early stages of carbonate formation: Geochem. J., v. 4, p. 183-206.

LINDHOLM, R. C., and FINKELMAN, R. B., 1972. Calcite staining: semiquantitative determination of ferrous iron: J. Sed. Pet., v. 42, n. 1, p. 239-242.

LLOYD, J. W., and HEATHCOTE, J. A., 1985. Natural inorganic hydrochemistry in relation to groundwater: Oxford, Clarendon Press, 294 pp.

LOHMANN, K. C., 1988. Geochemical patterns of meteoric diagenetic systems and their application to studies of paleokarst, in James, N. P., Choquette, P. W. (eds.), Paleokarst: Berlin, Springer-Verlag, p. 58-80.

LORENS, R. B., 1981. Sr, Cd, Mn, Co distribution coefficients in calcite as a function of precipitation rate: Geochim. Cosmochim. Acta, v. 45, p. 553-561.

LUDVIGSON, G. A., 1988. Geochemistry of fracture-filling calcites in the Plum River Fault Zone; Hydrogeologic and tectonic implications, in Ludvigson, G. A., Bunker B. A. (eds.), New Perspectives on the Paleozoic History of the Upper Mississippi Valey: An examination of the Plum River Fault Zone: S.E.P.M. Guidebook for the 18th Ann. Field Conf. Great Lakes Sect., pp. 171-196.

MCINTIRE, W. L., 1963. Trace element partition coefficients- a review of theory and applications to geology: Geochim. Cosmochim. Acta, v. 27, p. 1209-1264.

MEYERS, W. J., 1974. Carbonate cement stratigraphy of the Lake Valley Formation (Mississippian) Sacramento Mountains, New Mexico: J. Sed. Pet., v. 44, no. 3, p. 837-861.

MASON, R. A., 1987. Ion microprobe analysis of trace elements in calcite with an application to the cathodoluminescence zonation of limestone cements from the lower Carboniferous of South Wales, U.K.: Chem. Geol., v. 64, p. 209-224.

MILLER, D. E., 1966. Geology and ground-water resources of Miami County, Kansas: Kansas Geol. Survey Bull. 181, p. 1-66.

MITCHELL, J., C., 1981. Stratigraphy and depositional history of the Iola Limestone, Upper Pennsylvanian (Missourian), Northern Midcontinent, U.S.: Ph.D. dissertation, University of Iowa, 364 pp.

MORSE, J. W., and CASEY, W. H., 1988. Ostwald processes and mineral paragenesis in sediments: Amer. J. Sci., v. 288, p. 537-560.

MUCCI, A., 1988. Manganese uptake during calcite precipitation from seawater: Conditions leading to the formation of a pseudokutnahorite: Geochim. Cosmochim. Acta, v. 52, p. 1859-1868.

NEWELL, N. D., 1935. Pt. 1, Geology of Johnson and Miami Counties, Kansas: Kansas Geol. Survey Bull. 21, p. 1-150.

O'CONNOR, H. G., 1971. Geology and ground-water resources of Johnson County, northeastern Kansas: Kansas Geol. Survey Bull. 203, p. 1-68.

PINGITORE, N. E., 1978. The behavior of Zn^{2+} and Mn^{2+} during carbonate diagenesis: Theory and applications: J. Sed. Pet., v. 48, no. 3, p. 799-814.

REEDER R. J., and GRAMS, J. C., 1987. Sector zoning in calcite cement crystals: Implications for trace element distributions in carbonates: Geochim. Cosmochim. Acta, v. 51, p. 187-194.

SEEVERS, W. J., 1969. Geology and ground-water resources of Linn County, Kansas: Kansas Geol. Survey Bull. 193, 65 pp.

VEIZER, J., 1983. Chemical diagenesis of carbonates: theory and application of trace element technique, in Arthur, M. A., Anderson, T. F., Kaplan, I. R., Veizer, J., and Land, L. S. (eds.), Stable Isotopes in Sedimentary Geology, S.E.P.M. Short Course No. 10, p. 3-1 - 3-100.

WAYCHUNAS, G. A., 1988. Luminescence, X-ray emission, and new spectroscopies, in Hawthorne, F. C. (ed.), Spectroscopic Methods in Mineralogy and Geology, Reviews in Mineralogy, v. 18, Min. Soc. Amer., p. 639-698.

WRAY, J. L., 1964. Archaeolithophyllum, an abundant calcareous alga in limestones of the Lansing Group (Pennsylvanian), Southeast Kansas: Geol. Surv. Kansas Bull. 170, part 1, 14 pp.